NASA Contractor Report 2754

Real-Time Testing of Titanium Sheet and Extrusion Coupon Specimens Subjected to Mach 2.7 Supersonic Cruise Aircraft Wing Stresses and Temperatures

Tjerand Lunde

CONTRACT NAS1-13649
DECEMBER 1977

NASA

NASA Contractor Report 2754

Real-Time Testing of Titanium Sheet and Extrusion Coupon Specimens Subjected to Mach 2.7 Supersonic Cruise Aircraft Wing Stresses and Temperatures

Tjerand Lunde
Lockheed-California Company
Burbank, California

Prepared for
Langley Research Center
under Contract NAS1-13649

NASA
National Aeronautics
and Space Administration

**Scientific and Technical
Information Office**

1977

FOREWORD

The real-time testing program reported in this report was started in 1964 and was ended in 1976. The people associated with the research program over the years at Lockheed-California Company are too numerous for all to be named.

The Lockheed Project Leaders for the research program were Mr. Alexander J. McCulloch (1964-1965), Mr. Leon Bakow (1965-1970), and Mr. Tjerand Lunde (1970-1976).

All testing and metallurgical analyses were done at the Lockheed Research Facility at Rye Canyon, California. Mr. Russell L. Lowe (1964-1974) and Mr. E. Dwayne Black (1974-1976) were in charge of the testing. The metallurgical analyses were done by Mr. Jerry M. Van Orden and Mr. Frank T. Wimmer.

TABLE OF CONTENTS

TABLE OF CONTENTS (Continued)

LIST OF TABLES

LIST OF FIGURES

LIST OF FIGURES (Continued)

SUMMARY

A real-time testing program was undertaken to investigate the accuracy of three accelerated flight-by-flight test methods for material selection, and fatigue substantiation of supersonic cruise aircraft structure.

The real-time stresses and temperatures applied to the specimens were representative of the service conditions in the lower surface of a Mach 2.7 supersonic cruise aircraft wing root structure. Each real-time flight lasted about 65 minutes, including about one hour at 533 K (500 ^{o}F) in the cruise condition.

Center-notched coupon specimens from six titanium materials were tested: mill-annealed, duplex-annealed, and triplex-annealed Ti-8Al-1Mo-1V sheets; mill-annealed Ti-8Al-1Mo-1V extrusion; mill-annealed Ti-6Al-4V sheet; and solution-treated and aged Ti-6Al-4V extrusion. For duplex-annealed Ti-8Al-1Mo-1V sheet, specimens with single spotweld were also tested.

The test results were studied in conjunction with other related data from the literature for: material selection, structural fabrication, fatigue resistance of supersonic cruise aircraft structure, and fatigue test acceleration procedures for supersonic cruise aircraft.

INTRODUCTION

Prototypes of new subsonic aircraft are generally subjected to full-scale laboratory fatigue tests to detect fatigue sensitive areas and to verify the structural integrity. Fatigue tests of subsonic aircraft conducted under representative loading can be accelerated without invalidating the data, because metals are known to be insensitive to the frequency of fatigue loading over the range of interest at room temperature. However, supersonic aircraft, during most of each flight, will be subjected to elevated temperatures which must be considered in the fatigue tests. Long real-time tests are expensive and time consuming. Acceleration of full-scale fatigue tests for supersonic aircraft depends on knowledge of the effects of loading and long-time heating on the fatigue behavior of the materials considered for the primary structure.

The NASA Langley Research Center, Structural Integrity Branch, has been conducting a study of the effects of real-time loading and heating simulating the flight environment of a Mach 3 transport. The test program described and reported on in this report will provide fatigue data for an additional set of loading and specimen conditions (for Mach 2.7) to complement Langley's data.

The research program was initiated in 1964 by Air Force sponsorship. It was continued by sponsorship of the Federal Aviation Agency (1965-1971) and the National Aeronautices and Space Administration (1972-1976). The program was concluded in 1976.

The original program called for testing of duplex-annealed Ti-8Al-1Mo-1V, PH 14-8Mo and INCO 718 sheet specimens. Because of the superiority of the titanium alloy, demonstrated by the test results reported in References 1 and 2, the steel and nickel alloy specimens were replaced by specimens made from five additional titanium materials. These five materials were: mill-annealed and triplex-annealed Ti-8Al-1Mo-1V sheets, mill-annealed Ti-8Al-1Mo-1V extrusion, mill-annealed Ti-6Al-4V sheet, and solution-treated and aged Ti-6Al-4V extrusion. Center-notched specimens were tested for all the materials. For duplex-annealed Ti-8Al-1Mo-1V sheet, specimens with single spotweld were also tested.

During the period from 1964 to 1976, the test specimens were subjected to real-time flight-by-flight load and temperature cycles. The real-time stresses and temperatures applied to the specimens were representative of the service conditions in the lower surface of a Mach 2.7 supersonic cruise aircraft wing root structure. Each real-time flight lasted about 65 minutes, including about one hour at 533 K (500 ^{o}F) in the cruise condition. The real-time testing was terminated before all specimens had failed. After termination of the real-time testing, the specimens without cracks were subjected to accelerated testing at room temperature. The accelerated testing was performed to the same loading spectrum as the real-time testing, with the loading spectrum applied until failure occurred.

This report presents the real-time fatigue test results, and Lockheed-California Company results from similar, but accelerated fatigue tests. The results of the accelerated testing of unfailed real-time specimens are also included. The Lockheed-California Company results are discussed in conjunction with other related data from the literature.

Overall, the discussions and conclusions of the report identify the significance of the data for material selection, structural fabrication, fatigue resistance of supersonic cruise aircraft structure, and fatigue test acceleration procedures for supersonic cruise aircraft.

ABBREVIATIONS AND SYMBOLS

The measurements for physical quantities were made in U.S. Customary Units during the investigation. In this report, the units for physical quantities are given in both the International System of Units (SI) and the U.S. Customary Units. The conversion factors and SI abbreviations used are given in Appendix A.

Abbreviations

Acc.	-	Accelerated
Const.	-	Constant
cps	-	Cycles per second
D.A.	-	Duplex-annealed
^{o}F	-	Degrees fahrenheit
Flts.	-	Flights
ft	-	Foot
GAG	-	Ground-Air-Ground
hp	-	Horse Power
in.	-	Inch
ksi	-	Thousands of pounds per square inch
L	-	Longitudinal
lbf	-	Pound force
M.A.	-	Mill-annealed
Mag. 450X	-	Magnified 450 times
Min	-	Minutes
No.	-	Number
Ref(s).	-	Reference(s)
STA	-	Solution-treated and aged
T	-	Transverse
T.A.	-	Triplex-annealed
Temp.	-	Temperature
6-4	-	Ti-6Al-4V
8-1-1	-	Ti-8Al-1Mo-1V

Symbols

e	-	Percentage elongation in 5.08 cm (2.00 inch) gage length
$f_{1g_{Ref}}$	-	1 g reference stress, MPa (ksi)
f_{vary}	-	Varying stress, MPa (ksi)
F_{tu}	-	Ultimate tensile stress, MPa (ksi)
F_{ty}	-	Tensile yield stress, MPa (ksi)
W_1, W_2, W_3	-	Weights 1, 2, and 3, N (lbf)

MATERIALS

The materials were: mill-annealed, duplex-annealed, and triplex-annealed Ti-8Al-1Mo-1V sheets; mill-annealed Ti-8Al-1Mo-1V extrusion; mill-annealed Ti-6Al-4V sheet; and solution-treated and aged Ti-6Al-4V extrusion.

The static tensile properties of the titanium materials tested in the real-time test program are listed in Table 1. The listed static strengths and percentage elongations are typical for the titanium alloys tested.

Table 2 gives the mill histories and processes for the materials tested. The material processing was performed by the manufacturer of the individual alloys, except for triplex-annealed Ti-8Al-1Mo-1V sheet. For this, 1.52 mm (0.060 inch) thick mill-annealed Ti-8Al-1Mo-1V sheet was processed into 1.27 mm (0.050 inch) thick Ti-8Al-1Mo-1V sheet at Lockheed-California Company. A hydrogen analysis was performed on the 1.27 mm (0.050 inch) thick triplex-annealed Ti-8Al-1Mo-1V sheet. On a weight basis, a maximum of 150 parts of hydrogen per million is allowed (Ref. 3). Heat D6512 was found to have 85 parts of hydrogen per million, and heat D8647 was found to have 76 parts per million.

Titanium alloy samples were sectioned and examined. Photomicrographs of sections through the samples are given in Figure 1. The microstructures appear to be typical for all materials, except for Figure 1b. In Figure 1b, dark etching areas are seen adjacent to the beta particles. Metallurgical analyses of failed specimens are discussed in Appendix B.

SPECIMEN FABRICATION

Two types of specimens were tested in this program. These were thirty center-notched specimens and six single spotweld specimens having the geometries shown in Figure 2. Center-notched specimens were made from all the six materials and the single spotweld specimens were made from the duplex-annealed Ti-8Al-1Mo-1V sheet. The extrusion specimens were taken from the flange material of T-extrusions as shown in Figure 3. A minimum of 0.76 mm (0.030 inch) was machined from each surface of the extruded material. During the manufacture of the specimens, it was found that the material thicknesses were not exactly 1.27 mm (0.050 inch). Some were thicker and some were thinner. In order to compensate for this, the specimen widths were adjusted such that the net areas were as closely as possible the same as required to produce equal stresses under load.

The center-notch specimens, with two exceptions, had holes which were free from scratches and rough machining marks. The burrs were removed by light lapping with kerosene-soaked number 0 grit emery paper. The hole surface finish was smooth, about 635 nm (25 microinches) (arithmetic average) or better. There was no discoloration around any hole. This indicated that the material adjacent to the holes had not been overheated during the machining of the holes.

The specimens were not exposed to stress nor elevated temperature before the real-time testing.

All the specimens were fitted with thermocouple wires at points on the center line, in order to measure and control the specimen temperatures (see Figure 2). Two small holes were drilled through the specimen 1.27 cm (0.5 inch) on either side of the transverse axis. The holes were 0.81 mm (0.032 inch) in diameter to take the 0.79 mm (0.031 inch) thick thermocouple wires. The thermocouple wires were fed through these two holes (one in each hole) from the same side, gripped in a special holding fixture, then tapped lightly with a hammer (Ref. 1). This upset the thermocouple wires on either side of the specimen and prevented them from being pulled out and from rotating in the holes. The stress concentration at the thermocouple holes was less than at the center notch and single spotweld.

Due to the application of compressive loads, the specimens required supports against buckling. The buckling support was achieved with an edge support clamp arrangement. Each specimen was supported by four 6.35 mm (0.25 inch) diameter, detachable stainless steel rods held in place by four notched steel yokes, as shown in Figure 4. The whole assembly was centered on the specimen by four 4.78 mm (0.188 inch) attachment bolts (Ref. 1). The clamps were installed with a sliding contact, held fretting to a minimum and did not pick up specimen load.

REAL-TIME TESTING (1964-1976)

The real-time testing was started in 1964. The original program required twelve duplex-annealed titanium 8Al-1Mo-1V sheet specimens (six with center notch and six with single spotweld) together with specimens made from PH14-8Mo and INCO 718. The PH14-8Mo and INCO 718 were removed from the program in 1965, after 1728 simulated flights had been applied. Twenty-four center-notched titanium specimens were substituted in the program:

3 mill-annealed Ti-8Al-1Mo-1V sheet specimens
3 triplex-annealed Ti-8Al-1Mo-1V sheet specimens
6 mill-annealed Ti-8Al-1Mo-1V extrusion specimens
6 mill-annealed Ti-6Al-4V sheet specimens
6 solution-treated and aged Ti-6Al-4V extrusion specimens.

The test procedures and test equipment for the real-time testing are described in the following sections.

Procedures for Real-Time Testing

Thirty-six fatigue specimens were loaded in axial tension and compression with the magnitudes and sequences defined by Spectra "C" of Reference 1, and presented in Table 3, until specimen failure or until April 1, 1976. Prior to 1972, failure was defined as the initiation of visible cracking at the edge of the hole or spotweld. Specimens with cracks were taken out of the machine and failed statically. Starting in 1972, specimens which developed cracks were tested until complete failure had occurred across one side of each test section from the notch (or spotweld) to the edge. All specimens were inspected periodically for indication of crack initiation, and to monitor the growths of existing cracks. The crack lengths were measured twice a week.

Spectra "C", defined in Reference 1, simulate the service stresses in the lower surface of a supersonic cruise aircraft wing root structure. These stresses represent aerodynamic and thermal loadings which may occur at a point slightly inside the wing surface, such as a beam cap. At such a location, a significant tensile stress will be developed during heating due to thermal gradients.

Table 3 lists the ratios of the varying stress to the 1-g reference stress and their occurrences in 80 000 flights in the flight-by-flight sequences. All stresses are gross area stresses. The 1-g reference stress was 172 MPa (25 ksi). The varying stresses were applied at a rate of 1 Hz (1 cps). The unit flight-by-flight loading sequences and magnitudes of Spectra "C" are schematically shown in Figure 5, for the real-time tests, together with the once-per-flight temperature cycle. The duration of a simulated unit real-time flight was about 65 minutes.

Eleven specimens failed at the grips. To repair the specimens for continued testing, each specimen was first machined at the failed end to get a straight edge at right angles to the axis of the specimen. A mating piece of new material, to make up for the broken end of the specimen, was then electron beam welded to the specimen. The specimen edges and the weld areas were trimmed flush with the specimen surfaces after welding. The specimen was then reinstalled into the program.

All the specimens were taken out of the machine and the grip areas inspected, after several grip failures had occurred during October and November 1972. Fretting marks, due to contact with the grip attachment clamps, were polished off the specimens and 1.27 mm (0.050 inch) thick annealed copper shims were inserted between the specimen and the clamps at each end. Only two grip failures occurred after that.

Equipment for Real-Time Testing

The real-time testing machine consisted of six columns installed in parallel within a single reaction frame, with six specimens and a load-measuring transducer in each column. Each column was loaded by a double acting hydraulic jack through a bell crank lever. The test areas of the six series-connected specimens in each loading column were enclosed by heating-cooling ducts. The actions of the jacks were controlled so as to apply the loadings in the flight sequence which is shown in Figure 5. The specimen positions are shown in Figure 6. A block diagram of the control equipment is shown in Figure 7. Photographs of the test equipment are given in References 1 and 4.

The cyclic loads were controlled by a system that used load feedback. In that system, stepping switches programmed both the loadings, and the heating and cooling. The load sensing was obtained by using a trigger device along with one of the load transducers. On that trigger, a pair of preset voltages were used to represent the positive and negative halves of a load cycle. For every change in load on the specimen, the transducer generated a voltage increment. When the net voltage on the transducer was equal to one of the preset voltages on the trigger, the trigger fired to reverse the direction of oil flow in all of the hydraulic jacks. This reversal changed the action of the jacks on all of the specimens, with two such changes required to complete a loading cycle which was then recorded on a counter. When the required number of each varying load level had been applied, switches were rotated to a new position to establish the next varying load level to be applied to the specimens.

To apply the three differing mean load levels required for the climb, cruise, and descent phases of flight, sets of weights were used rather than electrically controlled hydraulic jacks. Use of the weights was dictated by the need to minimize the possiblity of inadvertent load change during the hour at constant load in each flight, which is defined in Figure 5. The load produced by the weights was applied, through a system of pulleys, to the pistons of the hydraulic jacks to generate the steady static load. During operation, the mean load produced by the weights was varied by the movement of a weight support platform. This platform movement was provided by the action of electric motor-driven Acme screws. The weight system is shown diagrammatically in Figure 8. The signals to the motor for moving the platform were supplied by points on the load control stepping switch. The position of the platform was controlled by a system of micro switches.

The specimen columns were restrained from buckling under compression loadings by using flexure plates at the specimen attachments, and edge support clamps on the specimens.

Quartz lamps were used to heat the specimens. These lamps were mounted immediately below and at right angles to the specimens. They were located in insulation-lined stainless steel tunnels which acted as cooling ducts during the last half of the temperature cycle. Power was supplied to these lamps by a 480-volt controller that operated at 100 amperes.

All the specimens were equipped with iron-constantan thermocouples. The temperatures were continuously recorded on a strip chart recorder. The temperature changes were monitored by the output from one of these thermocouples. Independent temperature surveys were periodically made on all specimens through the use of a portable temperature probe. This probe was lowered through each of the specimen observation slits (which were located along the tops of the heating-cooling tunnels, one directly above each of the specimens) and was held tightly against the central portion of the particular specimen being measured. Surface temperatures could be measured within ± 6 K (± 10 ^{o}F) by this means. The openings in the above slits were varied individually in order to obtain a uniform temperature distribution throughout the system.

During operation, a signal to the temperature controller was provided by a trigger action at the completion of loading cycles associated with the climb phase of the flight. Full power was applied to the heat lamp at the negative peak of the last load cycle applied during climb. When the load cycle had been completed, the mean load level for the cruise phase of the flight was applied. The maximum power was reduced in approximately six minutes to permit the specimens to reach the stabilized 533 K (500 ^{o}F) temperature. At the negative peak of the last cycle of the cruise loadings, the power to the lamps was shut off and a 11kW (15-horsepower) centrifugal blower was turned on to force ambient air across the specimens to reduce their temperature to 305 K (90 ^{o}F) for application of the descent load cycles. This cooling required approximately three minutes. The manifold from the blower was connected to each of the six stainless steel ducts. The temperature-loading relationships produced by the equipment are shown in Figure 5.

Several safeguards were designed into the equipment to minimize the possibility of accidental damage to the specimens through operator error or from malfunction of the equipment, in addition to the static weights for maintaining mean load levels:

1. During the automatically controlled flight-by-flight loading, the hydraulic pressures were limited to values a few percent over those required for the maximum loads during each flight.

2. Preset pressure regulators protected the specimens against accidental overloads which might have occurred during the manually controlled applications of the larger loadings which were required to represent the growth of peak loadings with time.

3. Mechanical stops were installed to prevent excessive and damaging deflections when a specimen failed.

4. In the event of a power failure, normally open by-pass valves acted to reduce the system oil pressure to zero. As an added safety feature, a 4-way solenoid valve operated to prevent large compressive loads on the specimens if the by-pass valves did not function.

5. In the event of a drop in operating pressure because of a malfunction of the hydraulic pump or because of a leak in the oil system, a pressure switch shut off the hydraulic pump and the heating.

6. To prevent overheating, a device was installed to shut off the hydraulic pump and the heating if the temperature measured by any of the thermocouples exceeded 550 K (530 °F).

7. A timer was installed in the system to shut off the power to the lamps if the heat stayed on for more than 66 minutes.

8. A hydraulic interlock circuit was installed which shut off the hydraulic pump whenever the power to the lamps was interrupted.

9. An additional interlocking device was installed to shut off the hydraulic pump and the heating in the event the cooling fan failed to operate.

FOLLOW-ON ACCELERATED TESTING OF UNFAILED REAL-TIME SPECIMENS

The real-time testing was terminated on April 1, 1976, and the fifteen uncracked real-time specimens were subjected to accelerated testing, at room temperature, until failure. The test procedures and test equipment for the accelerated testing are outlined in the following sections.

Procedures for Accelerated Testing

The accelerated testing of the unfailed real-time specimens was done with the same loading spectra, Spectra "C", as the real-time testing. All accelerated testing was done at room temperature. The duration of a simulated unit accelerated flight was about 0.09 minute. This was achieved by changing the mean stresses at a rate of 2.5 Hz (2.5 cps), applying the taxi half cycles at a rate of 10.00 Hz (10.00 cps), and applying the varying stresses at the following rates:

$\frac{f_{vary}}{f_{1g_{Ref}}}$	Rate of Applying Varying Stresses, Hz (cps)
0.15-0.35	20.00
0.45-0.75	15.15
0.85-1.65	10.00
1.75	5.00
1.85-2.05	2.00

Equipment for Accelerated Testing

Test machines of the type shown in Figure 9, and illustrated schematically in Figure 10, were employed to conduct the accelerated flight-by-flight testing. These machines have been designed and constructed at the Lockheed-California Company. Each machine consists of a pair of servo jacks mounted in parallel within a simple loading rack. Each jack loads two specimens, as shown in Figure 9. These specimens are connected in series with a calibrated load transducer. The loads applied by these dual jack machines were programmed by four-track magnetic tape units. In these machines, loads of $\pm$44.5 kN ($\pm$10 000 lbf) can be controlled within a scale accuracy of $\pm$2 percent at frequencies up to 45 Hz (45 cps).

During operation, the output voltage from the programmer was fed into the servo loop of each of the servo jacks through a summing junction, as shown schematically in Figure 10. This signal programmed the action of a servo valve to meter the cyclic flow of oil to the fore and aft ports of the servo jack. Loadings were applied to the specimens and the load transducer by the resulting movement of the jack piston. The servo loop was closed by feeding the resulting signal from the load cell back into the summing junction. The instantaneous summing of these opposing signals at the input side of the servo loop resulted in the specimens experiencing the same loading history as that represented by the signals on the magnetic tape.

As indicated in Figure 10, the loading system employed the following safeguards against specimen overload.

1. A load limiter was included to protect the specimens from spurious electrical signals as well as operator error by simply limiting the maximum amplitude of the signals to the pre-selected value.

2. A high-speed dump valve, located across the hydraulic lines between the servo valve and the servo jack protected the specimens from overload in the event of internal valve leakage from the hydraulic pressure reservoir to the high pressure side of the jack.

3. A high-speed relay was located within the servo valve amplifier. In the event the rate of increase in the command signal should have exceeded that which had been programmed, this relay would have locked the servo valve and opened the high-speed dump valve.

The specimen columns were restrained from buckling under compression loadings by using flexure plates at the specimen attachments, and edge support clamps on the specimens.

DISCUSSION OF TEST RESULTS

Introductory Information

Table 4 summarizes the test results for the real-time testing as well as accelerated test results for the fifteen unfailed real-time specimens. Table 4 gives the numbers of real-time flights applied to crack detection and to complete failure, and, as appropriate, the accelerated flights to crack detection and complete failure. The last column of Table 4 gives the size of the crack when first detected.

The crack propagation data recorded are given in Tables 5 through 10. Photomacrographs showing the mating fracture surfaces of the failed specimens are given in Figures 11 through 17. No photomacrograph is available for specimen G-1, nor is the specimen available, since it was cut up for metallurgical analysis (see Appendix B).

The log averages of the real-time test results are given in Table 11 for each type of specimen together with the log averages of the corresponding accelerated test results obtained from Reference 4. In the table, the ratios of

$$\frac{\text{Log Average Accelerated Flights}}{\text{Log Average Real-Time Flights}}$$

have been given. The log average real-time flights are based on the flights to crack detection when possible. Some specimens were tested to complete failure without a crack being detected. For those specimens, the flights to complete failure have been used in the evaluation of the log average real-time flights.

For the fifteen specimens which did not fail during the real-time testing, the flights accumulated for each specimen at the end of the real-time program have been used. However, for the groups those fifteen specimens belong to, log average values of the total applied flights to failure (i.e. including the follow-on accelerated testing) have also been given. For those groups, the ratios of

$$\frac{\text{Log Average Accelerated Flights}}{\text{Log Average (Real-Time + Accelerated) Flights}}$$

have been given.

Only the duplex-annealed Ti-8Al-1Mo-1V sheet specimens were in the program at the start of the testing. The other specimens were added after 1728 simulated flights had been applied, and are thus out of phase on the growth flights. Further, some specimens were out of the program due to grip failures until repaired. These specimens are also out of phase on the growth flights.

Also, in the first part of the program, the growth flights were applied by grouping growth cycles together in blocks rather than adding them to a unit flight periodically. Thus, although the specimens received the correct numbers of growth cycles, they received too few ground-air-ground (GAG) cycles. Separate GAG cycles were applied, to the unfailed specimens, to compensate for the loading which was eliminated by grouping growth cycles.

Three failure definitions have been used for the real-time testing: first detected crack; complete failure; and flights applied to unfailed specimens. The differences between these definitions involved more cycles than the out of phase inconsistencies discussed above, and have a greater effect on the test result comparisons. The accelerated test results obtained from Reference 4 were based on the first detected crack, unless the specimen did not fail.

The real-time test results given in Table 4 have been plotted in Figures 18 through 24. For the fifteen specimens which did not fail during real-time testing, the accelerated test flights have also been plotted. The maximum, minimum, and log average values of the corresponding accelerated test results from Reference 4 have also been given in Figures 18 through 24.

A summary of the accelerated test results for the fifteen specimens which did not fail during real-time testing together with the corresponding test results from Reference 4 are given in Table 12.

Table 13 gives the net area strengths of real-time specimens which were taken out of the test machine after cracks had developed.

To identify the significance of the data for material selection, structural fabrication, fatigue resistance of supersonic cruise aircraft structure, and fatigue test acceleration procedures for supersonic cruise aircraft, the following subject areas have been considered:

- Ultimate Tensile Strength
- Creep
- Residual Strength
- Stress Corrosion
- Constant Amplitude Tests
- Real-Time Fatigue Resistance
- Accelerated Testing
- Crack Propagation
- Test Scatter.

The sections on Creep, Stress Corrosion, and Constant Amplitude Tests are based entirely on data from the literature.

Ultimate Tensile Strength

The ultimate tensile strength values given in Table 1 apply only to the material thickness tested. Reference 5 reports that, for duplex-annealed

Ti-8Al-1Mo-1V sheet, 6.35 mm (0.250 inch) thick specimens had lower ultimate tensile strengths than 1.27 mm (0.050 inch) thick specimens. This is also indicated by the ultimate tensile strength values given in Reference 6.

For duplex-annealed Ti-8Al-1Mo-1V sheet, and annealed Ti-6Al-4V sheet, the ultimate tensile strengths were reduced by 21 and 28 percent respectively, at 561 K (550 °F), as compared with room temperature results (Ref. 7).

The ultimate tensile strength of triplex-annealed Ti-8Al-1Mo-1V sheet was reduced by about 14 percent at 561 K (550 °F), as compared with room temperature results (Ref. 8).

Solution-treated and aged Ti-6Al-4V sheet showed reductions in ultimate tensile strengths of about 20 percent when tested at 533 K (500 °F) as compared to room temperature (Ref. 9). For solution-treated and aged Ti-6Al-4V extrusion, no data were found.

Exposures for up to 30 000 hours without stress at 561 K (550 °F) had little effects on the room temperature ultimate tensile strengths of mill-annealed and duplex-annealed Ti-8Al-1Mo-1V sheets, and annealed Ti-6Al-4V sheet (References 10, 11, 12, 13, and 14). Both the notched and unnotched static tensile strengths were reduced by about 10 percent or less.

However, exposures at 561 K (550 °F) for spotwelded annealed Ti-8Al-1Mo-1V sheet, and annealed Ti-6Al-4V sheet showed a decrease in the spotweld tensile strengths with exposure time (Ref. 11). Spotwelded duplex-annealed Ti-8Al-1Mo-1V sheet may also show similar reduction in the spotweld tensile strength with exposure at elevated temperature. This must be investigated before spotwelded duplex-annealed Ti-8Al-1Mo-1V sheet is used on a supersonic cruise aircraft.

Solution-treated and aged Ti-6Al-4V extrusion had the highest ultimate tensile strength of the materials tested (Table 1). However, Table 4 shows that sheet materials, with lower ultimate tensile strengths, produced longer fatigue lives.

Creep

The discussion in this section is based entirely on the literature. For duplex-annealed Ti-8Al-1Mo-1V sheet, creep did not affect the fatigue lives for supersonic temperatures (Ref. 15). Creep is not considered to be a problem for titanium alloys at 561 K (550 °F) (Ref. 16). Thus, on the basis of creep alone, the heating period can be reduced, without an adverse effect, during representative fatigue testing of materials or structure for Mach 3.0 supersonic cruise aircraft. The heat-transfer characteristics of a structure will determine how much the hot and cold soaking times can be shortened. However, the effects of heat exposure on other material strength parameters must also be considered.

Residual Strength

The residual strength comparisons referred to below were based on evaluations using the unified notch-strength analysis method described in Reference 17. The fracture toughness concept was not used. All the tests were conducted on specimens containing central fatigue cracks.

The residual strength is sensitive to material thickness. Thus, 6.35 mm (0.250 inch) thick duplex-annealed Ti-8Al-1Mo-1V sheet has very much lower residual strength than 1.27 mm (0.050 inch) thick sheet (Ref. 5).

On the basis of the same thickness, duplex-annealed Ti-8Al-1Mo-1V sheet has superior residual strength as compared to mill-annealed and triplex-annealed Ti-8Al-1Mo-1V sheets, and annealed Ti-6Al-4V sheet (Refs. 5, 10, and 18). The residual strengths were compared at 195 K (-109 °F), room temperature (294-300 K (70-80 °F)), and 561 K (550 °F), and the exposure times were only long enough to produce the required crack lengths for the residual strength testing. Mill-annealed Ti-8Al-1Mo-1V sheet was found to have the lowest residual strengths at 195 K (-109 °F) and room temperature. This material is also very sensitive to delayed failure. Thus, a static tensile stress well below the residual strength may cause a static failure if sustained for a period of time even in air (Ref. 19). Mill-annealed Ti-8Al-1Mo-1V sheet therefore seems unsuitable as a wing skin material.

From Table 4, it is seen that four specimens failed during the real-time testing without a crack being observed. The four specimens were: mill-annealed Ti-8Al-1Mo-1V sheet specimen ET-4, which failed after 54 338 flights; and mill-annealed Ti-8Al-1Mo-1V extrusion specimens H-1, H-2, and H-3, which failed after 22 956, 22 725, and 19 618 flights respectively. Specimens H-2 and H-3 both failed, at different times, when resumption of testing was attempted after a shut-down period during which the specimens were held at small constant tensile stresses at room temperature. It thus appears that mill-annealed Ti-8Al-1Mo-1V extrusion is as notch sensitive as the sheet form of this material, and should be avoided in critical load carrying structure. Further data are required before it can be determined if this material can safely be used.

Several mill-annealed Ti-8Al-1Mo-1V extrusion specimens, including H-2 and H-3, were metallurgically analyzed. The results of these analyses are given in Appendix B.

Exposure for 1000 hours at 561 K (550 °F) reduced the residual strength for triplex-annealed Ti-8Al-1Mo-1V sheet (Ref. 20). However, exposure for 10 000 hours increased the residual strength above the unexposed strength. The reason for this is not known, but the lowest residual strength must of course be considered for material selection purposes.

The reductions in residual strengths of titanium alloys appear to be less with increasing temperatures than the reductions in the ultimate tensile strengths (Refs. 10 and 18).

The cracked real-time specimens which were taken out of the testing machine were failed statically in tension. The net area strengths of these specimens are given in Table 13. The failure strengths are from 68 to 94 percent of the room temperature ultimate strengths. The sheet specimens were tested in the transverse grain direction, and the extrusion specimens were tested in the longitudinal grain direction (see Figure 2).

Stress Corrosion

The discussion in this section is based entirely on the literature. Single-annealed Ti-8Al-1Mo-1V sheet is very much more susceptible to salt stress corrosion cracking than annealed Ti-6Al-4V sheet, at sustained stresses of 345 and 689 MPa (50 and 100 ksi) and 561 K (550 ^{o}F) exposure temperature (Ref. 21). The salt stress corrosion cracking susceptiblity of duplex-annealed Ti-8Al-1Mo-1V titanium sheet is similar to that of the single-annealed Ti-8Al-1Mo-1V sheet (Ref. 22). For duplex-annealed Ti-8Al-1Mo-1V sheet, salt stress corrosion cracking occurred after less than 20 hours at a residual stress of 483 MPa (70 ksi) and 561 K (550 ^{o}F) exposure temperature (Ref. 23). A thin salt layer was found to be more detrimental than a thick salt coating. At residual stresses of 172 to 448 MPa (25 to 65 ksi) and 533 K (500 ^{o}F) exposure temperature, salt stress corrosion cracking occurred in less than 200 hours (Ref. 24). Self-stressed specimens at 345 MPa (50 ksi) and 533 K (500 ^{o}F) exposure temperature produced salt stress corrosion cracking in about 1600 hours (Ref. 25).

The real-time specimens tested by Lockheed-California Company had a net area mean stress of 303 MPa (44 ksi) for the center-notched specimens and 248 MPa (36 ksi) for the single spotweld specimens, during the cruise condition. The cruise condition lasted for about 60 minutes during each flight and the temperature was 533 K (500 ^{o}F). For duplex-annealed Ti-8Al-1Mo-1V sheet, salt stress corrosion cracking may start at less than 262 MPa (38 ksi) for 10 000 hours at 533 K (500 ^{o}F) exposure temperature (Ref. 13). Later data (Ref. 25) show that for the same stress and soaking temperature, the material may produce salt stress corrosion cracks in less than 5000 hours.

A supersonic cruise aircraft will be flying at high altitudes most of the time where the oxygen content is relatively low and where the barometric pressure is low. Also, the elevated temperature soaking will not be continuous; it will be cyclic.

A reduction in the oxygen content reduced salt stress corrosion cracking for duplex-annealed Ti-8Al-1Mo-1V sheet (Ref. 22). The salt stress corrosion cracking was also reduced with reduction in atmospheric pressure. This can be explained with the reduction in oxygen. At high altitude, the effect of the air flow may compensate for the deficiency of oxygen, thus increasing the salt stress corrosion susceptibility (Ref. 26). Reference 26 suggests that a possible explanation for the greater severity of salt stress corrosion cracking with thin salt layers than with thick salt coatings may be the greater availability of oxygen with thin layers.

Short cyclic exposures to 561 K (550 °F), from room temperature, for 2 and 4 hours at a time produced less salt stress corrosion cracking than 6, 8, and 16 hours at a time, and less than for continuous exposure, for duplex-annealed Ti-8Al-1Mo-1V sheet (Ref. 23). However, the cracking was still considerable at 2-hour cycles.

The salt stress corrosion cracking investigations have been conducted on three different types of specimens (self-stressed; double-wave, seagull shaped; and single-bend). The compared test results are thus not always directly comparable. However, from the tests made, it appears that Ti-8Al-1Mo-1V sheet is not suitable for use in a supersonic cruise aircraft primary structure unless an effective protective treatment can be found. A supersonic cruise aircraft is required to have a service life of 50 000 flight hours, and the supersonic operation at Mach 2.7 subjects the aircraft to a temperature of 533 K (500 °F) (Refs. 16 and 27).

Stress relief annealing of duplex-annealed Ti-8Al-1Mo-1V sheet did not relieve the residual stress effects (Ref. 23). Some methods of alleviating or preventing salt stress corrosion are discussed in Reference 28. These include aluminum and nickel coatings. Before any coating is chosen for salt stress corrosion prevention on a supersonic cruise aircraft, the effect of the coating on the fatigue strength of the material must be established.

Because the Ti-8Al-1Mo-1V is more susceptible to salt stress corrosion cracking than Ti-6Al-4V, Ti-6Al-4V titanium has now been chosen as the primary material for supersonic cruise aircraft structure (Ref. 29).

However, it has since been found that duplex-annealed Ti-8Al-1Mo-1V sheet specimens subjected to a salt solution during real-time testing, with a maximum temperature of 616 K (650 °F), only showed a small detrimental effect on the fatigue lives (Refs. 7 and 30).

Constant-Amplitude Tests

The discussion in this section is based entirely on the literature. The fatigue strengths of notched and unnotched triplex-annealed Ti-8Al-1Mo-1V sheet were not appreciably affected when tested at 561 K (550 °F) as compared to room temperature (Refs. 8, 10, and 31). Similarly, the notched fatigue strength of duplex-annealed Ti-8Al-1Mo-1V sheet was not appreciably affected by testing at 561 K (550 °F) (Ref. 32). Some fatigue limits were higher and some were lower at 561 K (550 °F). It is not uncommon that the fatigue limit is higher at elevated temperatures than at room temperature.

For solution-treated and aged Ti-6Al-4V sheet, both the notched and the unnotched fatigue strengths show some reductions, for some stress ratios, at elevated temperatures of 478 K (400 °F) and above (Ref. 9).

Exposure at 561 K (550 °F) for up to three years did not significantly affect the fatigue strengths of notched, unnotched, and spotwelded specimens made of annealed and duplex-annealed Ti-8Al-1Mo-1V sheets, and annealed Ti-6Al-4V sheet (Refs. 12 and 14). However, edge-notched specimens of annealed Ti-8Al-1Mo-1V sheet showed an appreciable fatigue life reduction with exposures up to 8800 hours. All fatigue tests were conducted at a mean stress of 172 MPa (25 ksi). It is possible that another mean stress value would give different comparative results. Test results for solution-treated and aged Ti-6Al-4V sheet specimens without prior exposure indicate that the reductions are affected by the stress ratio (Ref. 9).

Prior exposure at 561 K (550 °F) for up to about 10 000 hours showed no significant change in the fatigue strengths of notched triplex-annealed Ti-8Al-1Mo-1V sheet specimens, at a mean stress of 172 MPa (25 ksi) (Ref. 20).

Residual compressive stresses greatly increased the fatigue lives of notched specimens made from duplex-annealed Ti-8Al-1Mo-1V sheet (Ref. 33). However, the beneficial effect was greatly reduced by exposure to a temperature of 561 K (550 °F) for only a few seconds. The beneficial effects of cold working can thus not be relied on as a means of providing fatigue life improvements for supersonic cruise aircraft.

The fatigue lives of duplex-annealed Ti-8Al-1Mo-1V, and solution-treated and aged Ti-6Al-4V sheet specimens were significantly reduced when tested outdoors at 561 K (550 °F) most of the time (Refs. 29, 34, and 35). There is thus a definite environmental effect. On the other hand, the fatigue lives of annealed Ti-6Al-4V sheet specimens were essentially unaffected by outdoor exposure both at ambient temperatures and at 561 K (550 °F) (Ref. 35).

The fatigue lives of annealed Ti-6Al-4V sheet specimens were also essentially unaffected by outdoor static load exposure both at ambient temperatures and at 561 K (550 °F), whereas the fatigue lives of solution-treated and aged Ti-6Al-4V sheet specimens were significantly reduced (Ref. 35).

Real-Time Fatigue Resistance

Table 4 shows that none of the duplex-annealed Ti-8Al-1Mo-1V sheet specimens with center notch failed during the real-time testing. Of the materials tested, this material is clearly superior in fatigue. The numbers of accelerated follow-on flights applied to four of these unfailed specimens (192, 194, 199, and 226) are of the same order as the numbers of accelerated flights applied to new specimens (Ref. 4), as shown in Table 12.

Mill-annealed and triplex-annealed Ti-8Al-1Mo-1V sheets appear, from Table 4, to have about the same fatigue strength, and both materials appear to be slightly better than mill-annealed Ti-6Al-4V sheet.

The extrusion materials exhibited the lowest fatigue lives. Solution-treated and aged Ti-6Al-4V extrusion has a lower fatigue strength than mill-annealed Ti-6Al-4V sheet. The mill-annealed Ti-8Al-1Mo-1V extrusion specimens gave fatigue lives of only about half the lives of the solution-treated and aged Ti-6Al-4V extrusion specimens.

All the specimens in a group were placed in the same column in the test machine (see Figure 6). No known significant load differences have been applied from column to column.

Further, all the sheet materials were made by one manufacturer and both the extrusion materials were made by another manufacturer. For any material, scatter must be expected between heats produced by different manufacturers. Even two heats made by the same manufacturer can vary greatly, as the test results show.

From Table 4, it is seen that mill-annealed Ti-8Al-1Mo-1V sheet specimen FT-15, made from heat number D8733, had a longer fatigue life than the specimens from heat number D8141 in this material group. Heat number D8733 also had a higher ultimate tensile strength than heat number D8141, as seen from Table 1.

For duplex-annealed Ti-8Al-1Mo-1V sheet, no heat comparisons can be made since only one heat was used for all specimens. It is thus possible that the fatigue test results may not have been so favorable if another heat had been used. However, this material gave longer fatigue lives than materials with higher ultimate tensile strengths.

The test results for the triplex-annealed Ti-8Al-1Mo-1V sheet specimens from the two heats used were about the same, as seen from Table 4.

The failures of the mill-annealed Ti-8Al-1Mo-1V extrusion specimens are clearly heat oriented. Heat number 3227 had the lower ultimate tensile strength, as seen from Table 1. The real-time specimens from this heat all failed before a failure of a specimen from heat number 3093 occurred, as seen from Table 4.

Table 4 shows that the mill-annealed Ti-6Al-4V sheet specimens from heat number D8103 gave the longest fatigue lives for this material. From Table 1, it is seen that this heat also had the higher ultimate tensile strength of the two heats tested in this material group.

The two heats tested for solution-treated and aged Ti-6Al-4V extrusion had about the same ultimate tensile strength, as seen from Table 1. Table 4 shows that the fatigue strengths of the two heats also were about the same.

The test results thus clearly show that, within a group of specimens, the specimens from the heat with the higher ultimate tensile strength gave the longest real-time fatigue lives.

Based on the log average flights, given in Table 11, the order of the real-time fatigue resistance for the center-notched specimens is as follows:

1. Ti-8Al-1Mo-1V duplex-annealed sheet
2. Ti-8Al-1Mo-1V triplex-annealed sheet
3. Ti-8Al-1Mo-1V mill-annealed sheet
4. Ti-6Al-4V mill-annealed sheet
5. Ti-6Al-4V solution-treated and aged extrusion
6. Ti-8Al-1Mo-1V mill-annealed extrusion.

However, since some specimens did not fail during real-time testing, it is difficult to establish a relative rating for the materials 2 through 5. For different material heats, specimen configuration, and test conditions, the real-time fatigue resistance of duplex-annealed Ti-8Al-1Mo-1V sheet was found generally to be less than that of annealed Ti-6Al-4V sheet (Refs. 7 and 30).

The ultimate tensile strengths of the duplex-annealed Ti-8Al-1Mo-1V sheet heats reported in Reference 7 are of the order given for this material in Table 1. However, the ultimate tensile strength for annealed Ti-6Al-4V sheet reported in Reference 7 is 1034 MPa (150 ksi), which is higher than for the heats tested in this program (see Table 1). This could explain the relatively higher fatigue lives reported in Reference 7. Allowing for scatter, it thus appears that the real-time fatigue resistance of mill-annealed Ti-6Al-4V sheet is comparable to that of duplex-annealed Ti-8Al-1Mo-1V sheet.

The above relative order of fatigue resistance would not have been predicted by any of the three accelerated fatigue testing methods, as seen from Table 11. Thus, all three accelerated fatigue test methods are unreliable for titanium material selection for supersonic cruise aircraft structure.

Accelerated Testing

The fatigue testing of a supersonic cruise aircraft (Mach 2.7 to Mach 3.0) will be very complex and expensive, unless a way can be found to simplify and accelerate the testing. For supersonic flying at Mach 2.7, the wing stagnation temperature will be about 533 K (500 ^{o}F) (Refs. 16 and 27). The Concorde, a supersonic cruise aircraft developed jointly by the British and French, flies at about Mach 2.0, and the skin temperatures vary from about 373 K (212 ^{o}F) to about 253 K (-4 ^{o}F) (Ref. 36). In the laboratory, a full-scale fatigue test article, weighing about 1 MN (120 tons) including simulated fuel, is being heated and cooled during each test cycle.

Reference 37 deals with the development of a general test time compression method applicable to a wide range of supersonic aircraft and the planning of a test program to substantiate that method.

Center-notched duplex-annealed Ti-8Al-1Mo-1V sheet specimens were fatigue tested to check various parts of this test time compression method (Ref. 15). In these tests, true GAG cycles were not applied. Accelerated testing at room temperature gave lives about 1.5 times the real-time fatigue lives at Mach 3.2 temperatures. Creep did not affect the fatigue lives up to Mach 3.2 temperatures. Cycle replacement was found to be unreliable. Multiflight techniques, i.e., grouping of flights within the temperature profile for one flight, gave too long fatigue lives. The fatigue lives were highest for the tests with the highest number of flights grouped together.

For complex structures, the cycle replacement technique is not valid since the effect of A cycles at one magnitude cannot be represented by B cycles of another higher magnitude at all critical points.

References 7, 30, 32, and 38 deal with accelerated flight-by-flight testing and real-time testing of center-notched coupon specimens. For duplex-annealed Ti-8Al-1Mo-1V sheet, annealed Ti-6Al-4V sheet, and solution-treated and aged Ti-6Al-4V sheet, it was shown that the fatigue lives for accelerated testing at room temperatures were about twice the fatigue lives for accelerated testing at 561 K (550 ^{o}F). The real-time test lives were generally between the accelerated test lives at 561 K (550 ^{o}F) and the room temperature test lives.

From Figures 18 through 24, for the Lockheed results, the sheet fatigue lives for accelerated testing at room temperature were about twice the fatigue lives for accelerated testing at 533 K (500 ^{o}F). However, with the exception of the triplex-annealed Ti-8Al-1Mo-1V, all the log average real-time test lives for sheet were longer than the accelerated test lives at both 533 K (500 ^{o}F) and room temperature.

Systematic simplification of tests, produced by omitting stress cycles, produced systematically longer lives (Ref. 7). Thus, test load simplification may give unrepresentative lives.

Table 11 shows that accelerated flight-by-flight testing at room temperature gave too long fatigue lives for triplex-annealed Ti-8Al-1Mo-1V sheet, mill-annealed Ti-8Al-1Mo-1V extrusion, and solution-treated and aged Ti-6Al-4V extrusion, as compared to the real-time fatigue test lives. The accelerated testing at room temperature was thus unconservative for these materials.

Table 11 also shows that accelerated testing at a constant elevated temperature of 533 K (500 ^{o}F) gave conservative test results for all groups of materials, as compared to the real-time fatigue test lives. The conservative factor was about 2 to 3.

For accelerated testing at cyclic temperatures of 305 to 533 K (90 to 500 °F), unconservative results were obtained for mill-annealed and triplex-annealed Ti-8Al-1Mo-1V sheets, and for mill-annealed Ti-8Al-1Mo-1V extrusion, as compared to the real-time fatigue test lives, as shown in Table 11.

For duplex-annealed Ti-8Al-1Mo-1V sheet, and mill-annealed Ti-6Al-4V sheet, Table 11 shows that all the accelerated testing methods gave conservative test results, as compared to the real-time fatigue test lives. Of the materials tested, these two materials are also the most likely candidates for supersonic cruise aircraft wing skins. It has been discussed earlier that other test programs have shown that the accelerated flight-by-flight testing at room temperature gave longer test lives than the real-time testing for both these materials (Refs. 7, 30, and 38). It thus appears that the test results are affected by the material heats, specimen configuration, and/or the test conditions.

Duplex-annealed Ti-8Al-1Mo-1V sheet gave longer test lives than mill-annealed Ti-6Al-4V sheet for both accelerated and real-time testing (see Table 11). However, References 7 and 30 indicate that, for different material heats, specimen configurations, and test conditions, the accelerated test lives (room temperature and 561 K (550 °F)) for duplex-annealed Ti-8Al-1Mo-1V sheet tended to be higher than for annealed Ti-6Al-4V sheet, whereas for real-time testing the Ti-8Al-1Mo-1V sheet tended to give lower lives than the Ti-6Al-4V sheet.

Most titanium specimens subjected to real-time testing have been simple coupon specimens. However, built-up skin-stiffener specimens made from annealed Ti-6Al-4V sheet have been tested with accelerated flight-by-flight loads and cyclic temperatures (Ref. 39). Additional specimens were tested at room temperature to accelerated flight-by-flight loads. Specimens which had been presoaked at 561 K (550 °F) for 500 hours gave good correlation with the baseline specimens. Accelerated tests on specimens which had not been presoaked gave too long lives as compared to the baseline test specimens.

Accelerated fatigue tests on riveted and spotwelded specimens made of triplex-annealed Ti-8Al-1Mo-1V sheet, using block loading spectra which included cruise temperature of 561 K (550 °F), showed that the riveted specimens had much longer lives than the spotwelded specimen (Ref. 40). Constant amplitude tests at room temperature and at 561 K (550 °F) showed similar fatigue lives for both types of specimen.

Crack Propagation

The available crack propagation records are given in Tables 5 through 10.

The number of crack propagation flights for each specimen can be seen from Table 4, which summarizes all test results. From Table 4, it is seen

that the crack in mill-annealed Ti-8Al-1Mo-1V sheet specimen ET-9 propagated from 2.03 mm (0.08 inch) to complete failure in only 427 real-time flights. The slowest crack propagation was exhibited by mill-annealed Ti-6Al-4V sheet specimen DT-9, whose crack only grew from 2.03 mm (0.08 inch) to 4.83 mm (0.19 inch) in 11 562 real-time flights. This specimen was failed in static tension at the end of the real-time testing. Four mill-annealed Ti-8Al-1Mo-1V specimens failed completely during the real-time testing without a crack being detected. These failures are discussed under Residual Strength.

Table 4 also shows that during the accelerated testing of the duplex-annealed Ti-8Al-1Mo-1V sheet specimens with single spotweld, four specimens failed completely without a crack having been observed. This could have been due to high crack propagation rates or due to low residual strength. The stresses applied to these specimens were only 83 percent of the net area stresses applied to the center-notched specimens.

Spotwelds have also produced relatively high crack propagation rates in triplex-annealed Ti-8Al-1Mo-1V sheet (Ref. 40). For riveted and spotwelded specimens tested to accelerated block spectrum loading with maximum temperature of 561 K (550 ^{o}F), the crack propagation rates in the spotwelded specimens were as much as four times the rates given when testing the riveted specimens.

The crack propagation rates for constant amplitude testing did not change appreciably at 561 K (550 ^{o}F), as compared to room temperature, for duplex-annealed and triplex-annealed Ti-8Al-1Mo-1V sheets, and annealed Ti-6Al-4V sheet (Refs. 10, 41, and 42). The duplex-annealed and triplex-annealed Ti-8Al-1Mo-1V sheets had about the same crack growth rates. The annealed Ti-6Al-4V sheet had higher crack growth rates than the other two materials.

Triplex-annealed Ti-8Al-1Mo-1V sheet specimens which had been subjected to a steady stress of 172 MPa (25 ksi) at 561 K (550 ^{o}F), for 8000 hours showed only slight increases in the crack growth rates as compared to room temperature crack growth rates for constant amplitude testing (Ref. 20).

The crack growth rates for duplex-annealed Ti-8Al-1Mo-1V sheet for constant amplitude testing were more than doubled due to soaking with sea water at room temperture (Ref. 19). Alternate sea water and thermal soaking at 561 K (550 ^{o}F) gave similar results, indicating that the elevated temperature did not have any appreciable added effect as compared to the sea water.

Calculated crack growth rates for duplex-annealed Ti-8Al-1Mo-1V sheet on the basis of available data, were found to be slower than the experimental rates (Ref. 43). The calculated rates agreed well for accelerated flight-by-flight testing at room temperature, but were not accurate for accelerated flight-by-flight testing at 561 K (550 ^{o}F), and were even less accurate for real-time testing.

Test Scatter

Table 14 gives the normal standard deviations corresponding to the log average test flights given in Table 11. Additional normal standard deviations have been given for the real-time test groups with specimens which were unfailed at the end of the real-time testing. For the unfailed specimens, the accelerated test flights at room temperature (see Table 4) were added to the real-time test flights. In all calculations, the flights to first seen crack have been used when available; if not available, the flights to complete failure have been used.

Titanium alloys appeared to exhibit more scatter than both steel and aluminum alloys (Ref. 44). However, based on more testing, as yet unpublished Lockheed data indicate that the titanium alloy scatter is between those of aluminum and steel alloys. Thus, unless the selected titanium alloys, and the processes they are subjected to, can be refined to reduce the fatigue life scatter, a larger scatter factor may be required for titanium alloys than for aluminum alloys.

Summary of Discussions

The significance of the data from the reported real-time program, and the referenced data from the literature, is summarized below for: material selection, structural fabrication, fatigue resistance of supersonic cruise aircraft structure, and fatigue test acceleration procedures for supersonic cruise aircraft.

Material selection. - Reductions in the ultimate tensile strengths at elevated temperatures vary from about 14 to 28 percent, and long exposures at 561 K (550 °F) do not appreciably affect the ultimate tensile strengths of the titanium sheet materials. The effects on titanium extrusion materials are not known.

Mill-annealed Ti-8Al-1Mo-1V sheet is very sensitive to delayed failure at low tensile stresses after a crack has formed. This material is also very susceptible to salt stress corrosion. Further, edge-notched specimens of annealed Ti-8Al-1Mo-1V sheet showed an appreciable fatigue life reduction with exposure up to one year at 561 K (550 °F). Mill-annealed Ti-8Al-1Mo-1V sheet thus seems unsuitable for main load carrying supersonic cruise aircraft structure.

Duplex-annealed Ti-8Al-1Mo-1V sheet has the highest residual strength of the sheet materials in this program. However, the material is very susceptible to salt stress corrosion, and outdoor testing at 561 K (550 °F) greatly reduces the fatigue lives. Duplex-annealed Ti-8Al-1Mo-1V sheet thus appears not to be suitable for main load carrying supersonic cruise aircraft structure unless a protective treatment, which does not reduce the fatigue strength, can be found.

Triplex-annealed Ti-8Al-1Mo-1V sheet has a high real-time fatigue strength. However, if it is as susceptible to salt stress corrosion as mill-annealed and duplex-annealed Ti-8Al-1Mo-1V sheets, it may not be suitable for main load carrying supersonic cruise aircraft structure.

Mill-annealed Ti-8Al-1Mo-1V extrusion may, for some heats, be as notch sensitive as the sheet form of this material. The material may therefore not be suitable for main load carrying supersonic cruise aircraft structure.

Mill-annealed Ti-6Al-4V sheet is not very sensitive to salt stress corrosion, and is virtually unaffected by the environment when fatigue tested outdoors at 561 K (550 ^{o}F). Allowing for scatter, it appears that the real-time fatigue resistance of mill-annealed Ti-6Al-4V sheet is comparable to that of duplex-annealed Ti-8Al-1Mo-1V sheet. Thus, on the basis of the discussed data, mill-annealed Ti-6Al-4V sheet appears to be the most suitable sheet material, of those included in this program, for use in main load carrying supersonic cruise aircraft structure.

Solution-treated and aged Ti-6Al-4V extrusion is the better of the two extrusion materials tested. However, salt stress corrosion data are needed on this material before it is selected for use in main load carrying supersonic cruise aircraft structure.

The three methods of accelerated testing are not reliable for material selection purposes, as seen from the results of this real-time test program. The mill-annealed Ti-8Al-1Mo-1V extrusion had a real-time life of only about a third of that of duplex-annealed Ti-8Al-1Mo-1V sheet. However, on the basis of accelerated testing at room temperature, the two materials would have been considered equivalent.

Also, on the basis of accelerated testing at 533 K (500 ^{o}F), duplex-annealed Ti-8Al-1Mo-1V sheet would appear to be only slightly better than mill-annealed Ti-8Al-1Mo-1V extrusion. Further, accelerated testing with cyclic temperature from 305 to 533 K (90 to 500 ^{o}F) would make mill-annealed Ti-8Al-1Mo-1V extrusion appear superior to duplex-annealed Ti-8Al-1Mo-1V sheet. Thus, accelerated testing for titanium material selection, for supersonic cruise aircraft structure, can give very misleading results.

Structural fabrication. - The ultimate tensile strengths of spotwelds in annealed Ti-8Al-1Mo-1V and annealed Ti-6Al-4V sheets decrease with exposure time at 561 K (550 ^{o}F). Spotwelded triplex-annealed Ti-8Al-1Mo-1V sheet specimens produced much shorter fatigue lives than riveted specimens at 561 K (550 ^{o}F). The spotwelded specimens also had four times as high crack propagation rates as the riveted specimens. Spotwelding should, therefore, be used with great care in supersonic cruise aircraft structure.

The beneficial effects of cold working are rapidly lost at 561 K (550 ^{o}F). Thus, cold working can not be used for providing fatigue life improvements for supersonic cruise aircraft structures.

Annealed titanium material is generally preferred, over solution-treated and aged material, for ease of fabrication (Ref. 45). At the surface of titanium alloys, scale and/or "alpha case" is formed which is brittle and lowers the fatigue strength. The surface layer may range from 0.051 to 0.762 mm (0.002 to 0.030 inch) thick, and must be removed by machining all raw forgings, extrusions, bars, and plates (Ref. 45). Machining or chemical removal is also required after heat treating and hot forming.

Fatigue resistance of supersonic cruise aircraft structure. - All the specimens tested in this program were small coupon specimens. It is not possible to determine the fatigue resistance of supersonic cruise aircraft structure on the basis of these specimen results, nor on the basis of the discussed data from the literature. There is not yet a reliable method available for evaluating the fatigue resistance of supersonic cruise aircraft structure, allowing for temperature degrading and thermally induced stresses, based on coupon specimen test results.

Fatigue test programs using built-up structures are required to assist in the development of reliable fatigue strength evaluation methods for supersonic cruise aircraft.

Further, unless the selected titanium alloys, and the processes they are subjected to, can be refined to reduce the fatigue life scatter, a larger scatter factor may be required for titanium alloys than for aluminum alloys.

Fatigue test acceleration procedures for supersonic cruise aircraft. - The longest flight condition in a supersonic flight is the cruise condition at elevated temperatures. This exposure period does not appreciably affect the vital characteristics of the titanium materials which are possible candidates for use in main load carrying structure, with the exception of salt stress corrosion.

Creep is not considered to be a problem for titanium alloys at 561 K (550 ^{o}F).

Exposures of up to 30 000 hours without stress had little effect on the ultimate tensile strengths of duplex-annealed Ti-8Al-1Mo-1V sheet and annealed Ti-6Al-4V sheet.

The residual strengths of titanium alloys appear to be less affected by elevated temperatures than do their ultimate tensile strengths.

Exposure at 561 K (550 ^{o}F) for up to three years did not significantly affect the constant amplitude fatigue strengths of notched and unnotched specimens made of duplex-annealed Ti-8Al-1Mo-1V sheet and annealed Ti-6Al-4V sheet.

The crack propagation rates for duplex-annealed and triplex-annealed Ti-8Al-1Mo-1V sheets, and annealed Ti-6Al-4V sheet are not appreciably

affected by increasing the temperature from room temperature to 561 K (550 ^{o}F). Triplex-annealed Ti-8Al-1Mo-1V sheet showed only slight increases in crack growth rates after having been subjected to a steady stress for almost a year at 561 K (550 ^{o}F). In this program, triplex-annealed Ti-8Al-1Mo-1V sheet and mill-annealed Ti-6Al-4V sheet both gave similar, relatively slow, crack growth rates. It is therefore expected that the mill-annealed Ti-6Al-4V sheet crack growth rates are not more affected by exposure than those of triplex-annealed Ti-8Al-1Mo-1V sheet.

It thus appears that the heating time can be greatly shortened. Any slight detrimental effects, not covered on a test with shortened heating time, should be allowed for by a factor on the allowable design stresses or the test loads. The applied loads at the elevated temperature can be applied at accelerated rates, as can the applied loads at the ambient temperatures.

The amount of shortening of the flight-by-flight testing with representative heating will depend on the heat exchange characteristics of the tested structure, and the practical rates of heating and cooling of the test specimen.

Too little data are available to determine if the thermal stresses can be adequately represented by applied loads. Temperature soaking and allowing for thermal stress effects is promising, but too few specimens have been tested to be able to rely on this approach. Stresses are induced due to temperature differentials between the external and internal aircraft structure during climb and descent. Thermal stresses are also induced where materials of different coefficients of thermal expansion are restraining each other. These induced stresses are superimposed on the stresses from the externally applied flight loads. Thus, representative testing of a full-scale supersonic cruise aircraft assembly at room temperature, or at a constant elevated temperature, would not be strictly correct. All the induced effects due to heating and cooling would then not be accounted for. To cover these uncertainties by increased loads would tend to overload some areas of the assembly.

The fatigue test loading spectrum can be simplified by eliminating extremely low stress levels. However, an adequate number of cycles must be included to produce representative fretting at all critical joints.

Substitution of a few cycles of high loads to replace many cycles of low value loads will not give representative structural responses at all critical areas. Further, to use cumulative fatigue damage calculations to evaluate the equivalent number of load cycles for the substitution, partly defeats the object of the test; namely, to verify the assumptions made in sizing the structure for fatigue, including the imprecise cumulative damage assumptions.

CONCLUSIONS

The reported real-time testing program was undertaken to investigate the accuracy of three accelerated flight-by-flight test methods for material selection, and fatigue substantiation for supersonic cruise aircraft structure.

The real-time stresses and temperatures applied to the specimens were representative of the service conditions in the lower surface of a Mach 2.7 supersonic cruise aircraft wing root structure. Each real-time flight lasted about 65 minutes, including about one hour at 533 K (500 ^{o}F) in the cruise condition.

Center-notched coupon specimens from six titanium materials were tested: mill-annealed, duplex-annealed, and triplex-annealed Ti-8Al-1Mo-1V sheets; mill-annealed Ti-8Al-1Mo-1V extrusion; mill-annealed Ti-6Al-4V sheet; and solution-treated and aged Ti-6Al-4V extrusion. For duplex-annealed Ti-8Al-1Mo-1V sheet, specimens with a single spotweld were also tested.

The test results were studied in conjunction with other related data from the literature, for material selection, structural fabrication, fatigue resistance of supersonic cruise aircraft structure; and fatigue test acceleration procedures for supersonic cruise aircraft. The overall conclusions drawn are:

1. Mill-annealed Ti-6Al-4V sheet appears to be the most suitable sheet material, of those included in this program, for use in main load carrying supersonic cruise aircraft structure; because it is not very sensitive to salt stress corrosion, it is virtually unaffected by the environment when fatigue tested outdoors, and its real-time fatigue resistance appears to be comparable to that of duplex-annealed Ti-8Al-1Mo-1V sheet.

2. Duplex-annealed Ti-8Al-1Mo-1V sheet had the highest fatigue resistance in this program, but a protective treatment against salt stress corrosion appears to be required before it can be safely used for main load carrying supersonic cruise aircraft structure.

3. Mill-annealed Ti-8Al-1Mo-1V sheet and extrusion should not be used for supersonic cruise aircraft structure. Mill-annealed Ti-8Al-1Mo-1V sheet is very sensitive to delayed failure at low tensile stresses after a crack has formed. Mill-annealed Ti-8Al-1Mo-1V extrusion may also be very notch sensitive; further data are required before it can be determined if this material can safely be used.

4. Salt stress corrosion data are required before determining if triplex-annealed Ti-8Al-1Mo-1V sheet, and solution-treated and aged Ti-6Al-4V extrusion are suitable for supersonic cruise aircraft structure.

5. The accelerated flight-by-flight fatigue testing methods (at room temperature, at a constant temperature of 533 K (500 °F), and with cyclic temperatures 305 to 533 K (90 to 500 °F)) are unreliable for titanium material selection for supersonic cruise aircraft structure.

6. Spotwelding should not be used in primary structure on supersonic cruise aircraft unless better spotwelding techniques are developed, because spotwelded specimens appear to produce shorter fatigue lives and higher crack propagation rates than riveted specimens when subjected to elevated temperatures of 561 K (550 °F).

7. Cold working cannot be relied on for providing fatigue life improvements for supersonic cruise aircraft structure, because the beneficial effects of cold working are rapidly lost at 561 K (550 °F).

8. Fatigue tests of built-up structures are required to assist in the development of reliable fatigue strength evaluation methods for supersonic cruise aircraft structure.

9. Further studies are required to determine if a larger scatter factor is required for titanium alloys than for aluminum alloys.

10. For fatigue testing of supersonic cruise aircraft assemblies, it appears that the heating time can be greatly shortened. The amount of shortening of the flight-by-flight testing with representative heating will depend on the heat exchange characteristics of the tested structure, and the practical rates of heating and cooling of the test specimen.

11. Too little data are available to determine if the thermal stresses can be adequately represented by applied loads.

12. In the simplification of the fatigue test loading spectra, sufficient loading cycles must be included to produce representative fretting at critical joints.

Conclusions 4, 7, 8, 9, 11, and 12 are based primarily on the literature.

Lockheed-California Company,
Lockheed Aircraft Corporation,
Burbank, California, September 27, 1976.

APPENDIX A

CONVERSION OF THE INTERNATIONAL SYSTEM OF UNITS TO U.S. CUSTOMARY UNITS

The International System of Units (SI) is the system of units of measurement which has been adopted by the principal industrial nations of the world. The conversion factors for the units used in this report were obtained from Reference 46, and are given in the following table:

Physical Quantity	SI Unit	Conversion Factor (a)	U.S. Customary Unit (b)
Frequency	Hertz (Hz)	1.0	cps
Force	Newtons (N)	0.224809	lbf
Length	Meters (m)	39.3701	in.
Stress	Newtons/meter^2 (N/m^2) or (Pascal (Pa))	1.450377×10^{-7}	ksi = 1000 lbf/in^2
Power	Watts (W)	0.001340	hp
Temperature	Kelvin (K)	$^oF = 9/5\ (K-255.37)$	^oF

Notes: (a) Multiply value given in SI units by the conversion factor to obtain the equivalent value in the U.S. Customary Units or apply the conversion formula.

(b) For the abbreviations used, see ABBREVIATIONS AND SYMBOLS.

Prefixes used to indicate multiples of SI units are as follows:

Prefix	Multiple
nano (n)	10^{-9}
milli (m)	10^{-3}
centi (c)	10^{-2}
kilo (k)	10^3
mega (M)	10^6

APPENDIX B

METALLURGICAL ANALYSES OF MILL-ANNEALED Ti-8Al-1Mo-1V EXTRUSION SPECIMENS

CONTENTS

APPENDIX B

METALLURGICAL ANALYSES OF MILL-ANNEALED Ti-8Al-1Mo-1V EXTRUSION SPECIMENS

This appendix presents the results of the metallurgical analyses of failed mill-annealed Ti-8Al-1Mo-1V extrusion specimens. The failed specimens subjected to metallurgical analyses are listed in Table 15 in alphanumerical specimen number order.

The first five mill-annealed Ti-8Al-1Mo-1V extrusion real-time specimens to fail were metallurgically analyzed to varying degrees. The first real-time specimen to fail was mill-annealed Ti-8Al-1Mo-1V extrusion specimen H-3. This specimen was extensively analyzed to see if the fatigue life was abnormally short because of some unexpected condition of the material. Mill-annealed Ti-8Al-1Mo-1V extrusion specimens which had failed during accelerated testing were also metallurgically analyzed for comparison with the real-time specimens.

All specimens subjected to real-time testing and accelerated testing at elevated temperatures at 533 K (500 °F) displayed a straw, gold or brown color on the fatigue cracked portions of the fracture surfaces. The colors resulted from oxidation of the fatigue surfaces at the high test temperature as the cracks developed. Rapid failures occurred over the remainders of the specimen widths. The delineations between the short colored fatigue crack areas and the rapid failure areas were very marked. Delineations are indicated by arrows in the photomacrographs of metallurgically analyzed real-time specimens (Figures 15b-15e (and 16b)). During the microfractographic analyses, repeated replications of the colored regions did not remove the colors, indicating that adherent oxide films were present.

The external surfaces of most specimens exhibited evidence of slight oxidation (brown or straw color), usually associated with exposure at temperatures of 505-561 K (450-550 °F). Areas near the holes exhibited a blue or purple color indicating somewhat higher exposure temperatures (589-616 K (600-650 °F)). A short exposure to these temperatures will produce the blue or purple color. However, long exposure at temperatures below 589 K (600 °F) can also produce these colors, especially if the specimens have been touched by hand. The discoloration was very slight on many of the specimens. The thickness of the oxide layer was very small on all the discolored specimens. Thus, the discoloration comes off very easily.

The microfractographic analyses of the fatigue crack areas of real-time specimens G-1 and H-3, and specimen HL-10, which had been subjected to accelerated testing at cyclic temperatures of 305-533 K (90-500 °F) indicated predominantly fatigue striations interrupted by cleavage steps. Also, the fatigue crack areas of specimen HL-9, which had been subjected to accelerated testing at a constant temperature of 533 K (500 °F), exhibited some areas of fatigue striations interrupted by cleavage steps. Specimen

GL-10, which had been subjected to accelerated testing at room temperature (305 K (90 °F)), exhibited the more conventional fatigue striations without interruptions.

Fatigue striations interrupted by cleavage steps may suggest embrittlement. However, the overload sections of specimens G-1, GL-10, H-3, HL-9, and HL-10 all showed dimpled failure modes, indicating a ductile failure. In the overload section of specimen H-3, some cleavage-type fractures were apparent. However, no evidence of Ti_3Al was found in this specimen, nor in any other specimen subjected to x-ray diffraction analysis. Thus, the mill-annealed Ti-8Al-1Mo-1V extrusion material did not appear to be embrittled due to the elevated temperature exposure.

Under microfractographic analysis, it is not unusual to identify various fracture modes, i.e., fatigue striations, fatigue striations interrupted by cleavage steps, fatigue striations with tear ridges, cleavage fracture, and dimple rupture, etc. In the individual analysis, the predominant fracture mode has been indicated.

Methods of Metallurgical Analyses

The metallurgical analyses methods used for the analyses of failed test specimens are briefly described below.

Visual examination. - The specimens were neither sectioned nor polished for the visual examination. The external surfaces were examined with the unaided eye. Also, for some specimens, the fracture surfaces were examined with a binocular microscope at magnifications up to 50 times.

Macrostructural examination. - Samples were cut from both strained and unstrained areas of the specimens for macrostructural examination. The samples were mounted in plastic and polished. The polished samples were then macroetched in order to reveal any gross defects, segregation, or banding that might be present. The macroetched samples were examined with the aid of a binocular microscope at magnifications up to 50 times.

Microstructural examination. - Samples were cut from both strained and unstrained areas of the specimens for microstructural examination. The samples were mounted in plastic and polished. The polished samples were then microetched and the microstructure was examined at various magnifications of from about 100 times to about 3000 times utilizing a polarized light metallograph. The microstructure was examined for defects and inclusions in the grains and at the grain boundaries, for relative amounts of alpha and beta phases, and for deformation.

Electron microfractography. - Microfractographic analysis was conducted employing a two-stage plastic/carbon replication technique and a transmission electron microscope for observation. The two-stage plastic/carbon replica is prepared by applying a strip of cellulose acetate wetted in acetone to the fracture surface. The strip is allowed to dry, and it is

then pulled from the surface, coated with carbon and shadowed with chromium. The cellulose acetate is then dissolved and the remaining carbon replica is examined in the transmission electron microscope. The resulting images are analyzed and compared with known standards (Ref. 47).

X-ray diffraction analysis. - Samples were cut from both strained and unstrained areas of the specimens. Standard sample thicknesses were examined. Complete x-ray diffraction patterns were obtained on these samples by using a diffraction unit with copper target K-alpha radiation.

X-ray diffraction techniques will reveal texture influences, if present, and, on a submicroscopic level, any order/disorder reaction that may be associated with the material conditions. The diffraction patterns obtained were analyzed in terms of peak position, relative intensity (height basis), and integrated intensity, and compared with known standards (Ref. 48).

Transmission electron microscopy. - Thin foils were obtained from the specimens by using an electropolisher to prepare the specimens. To prepare the thin foil, a bulk sample is cut from the material, mechanically thinned by grinding and successively finer grit paper to a final thickness of about 0.08-0.13 mm (0.003-0.005 inch). The sample is then electrochemically thinned utilizing a twin jet electropolisher until perforation at the jets, which are facing each other. The thin edges of the resulting hole are examined in a transmission electron microscope.

This technique will identify the character of the substructure. The thin foils are taken from material in areas of the specimen that are representative of specific failure modes, and are examined at magnifications up to 40 000 times.

Metallurgical Analysis of Specimen G-1

Specimen G-1 had been subjected to 27 612 real-time flights when two cracks were found. The specimen was failed in static tension.

Visual examination. - The two cracks, one on each side of the center hole, were 3.05 mm (0.12 inch) long and 1.02 mm (0.04 inch) long. Abrupt transitions to the slant type of fracture were evident for both cracks, and these portions extended across the remaining width of the specimen to both outer edges. The fracture surfaces of specimen G-1 were similar to those of other examined specimens of this material.

Electron microfractography. - Specimen G-1 was subjected to an extensive microfractography study. Replicas were taken in seven different areas of the fracture surfaces. The areas were located as follows: (1) and (2) - within each of the two macroscopic fatigue crack regions; (3) - adjacent to the larger fatigue crack; (4) and (5) - approximately mid-length along each slant type portion; and (6) and (7) - at the end of each slant type portion (at the outer edges of the specimen).

Both of the macroscopic fatigue regions exhibited predominantly fatigue striations interrupted by cleavage steps, as shown in Figures 25a and 25b, with some areas of uninterrupted fatigue striations, and some areas of cleavage. The region adjacent to the larger fatigue crack exhibited both dimple rupture and cleavage, as shown in Figures 25c and 25d, respectively. The areas midway along, and at the ends of the slant portions, revealed predominantly well formed dimples of both equiaxed and elongated types, as shown in Figures 25e and 25f, with very few areas of cleavage.

Metallurgical Analysis of Specimen G-3

Specimen G-3 was visually examined only (no sectioning). The specimen had been subjected to 23 470 real-time flights, and a 3.05 mm (0.12 inch) crack had developed at one side of the hole. The specimen was failed in static tension. A photomacrograph showing the fracture surfaces of specimen G-3 is given in Figure 15b. The fracture surfaces of specimen G-3 were similar to those of other examined specimens of this material.

Metallurgical Analysis of Specimen GL-10

Specimen GL-10 had been subjected to 42 800 accelerated flights at room temperature. The center hole was deformed, and the specimen had been classified as nonstandard (Ref. 4). The test result is not included in the comparisons between accelerated and real-time test resuts.

Visual examination. - The specimen had two cracks, one at each side of the center hole. They extended 1.78 mm (0.07 inch) and 3.30 mm (0.13 inch) towards the outer edges of the specimen. Both had progressed through a transition region from a flat fatigue crack type fracture surface into a rougher, slant type of fracture surface oriented approximately 45 degrees to the load axis. All fracture surfaces were clean and showed no oxide coloration.

Electron microfractography - Replicas were obtained for both the macroscopic fatigue regions and the adjacent transition regions to shear mode failures.

The two macroscopic fatigue regions each exhibited numerous areas of well defined fatigue striations, with very little cleavage, as shown in Figures 26a and 26b. In the adjacent transition-to-shear regions, some fatigue striations were present, as shown in Figure 26c. However, these fracture surfaces consisted predominantly of well formed dimples of both the elongated and the equiaxed types, characteristic of a ductile microvoid coalescense process such as is typical for a ductile overload fracture. These features are shown in Figure 26d.

The fatigue crack propagation by the formation of ductile fatigue striations is typical of those seen in alpha/beta titanium alloys fatigue tested at room temperature.

Metallurgical Analysis of Specimen H-1

Specimen H-1 was visually examined only (no sectioning). The specimen had been subjected to 22 956 real-time flights and failed completely during testing. A photomacrograph showing the fracture surfaces of specimen H-1 is given in Figure 15c. The fracture surfaces of specimen H-1 were similar to the fracture surfaces of other examined specimens of this material. This material is usually extruded above the beta transus temperture and the coarse fracture surface is characteristic of the large grain size of the material.

Metallurgical Analysis of Specimen H-2

Specimen H-2 was visually examined only (no sectioning). The specimen had been subjected to 22 725 real-time flights, and failed during an attempted resumption of testing after a five day shutdown period during which the specimen was held under a constant gross area tensile stress of 250 MPa (36.3 ksi) at room temperature. A photomacrograph showing the fracture surfaces of specimen H-2 is given in Figure 15d. The fracture surfaces of specimen H-2 were similar to those of specimen H-1.

Metallurgical Analysis of Specimen H-3

Specimen H-3 was the first real-time specimen to fail; after 19 618 simulated flights had been applied. An overall view of the failed specimen is shown in Figure 27. The specimen failed during an attempted resumption of testing after a shutdown period.

Visual examination. - A photomacrograph showing the fracture surfaces of specimen H-3 is given in Figure 15e. Visual examination of the fracture surfaces revealed that a short fatigue crack had grown from one side of the hole to a length of about 1.27 mm (0.05 inch). Rapid failure had apparently occurred over the remainder of the specimen width. However, unique to specimen H-3, no abrupt transition to a slant type of fracture was present, but rather the flat crack extended (with no discoloration) approximately 12.7 mm (0.5 inch) further towards the outer edge of the specimen. Only within the last 1.78 mm (0.07 inch), very near the specimen's outer edge, did the fracture surface assume the slant type of fracture orientation. The crack on the other side of the center hole, which extended across the whole half section to the outer edge, was entirely of slant type fracture. No portion of it exhibited any discoloration. The flat macroscopic fatigue crack portions were relatively coarse (see Figures 15e, 28a, and 28b) because the grain size resulting from the beta field extrusion process used on the Ti-8Al-1Mo-1V extrusion material is comparatively large (see Figures 29a and 29b), and influences the local microscopic crack path.

A re-evaluation of the hole confirmed the initial evaluation: rough, scored surfaces; raised annular rings; and slightly deformed radius. These

conditions are shown in Figures 28a and 28b. The original evaluation noted that specimen H-3 had a sizable burr on the hole wall. The burr was located, but it was not associated with the fracture surfaces.

Electron microfractography. - Initially replicas were obtained for the oxidized macroscopic fatigue region and the rapid tensile overload region.

The single macroscopic fatigue region exhibited predominantly fatigue striations with occasional striation cracking, as shown in Figure 30a. Similarly, the rapid tensile overload portion exhibited a cleavage rupture mode, as shown in Figure 30b.

Additional replicas were obtained from seven different areas of the fracture surfaces. The areas were located as follows: (1) - within the macroscopic fatigue region; (2) - adjacent to the fatigue region; (3) - midway along the flat fracture surface extending from the fatigue crack; (4) - at the outer edge of the preceding surface where the fracture changed suddenly to a slant type; (5) - at a point approximately 5 mm (0.2 inch) from the center hole on the fracture surface opposite the fatigue crack side; (6) - at a point approximately half-way along the preceding surface; and (7) - at the outer edge of the preceding surface.

The macroscopic fatigue region exhibited many areas of cleavage, as shown in Figures 30c and 30d, many areas of fatigue striations interrupted by cleavage steps, as indicated by Figure 30e, and some areas of uninterrupted fatigue striations, as shown in Figure 30f. The area adjacent to the fatigue region, and the area half-way toward the outer edge both possessed predominantly cleavage-type features, as shown in Figures 30g and 30h respectively. These were intermixed with some dimples, as shown in Figure 30i, and occasionally, near the fatigue crack, an area of fatigue striations, as shown in Figure 30j. Even macrofractographically, this area was unique in that the fracture plane remained normal to the specimen load axis, except at the very outer edge, and it was clean, with no discoloration, except for the fatigue crack portion. The three areas examined on the slant type fracture surface on the opposite side of the center hole all exhibited predominantly dimples of both elongated and equiaxed types, typical for a ductile overload failure, as shown in Figures 30k and 30l, with very little cleavage.

Macrostructural examination. - Specimens H-3, H-8, H-9, H-10, HL-6, and HL-8 were examined together for comparison. For details of the other specimens, see their metallurgical analyses sections and Table 15.

For each fatigue specimen, samples were cut from both the area adjacent to the fatigue crack(s), and in the relatively unstrained grip area, to facilitate a complete comparison. Samples from both areas of each specimen were macroetched in order to reveal any gross defects, segregation, or banding that might be present. No such gross material defects were found in any of the six specimens examined.

Microstructural examination. - Specimens H-3, H-8, H-9, H-10, HL-6, and HL-8 were examined together for comparison. For details of the other specimens, see their metallurgical analyses sections and Table 15.

Microstructural mounts were made for two transverse sections from each fatigue specimen; one from the fatigued area near the notch hole, and the other from the relatively strain free grip area. In each area, for all specimens, a normal microstructure for this material (Ti-8Al-1Mo-1V) and condition was found. A typical microstruture is shown in Figure 29a from the grip area of specimen H-3. In each case, the microstructure consisted of a network of lamellae of transformed product (predominantly alpha with some beta). The large beta grain boundaries were clearly outlined. This is similar to the microstructures shown in Figures 1f and 1g. The samples from the fatigue areas showed regions of highly localized plastic deformation near the fatigue cracks. This was evidenced by pronounced slip lines and offset lamallae, as shown in Figure 29b. This is as expected, since the formation and propagation of a fatigue crack is preceded by the movement of dislocations, and associated localized plastic deformation. A metallographic survey of the samples at high magnification utilizing polarized light was made to ascertain the distribution of the beta phase. No regions of unusual beta segregation were noted.

X-ray diffraction analysis. - Specimens H-3, H-8, H-9, H-10, HL-6, and HL-8 were analyzed together for comparison. For details of the other specimens, see their metallurgical analyses sections and Table 15.

Complete x-ray diffraction patterns were obtained on samples from both the fatigued area and the grip area of each fatigue specimen. The diffraction patterns obtained were analyzed in terms of peak position, relative intensity (height basis), and integrated intensity. In particular, a comparison was made between specimens as to the type and degree of preferred orientation (i.e., texture) of the alpha phase, the presence or absence of the beta phase and the nature of its preferred orientation, and the possible presence of the additional peaks of an ordered precipitate phase (Ti_3Al) known to occur in titanium-aluminum alloy systems. Work at Lockheed-California Company has confirmed the unexpected appearance of this phase in commercially fabricated material. No evidence of Ti_3Al was found in the present study.

All the fatigue specimens submitted were cut from adjacent positions in the same extrusion. In light of this fact, the preferred orientation of the alpha phase showed considerable variation among specimens. The exact nature of the variation could not be ascertained because complete pole figures were not determined for time limitation and cost reasons. In the technique employed herein, variations in preferred orientation were studied by their effect on the relative intensities of the diffraction peaks. It is not believed that the variation in texture by itself was important to the failure of fatigue specimen H-3. Some variation in the amount of the beta phase was observed among the specimens ranging from none, through trace, to slight. Those variations were expected since the accuracy of the determination is poor at low levels. The metallographic examination did not reveal

significant localized concentrations of the beta phase. No evidence of any other phase, e.g. Ti_3Al, was found. However, the presence of Ti_3Al in small amounts is not readily detectable, because of the nature and distribution of the precipitate.

Transmission electron microscopy. - Specimens H-3, H-8, H-9, H-10, HL-6, and HL-8 were analyzed together for comparison. For details of the other specimens, see their metallurgical analyses sections and Table 15.

Thin foils were obtained from several of the fatigue coupons for electron transmission microscopy. An effort was made to find significant differences between the several specimens examined rather than to describe specific features. A general survey of specimen foils failed to reveal any significant differences between the substructures of specimen H-3 and the others examined. Some electron transmission micrographs typical of areas in the specimens examined are shown in Figure 31.

Metallurgical Analysis of Specimen H-8

Specimen H-8 had been subjected to 46 000 acclerated flights at room temperature, and a 3.30 mm (0.13 inch) crack had developed at one side of the center hole.

Together with specimens H-3, H-9, H-10, HL-6, and HL-8, specimen H-8 was subjected to:

- Macrostructural examination
- Microstructural examination
- X-ray diffraction analysis
- Transmission electron microscopy.

For the results of these analyses, see the metallurgical analysis section for specimen H-3.

Metallurgical Analysis of Specimen H-9

Specimen H-9 had been subjected to 15 700 accelerated flights at a constant temperature of 533 K (500 ^{o}F), and had developed two cracks, one on each side of the center hole. One crack was 4.57 mm (0.18 inch) long, the other was 5.08 mm (0.20 inch) long.

The specimen was subjected to the same metallurgical analyses methods as specimen H-8. See the metallurgical analysis section for specimen H-8.

Metallurgical Analysis of Specimen H-10

Specimen H-10 had been subjected to 35 000 accelerated flights at room temperature, and a 6.60 mm (0.26 inch) crack had developed at one side of the center hole.

The specimen was subjected to the same metallurgical analyses methods as specimen H-8. See the metallurgical analysis section for specimen H-8.

Metallurgical Analysis of Specimen HL-6

Specimen HL-6 had been subjected to 11 800 accelerated flights at a constant temperature of 533 K (500 °F), and had developed two cracks, one on each side of the center hole. One crack was 4.06 mm (0.16 inch) long, the other was 5.08 mm (0.20 inch) long.

The specimen was subjected to the same metallurgical analyses methods as specimen H-8. See the metallurgical analysis section for specimen H-8.

Metallurgical Analysis of Specimen HL-8

Specimen HL-8 had been subjected to 67 000 accelerated flights at cyclic temperatures of 305-533 K (90-500 °F), and a 4.57 mm (0.18 inch) crack had developed at one side of the center hole.

The specimen was subjected to the same metallurgical analyses methods as specimen H-8. See the metallurgical analysis section for specimen H-8.

Metallurgical Analysis of Specimen HL-9

Specimen HL-9 had been subjected to 14 000 accelerated flights at a constant temperature of 533 K (500 °F). The center hole was deformed, and the specimen had been classified as nonstandard (Ref. 4). The test result is not included in the comparisons between accelerated and real-time test results.

Visual examination. - The specimen exhibited one macroscopic fatigue crack emanating from the center hole. It also had entered into the transition from a flat to a slant type fracture surface. The fracture opposite the fatigue crack at the center hole consisted entirely of a slant type shear mode failure. The flat, fatigue crack portion extended 1.78 mm (0.07 inch) from the hole. Both slant type fracture regions were clean and showed no discoloration, indicating they had accumulated little time at 533 K (500 °F).

Electron microfractography. - Replicas were obtained for both the macroscopic fatigue region and the adjacent transition region to shear mode failures.

The single macroscopic fatigue region had numerous areas of uninterrupted fatigue striations, some areas of fatigue striations interrupted by cleavage steps, and very little cleavage, as shown in Figures 32a and 32b. In the adjacent final fracture region, well formed dimples, of both elongated and equiaxed types, were the predominant features, as shown in Figures 32c and 32d.

Metallurgical Analysis of Specimen HL-10

Specimen HL-10 had been subjected to 21 000 accelerated flights at cyclic temperatures of 305-533 K (90-500 ^{o}F). The center hole was deformed, and the specimen had been classified as nonstandard (Ref. 4). The test result is not included in the comparisons between accelerated and real-time test results.

Macrostructural examination. - The specimen had one macroscopic fatigue crack, which extended approximately 2.03 mm (0.08 inch), before entering the transition to a slant type fracture surface. The fracture on the opposite side of the center hole from the fatigue crack was entirely of a slant type shear mode failure.

Electron microfractography. - Replicas were obtained for both the macroscopic fatigue region and the adjacent transition region to shear mode failures.

The single macroscopic fatigue region exhibited predominantly fatigue striations interrupted by cleavage steps, with some areas of uninterrupted fatigue striations, and some areas of cleavage, as shown in Figures 33a and 33b. The area adjacent to the fatigue region consisted predominantly of well formed dimples of both elongated and equiaxed types, as shown in Figures 33c and 33d.

REFERENCES

1. McCulloch, A. J.; Melcon, M. A.; and Young, L.: Fatigue Behavior of Sheet Materials for the Supersonic Transport; Volume I - Summary and Analysis of Fatigue and Static Test Data. AFML-TR-64-399, Volume I, U. S. Air Force, Jan. 1965.

2. McCulloch, A. J.; Melcon, M. A.; and Young, L.: Fatigue Behavior of Sheet Materials for the Supersonic Transport; Volume II - Static Test Data, S-N Test Data and S-N Diagrams. AFML-TR-64-399, Volume II, U. S. Air Force, Jan. 1965.

3. Military Specification. Titanium and Titanium Alloy, Sheet, Strip and Plate. MIL-T-9046F, April 1967, and MIL-T-009046G (USAF), Oct. 1970.

4. Fatigue Strength Evaluation of Titanium Materials for the Supersonic Transport Under Flight-by-Flight Loading Spectra. SST-66-2, Federal Aviation Agency, Jan. 1966.

5. Figge, I. E.: Residual Strength of Alloys Potentially Useful in Supersonic Aircraft. NASA TN D-2613, 1965.

6. Metallic Materials and Elements for Aerospace Vehicle Structures. MIL-HDBK-5B, Aug. 1974.

7. Imig, L. A.; and Garrett, L. E.: Fatigue-Test Acceleration with Flight-by-Flight Loading and Heating to Simulate Supersonic-Transport Operation. NASA TN D-7380, 1973.

8. Gideon, D. N.; Marschall, C. W.; Holden, F. C.; and Hyler, W. S.: Exploratory Studies of Mechanical Cycling Fatigue Behavior of Materials for the Supersonic Transport. NASA CR-28, 1964.

9. Determination of Design Data for Heat Treated Titanium Alloy Sheet. ASD-TDR-62-335, Volumes 1-3, U. S. Air Force, Dec. 1962.

10. Hardrath, Herbert F.; and Heimerl, George J.: NASA Research on Materials Applicable to Supersonic Transports. NASA TM X-1013, 1964.

11. Heimerl, George J.; Baucom, Robert M.; Manning, Charles R., Jr.; and Braski, David N.: Stability of Four Titanium-Alloy and Four Stainless-Steel Sheet Materials after Exposures up to 22 000 Hours at 550° F (561° K). NASA TN D-2607, 1965.

12. Illg, Walter; and Castle, Claude B.: Fatigue of Four Stainless Steels and Three Titanium Alloys Before and After Exposure to 550° F (561° K) up to 8800 Hours. NASA TN D-2899, 1965.

13. Pride, Richard A.; Royster, Dick M.; Stein, Bland A.; and Gardner, James E.: Effects of Longtime Environmental Exposure on Mechanical Properties of Sheet Materials for a Supersonic Transport. NASA TN D-4318, 1968.

14. Illg, Walter; and Imig, L. A.: Fatigue of Four Stainless Steels, Four Titanium Alloys, and Two Aluminum Alloys Before and After Exposure to Elevated Temperatures for up to Three Years. NASA TN D-6145, 1971.

15. Dill, H. D.; and Newman, J. A.: Experimental Verification of the Suitability of Compressing the Time of Mission Profile During Elevated Temperature Fatigue Testing. AFFDL-TR-70-113, U. S. Air Force, Feb. 1971.

16. Heimerl, George J.; and Hardrath, Herbert F.: An Assessment of a Titanium Alloy for Supersonic Transport Operations. NASA SP-83, 1965, pp. 215-226.

17. Kuhn, Paul; and Figge, I. E.: Unified Notch-Strength Analysis for Wrought Aluminum Alloys. NASA TN D-1259, 1962.

18. Figge, I. E.: Residual Static Strength of Several Titanium and Stainless-Steel Alloys and One Superalloy at -109° F, 70° F, and 550° F. NASA TN D-2045, 1963.

19. Figge, I. E.; and Hudson, C. Michael: Crack Propagation, Delayed Failure, and Residual Static Strength of Titanium, Aluminum, and Stainless Steel Alloys in Aqueous Environments. NASA TN D-3825, 1967.

20. Healy, M. S.; Marschall, C. W.; Holden, F. C.; and Hyler, W. S.: The Fatigue Behavior of Materials for the Supersonic Transport. NASA CR-215, 1965.

21. Braski, David N.; and Heimerl, George J.: The Relative Susceptibility of Four Commercial Titanium Alloys to Salt Stress Corrosion at 550° F. NASA TN D-2011, 1963.

22. Braski, David N.: Preliminary Investigation of Effect of Environmental Factors on Salt Stress Corrosion Cracking of Ti-8Al-1Mo-1V at Elevated Temperatures. NASA TM X-1048, 1964.

23. Pride, Richard A.; and Woodard, John M.: Salt-Stress-Corrosion Cracking of Residually Stressed Ti-8Al-1Mo-1V Brake-Formed Sheet at 550° F (561° K). NASA TM X-1082, 1965.

24. Dexter, Howard B.: Salt Stress Corrosion of Residually Stressed Ti-8Al-1Mo-1V Alloy Sheet After Exposure at Elevated Temperatures. NASA TN D-3299, 1966.

25. Royster, Dick M.: Hot-Salt-Stress-Corrosion Cracking and Its Effect on Tensile Properties of Ti-8Al-1Mo-1V Titanium-Alloy Sheet. NASA TN D-4674, 1968.

26. Heimerl, G. J.; Braski, D. N.; Royster, D. M.; and Dexter, H. B.: Salt Stress Corrosion of Ti-8Al-1Mo-1V Alloy Sheet at Elevated Temperatures. Stress-Corrosion Cracking of Titanium, Spec. Tech. Publ. No. 397, Amer. Soc. Testing Mater., 1966, pp. 194-214.

27. Doty, Ralph J.: Fatigue Design Procedure for the American SST Prototype. Advanced Approaches to Fatigue Evaluation, NASA SP-309, 1972, pp. 365-403.

28. Stein, Bland A.; Dexter, H. Benson; and Royster, Dick M.: Coatings and Surface Treatments for Longtime Protection of Ti-8Al-1Mo-1V Alloy Sheet from Hot-Salt Stress Corrosion. NASA TN D-4319, 1968.

29. Hardrath, H. F.: Environmental Effects on Fatigue of Structural Materials for a Supersonic Transport. Advanced Testing Techniques, Spec. Tech. Publ. No. 476, Amer. Soc. Testing. Mater., 1970, pp. 79-95.

30. Imig, L. A.: Fatigue of Supersonic Transport Materials Using Simulated Flight-by-Flight Loading. Fatigue at Elevated Temperatures, Spec. Tech. Publ. No. 520, Amer. Soc. Testing Mater., 1973, pp. 264-272.

31. Peterson, John J.: Fatigue Behavior of AM-350 Stainless Steel and Titanium-8Al-1Mo-1V Sheet at Room Temperature, 550° F and 800° F. NASA CR-23, 1964.

32. Imig, L. A.; and Illg, Walter: Fatigue of Notched Ti-8Al-1Mo-1V Titanium Alloy at Room Temperature and 550° F (560° K) with Flight-by-Flight Loading Representative of a Supersonic Transport. NASA TN D-5294, 1969.

33. Imig, L. A.: Effect of Initial Loads and of Moderately Elevated Temperature on the Room-Temperature Fatigue Life of Ti-8Al-1Mo-1V Titanium-Alloy Sheet. NASA TN D-4061, 1967.

34. Phillips, Edward P.: Effect of Outdoor Exposure at Elevated Temperature on the Fatigue Life of Ti-8Al-1Mo-1V Titanium Alloy and AM 350 Stainless Steel Sheet. NASA TN D-5362, 1969.

35. Phillips, Edward P.: Effect of Outdoor Exposure at Ambient and Elevated Temperatures on Fatigue Life of Ti-6Al-4V Titanium Alloy Sheet in the Annealed and the Solution-Treated and Aged Condition. NASA TN D-7540, 1974.

36. Ripley, E. L.: The Philosophy which Underlies the Structural Tests of a Supersonic Transport Aircraft with Particular Attention to the Thermal Cycle. Advanced Approaches to Fatigue Evaluation, NASA SP-309, 1972, pp. 1-91.

37. Study to Determine the Suitability of Compressing the Time of Mission Profile During Elevated Temperature Fatigue Testing on Large or Full Scale Vehicles. FDL-TDR-64-52, U. S. Air Force, Sept. 1964.

38. Imig, L. A.: An Investigation of Fatigue in a Supersonic Transport Operating Environment. Paper No. 700033, Soc. Automot. Eng., Jan. 1970.

39. Watanabe, R. T.: Acceleration of Fatigue Tests for Built-up Titanium Components. NASA CR-2658, 1975.

40. Peterson, John J.: Fatigue Behavior of Ti-8Al-1Mo-1V Sheet in a Simulated Wing Structure Under the Environment of a Supersonic Transport. NASA CR-333, 1965.

41. Hudson, C. Michael: Fatigue-Crack Propagation in Several Titanium and Stainless-Steel Alloys and One Superalloy. NASA TN D-2331, 1964.

42. Hudson, C. Michael: Studies of Fatigue Crack Growth in Alloys Suitable for Elevated-Temperature Applications. NASA TN D-2743, 1965.

43. Imig, L. A.: Crack-Growth in Ti-8Al-1Mo-1V with Real-Time and Accelerated Flight-by-Flight Loading. NASA TM X-72754, 1975.

44. Crichlow, Walter J.; and Lunde, Tjerand: High Cycle Fatigue Properties of Titanium in Aircraft Application. Titanium Science and Technology, Volume 2, R. I. Jaffee and H. M. Burte, eds., Plenum Press, 1973, pp. 1257-1270.

45. Lunde, Tjerand: Fatigue and Stress Corrosion Guidelines. Lockheed-California Company, 1976.

46. Mechtly, E. A.: The International System of Units. NASA SP-7012, 1973.

47. Phillips, A.; Kerlins, V.; and Whiteson, B. V.: Electron Fractography Handbook. ML-TDR-64-416, U.S. Air Force, Jan. 1965.

48. Pearson, W. B.: A Handbook of Lattice Spacings and Structures of Metals and Alloys. Volume 2, Pergamon Press, 1967.

TABLE 1. - STATIC TENSILE PROPERTIES OF THE MATERIALS (ROOM TEMPERATURE)

Titanium Material(a)	Manufacturer	Heat Number	Grain Direction(b)	F_{tu}		F_{ty}		e
				MPa	ksi	MPa	ksi	
Ti-8Al-1Mo-1V Mill-Annealed Sheet	Titanium Metals Corporation of America	D8141	L	1063.9	154.3	1027.3	149.0	13
		D8141	T	1104.5	160.2	1058.3	153.5	15
		D8733	L	1132.1	164.2	1065.9	154.6	15
		D8733	T	1097.0	159.1	1041.1	151.0	14
Ti-8Al-1Mo-1V Duplex-Annealed Sheet (c)	Titanium Metals Corporation of America	D4539	L	1011.5	146.7	930.8	135.0	15
				1039.7	150.8	966.6	140.2	15
				992.8	144.0	908.0	131.7	14
				997.7	144.7	918.4	133.2	15
				998.4	144.8	932.9	135.3	14
				1032.8	149.8	934.2	135.5	13.5
				1021.8	148.2	934.9	135.6	14
				1017.0	147.5	939.1	136.2	15
				1027.3	149.0	950.8	137.9	14
			L	1009.4	146.4	932.2	135.2	14
			T	1020.4	148.0	938.4	136.1	15
				1020.4	148.0	939.1	136.2	15
				1010.1	146.5	934.9	135.6	15
				1020.4	148.0	942.5	136.7	15
				1021.8	148.2	941.8	136.6	15
				1056.3	153.2	966.6	140.2	15
				1062.5	154.1	968.7	140.5	15
				1020.4	148.0	944.6	137.0	15
				1034.2	150.0	953.5	138.3	14
		D4539	T	1034.2	150.0	950.8	137.9	15
Ti-8Al-1Mo-1V Triplex-Annealed Sheet	Titanium Metals Corporation of America	D6512	L	1059.7	153.7	977.0	141.7	15
		D6512	T	1101.8	159.8	1027.3	149.0	13
		D8647	L	1088.0	157.8	996.3	144.5	12
		D8647	T	1014.2	147.1	953.5	138.3	10

TABLE 1. - Concluded

Titanium Material(a)	Manufacturer	Heat Number	Grain Direction(b)	F_{tu}		F_{ty}		e
				MPa	ksi	MPa	ksi	
Ti-8Al-1Mo-1V Mill-Annealed Extrusion (d)	Harvey Aluminum	3093	L	1017.7	147.6	927.3	134.5	13.5
		3227	L	991.5	143.8	911.5	132.2	14.0
Ti-6Al-4V Mill-Annealed Sheet	Titanium Metals Corporation of America	D8103	L	1008.7	146.3	973.5	141.2	12
		D8103	T	1012.2	146.8	957.7	138.9	12
		D8673	L	970.1	140.7	939.8	136.3	12
		D8673	T	987.3	143.2	941.8	136.6	13
Ti-6Al-4V Solution-Treated and Aged Extrusion (d)	Harvey Aluminum	3701	L	1219.0	176.8	1052.8	152.7	7.0
		3712	L	1212.8	175.9	1057.7	153.4	7.0

NOTES: (a) Nominal thickness 1.27 mm (0.050 inch).

(b) L - Longitudinal
T - Transverse

(c) Obtained from Reference 2.

(d) Machined from extrusion to 1.27 mm (0.050 inch) thickness.

TABLE 2. - MILL HISTORIES AND PROCESSES FOR THE TITANIUM ALLOYS AND PRODUCTS TESTED (REF. 4)

Ti-8Al-1Mo-1V Mill-Annealed Sheet (Titanium Metals Corporation of America)
1. Ingot hot forged until 48.3 cm (19 inches) square 2. Ingot reheated 3. Ingot hot forged until 38.1 cm (15 inches) square 4. Ingot ground and forged to 17.8 x 27.9 cm (7 x 11 inches) 5. Ingot ground and forged to 7.3 x 30.5 cm (2-7/8 x 12 inches) bar 6. Bar given ultra-sonic test 7. Bar ground and cut to length 8. Bar pickled and rolled to 1.27 or 1.52 mm (0.050 or 0.060 inch) sheet 9. Sheet annealed; heated to 1061 K ±14 K (1450 °F ± 25 °F) and held 8 hours; furnace cooled at 28 K (50 °F) per hour to below 700 K (800 °F); air cooled; sheet descaled 10. Sheet pickled and scrubbed for uniform color
Ti-8Al-1Mo-1V Duplex-Annealed Sheet (Titanium Metals Corporation of America)
1. to 9. Same as above for mill-annealed sheet 10. Sheet annealed; heated to 1061 K ±14 K (1450 °F ±25 °F) and held 1 hour; air cooled; sheet blasted by grit 11. Sheet pickled and scrubbed for uniform color
Ti-8Al-Mo-1V Triplex-Annealed Sheet (Processed by the Lockheed-California Company from 1.52 mm (0.060 inch) Ti-8Al-1Mo-1V Mill-Annealed Sheet Produced by Titanium Corporation of America)
1. to 10. Same as above for mill-annealed sheet 11. Sheet cleaned and pickled 12. Sheet heated in air to 1283 K ±14 K (1850 °F ±25 °F) and held for 5 minutes; air cooled; heated in air to 1019 K ± 14 K (1375 °F ±25 °F) and held for 15 minutes; air cooled 13. Sheet descaled by vapor blasting 14. Sheet pickled in HNO_3-HF solution to remove 0.13 to 0.15 mm (0.005 to 0.006 inch) thickness from each surface. (Pickling procedure included necessary rinsing and drying cycles)
Ti-8Al-1Mo-1V Mill-Annealed Extrusion (Harvey Aluminum Company)
1. Ingot hot forged to an approximate 15 cm (6-inch) container diameter 2. Billet machined and cut to length for extruding 3. Billet preheated

TABLE 2. - Concluded

4. Glass lubricant applied to billet 5. Billet extruded at 1394 K (2050 °F) for heat 3093 and 1353 K (1975 °F) for heat 3227 6. Extrusion straightened 7. Extrusion heat treated to anneal condition: heated to 1061 K ±14 K (1450 °F ±25 °F) and held 1 hour; furnace cooled to 728 K (850 °F) at a maximum rate of 28 K (50 °F) per hour; air cooled
Ti-6Al-4V Mill-Annealed Sheet (Titanium Corporation of America)
1. to 10. Same as above for Ti-8Al-1Mo-1V mill-annealed sheet except anneal cycle: heated to 991 K ±14 K (1325 °F ± 25 °F) and held 1 hour; furnace cooled at 28 K (50 °F) per hour to below 700 K (800 °F); air cooled
Ti-6Al-4V Solution-Treated and Aged Extrusion (Harvey Aluminum Company)
1. Ingot hot forged to an approximate 15 cm (6-inch) container diameter 2. Billet machined and cut to length for extruding 3. Billet preheated 4. Glass lubricant applied to billet 5. Billet extruded at 1333 K (1940 °F) for heat 3701 and 1347 K (1965 °F) for heat 3712 6. Extrusion straightened 7. Extrusion heat treated to STA condition: heated to 1200 K ±14 K (1700 °F ±25 °F) and held 1 hour; water quenched; heated to 811 K ±14 K (1000 °F ±25 °F) and held 3 hours; air cooled

TABLE 3. - LOADING SPECTRA "C"

$\frac{f_{vary}}{f_{lg_{Ref}}}$	Unit Spectrum (a)	Additional Number if Discrete Cycles of $\frac{f_{vary}}{f_{lg_{Ref}}}$ Applied Every (b)								Total Number of Discrete Loadings in 8×10^4 Flts.
		100 Flights	500 Flights	1000 Flights	5000 Flights	10 000 Flights	20 000 Flights	40 000 Flights	80 000 Flights	
Taxi Spectrum (c)										
0.95	1									80 000
1.05		22	1	1						17 840
1.15		2	2							1 920
1.25			1	1	1	1				264
1.35					2					32
1.45							1			4
Climb Spectrum										
0.15	7									560 000
0.25	2									160 000
0.35		62								49 600
0.45		22								17 600
0.55		7								5 600
0.65			13							2 080
0.75			6							960
0.85			2							320
0.95			1							160
1.05				1						80
1.15					2					32
1.25					1					16
1.35						1				8
1.45							2			8
1.55							1			4
1.65								1	1	3
1.75									1	1
1.85									1	1
1.95									1	1
2.05									1	1
Cruise Spectrum										
0.15	3	80								304 000
0.25		48								38 400
0.35		7								5 600
0.45		1								800
0.55				1	3					128
0.65					1	1				24
0.75							1	1		6
0.85									1	1
0.95									1	1
Descent Spectrum										
0.15	7	75								620 000
0.25	1	30								104 000
0.35		25								20 000
0.45		5	2							4 320
0.55		1	1							960
0.65				3	1					256
0.75				1						80
0.85						3				24
0.95							2	1		10
1.05								2		4
1.15								1		2
1.25									1	1
1.35									1	1

NOTES: (a) Automatically controlled on a flight-by-flight basis.
(b) Manually controlled.
(c) The discrete taxi loadings are applied as negative half cycles below the descent spectrum mean (see Figure 5).
(d) $f_{lg_{Ref}}$ = 172 MPa (25 ksi).

TABLE 4. - TEST RESULTS FOR REAL-TIME TITANIUM SPECIMENS

Specimen Material and Geometry (a)	Heat No.	Specimen No.	Real-Time (b) Flights Applied to		Accelerated Flights Applied to		Size of Fatigue Crack When Detected (f)
			Crack Detection	Complete Failure	Crack Detection	Complete Failure	
1.27 mm (0.050 in.) Ti-8Al-1Mo-1V Sheet (Mill-Annealed); Center-Notched	D8141	ET-4		54 338			No crack seen
	D8141	ET-9	46 364	46 791			0/2.03 mm (0/0.08 in.)
	D8733	FT-15	>65 713 (d)		35 000	36 191	0/4.57 mm (0/0.18 in.)(j)
1.27 mm (0.050 in.) Ti-8Al-1Mo-1V Sheet (Duplex-Annealed); Center-Notched	D4539	192	>66 243 (d)		48 000	50 254	0/2.54 mm (0/0.10 in.)(h)
	D4539	194	>65 784 (d)		24 500	26 499	0/2.29 mm (0/0.09 in.)(h)(k)
	D4539	199	>66 918 (d)		78 500	82 813	0/0.51 mm (0/0.02 in.)(h)(j)
	D4539	215	>66 624 (d)		9400	12 400	0/0.51 mm (0/0.02 in.)(h)
	D4539	216	>67 441 (a)		9000	9653	0/6.10 mm (0/0.24 in.)
	D4539	226	>64 216 (d)		59 000	61 194	0/3.56 mm (0/0.14 in.)(h)
1.27 mm (0.050 in.) Ti-8Al-1Mo-1V Sheet (Duplex-Annealed); Single Spotweld	D4539	33	>65 859 (d)			5000	No crack seen (h)
	D4539	35	59 317	66 702			2.03 mm (0.08 in.)
	D4539	38	>67 441 (d)			35 300	No crack seen
	D4539	39	>67 441 (d)		40 000	44 040	2.54 mm (0.10 in.)
	D4539	41	>67 441 (d)			15 625	No crack seen (k)
	D4539	42	>66 858 (d)			22 200	No crack seen (h)(k)
1.27 mm (0.050 in.) Ti-8Al-1Mo-1V Sheet (Triplex-Annealed); Center-Notched	D8647	AT-1	49 478	58 945			0/0.25 mm (0/0.01 in.)
	D8647	AT-2	65 399	65 713 (e)			0/3.05 mm (0/0.12 in.)
	D6512	BT-1	62 962	65 713 (e)			0/3.56 mm (0/0.14 in.)
1.27 mm (0.050 in.) Ti-8Al-1Mo-1V Extrusion (Mill-Annealed); Center-Notched	3093	G-1	27 612 (c)				1.02/3.05 mm (0.04/0.12 in.) (g)
	3093	G-2	34 810 (c)				0/1.27 mm (0/0.05 in.)
	3093	G-3	23 470 (c)				0/3.05 mm (0/0.12 in.) (g)
	3227	H-1		22 956			No crack seen (g)
	3227	H-2		22 725			No crack seen (g)
	3227	H-3		19 618			No crack seen (g)

TABLE 4. - Concluded

Specimen Material and Geometry (a)	Heat No.	Specimen No.	Real-Time (b) Flights Applied to		Accelerated Flights Applied to		Size of Fatigue Crack When Detected (f)
			Crack Detection	Complete Failure	Crack Detection	Complete Failure	
1.27 mm (0.050 in.) Ti-6Al-4V Sheet (Mill-Annealed); Center-Notched	D8673	CT-3	46 379	53 617			0/0.25 mm (0/0.01 in.)(h)
	D8673	CT-14	22 725 (c)				0/1.52 mm (0/0.06 in.)
	D8673	CT-16	>41 726 (d)		13 000	17 996	0/0.76 mm (0/0.03 in.)(i)
	D8103	DT-4	>64 546 (d)			35 900	No crack seen (h)
	D8103	DT-9	54 151	65 713 (e)			0/2.03 mm (0/0.08 in.)
	D8103	DT-16	>65 713 (d)		32 400	33 100	5.59/5.33 mm (0.22/0.21 in.)(j)
1.27 mm (0.050 in.) Ti-6Al-4V Extrusion (Solution-Treated and Aged); Center-Notched	3701	J-1	57 172	58 195			0/2.03 mm (0/0.08 in.)
	3701	J-2	40 779	42 830			0/1.27 mm (0/0.05 in.)
	3701	J-3	39 062 (c)				0/2.54 mm (0/0.10 in.)
	3712	K-1	53 434	56 720			0/1.52 mm (0/0.06 in.)(h)
	3712	K-2	42 866	45 763			0/3.05 mm (0/0.12 in.)
	3712	K-3	46 354	51 210			0/0.76 mm (0/0.03 in.)

NOTES: (a) For specimen dimensions, see Figure 2.

(b) Prior to 1972, specimens with cracks were taken out of the machine. Starting in 1972, specimens which developed cracks were tested to complete failure.

(c) Testing was stopped, and specimen was failed statically in tension.

(d) Specimen did not crack during real-time testing, and was subjected to accelerated testing.

(e) Specimen did not fail completely during real-time testing. It was failed statically after the real-time testing was stopped (see Table 13).

(f) For center-notched specimens, the table indicates crack lengths on both sides of the hole. Thus, 0/3.05 mm (0/0.12 in.) indicates no crack on one side of the hole and 3.05 mm (0.12 in.) crack on the other side of the hole.

(g) Specimen was subjected to metallurgical analysis. See Appendix B.

(h) Specimen failed at the grip during real-time testing. It was repaired and reinstalled into the program.

(i) Specimen failed at both grips and was for years considered unrepairable. It was repaired with only a small misalignment and reinstalled into the program.

(j) Specimen failed at the grip during accelerated testing. It was repaired and reinstalled into the program.

(k) Specimen slipped at the grips during accelerated testing and was slightly buckled. It was repaired and reinstalled into the program.

TABLE 5. - CRACK PROPAGATION RECORDS FOR MILL-ANNEALED Ti-8Al-1Mo-1V SHEET SPECIMENS

(a) Specimen ET-9

Applied No. of Real-Time Flights	Crack Length (One Side of Hole)	
	mm	in.
46 364	2.03	0.08
46 416	2.03	0.08
46 489	2.29	0.09
46 570	5.08	0.20
46 713	9.91	0.39
46 791	Complete failure	

(b) Specimen FT-15

Applied No. of Accelerated Flights (a)	Crack Length (One Side of Hole)	
	mm	in.
35 000	4.57	0.18
35 700	7.11	0.28
36 000	10.67	0.42
36 160	15.88	0.625
36 191	Complete failure	

NOTE: (a) Specimen FT-15 had been subjected to 65 713 real-time flights prior to the accelerated testing.

TABLE 6. - CRACK PROPAGATION RECORDS FOR DUPLEX-ANNEALED Ti-8Al-1Mo-1V SHEET SPECIMENS WITH CENTER NOTCH

(a) Specimen 192

Applied No. of Accelerated Flights (a)	Crack Length (One Side of Hole)	
	mm	in.
48 000	2.54	0.10
49 000	4.06	0.16
49 500	4.83	0.19
50 000	7.62	0.30
50 254	Complete failure	

(b) Specimen 194

Applied No. of Accelerated Flights (a)	Crack Length (One Side of Hole)	
	mm	in.
24 500	2.29	0.09
24 800	3.05	0.12
25 000	4.06	0.16
25 400	5.08	0.20
25 800	6.10	0.24
26 000	6.86	0.27
26 200	8.13	0.32
26 300	9.14	0.36
26 499	Complete failure	

NOTE: (a) The specimens were subjected to the following numbers of real-time flights prior to accelerated testing:

Specimen 192, 66 243 Real-Time Flights,
Specimen 194, 65 784 Real-Time Flights.

TABLE 6. - Concluded

(c) Specimen 199

Applied No. of Accelerated Flights (a)	Crack Length (One Side of Hole)	
	mm	in.
78 500	0.51	0.02
79 000	1.02	0.04
79 900	1.78	0.07
80 000	2.03	0.08
81 000	2.79	0.11
81 500	3.81	0.15
81 900	4.57	0.18
82 000	5.08	0.20
82 200	5.84	0.23
82 400	6.60	0.26
82 500	7.37	0.29
82 600	8.38	0.33
82 700	10.16	0.40
82 760	15.88	0.625
82 813	Complete failure	

(d) Specimen 215

Applied No. of Accelerated Flights (a)	Crack Length (One Side of Hole)	
	mm	in.
9 400	0.51	0.02
9 800	1.02	0.04
10 000	2.03	0.08
10 300	2.54	0.10
10 800	3.05	0.12
11 000	3.56	0.14
11 300	4.32	0.17
11 500	5.08	0.20
11 700	5.59	0.22
11 800	6.60	0.26
12 000	7.62	0.30
12 100	8.64	0.34
12 200	9.65	0.38
12 300	11.18	0.44
12 350	15.88	0.625
12 400	Complete failure	

(e) Specimen 216

Applied No. of Accelerated Flights (a)	Crack Length (One Side of Hole)	
	mm	in.
9 000	6.10	0.24
9 200	7.62	0.30
9 300	8.64	0.34
9 400	9.65	0.38
9 500	15.88	0.625
9 653	Complete failure	

(f) Specimen 226

Applied No. of Accelerated Flights (a)	Crack Length (One Side of Hole)	
	mm	in.
59 000	3.56	0.14
59 800	5.33	0.21
59 900	5.84	0.23
60 000	6.86	0.27
61 000	9.65	0.38
61 194	Complete failure	

NOTE: (a) The specimens were subjected to the following numbers of real-time flights prior to accelerated testing:

Specimen 199, 66 918 Real-Time Flights,
Specimen 215, 66 624 Real-Time Flights,
Specimen 216, 67 441 Real-Time Flights,
Specimen 226, 64 216 Real-Time Flights.

TABLE 7. - CRACK PROPAGATION RECORDS FOR DUPLEX-ANNEALED Ti-8Al-1Mo-1V SHEET SPECIMENS WITH SINGLE SPOTWELD

(a) Specimen 35

Applied No. of Real-Time Flights	Crack Length		Applied No. of Real-Time Flights	Crack Length	
	mm	in.		mm	in.
59 317	2.03	0.08	64 112	9.14	0.36
59 457	2.79	0.11	64 193	9.14	0.36
59 637	2.79	0.11	64 289	9.65	0.38
59 676	3.05	0.12	63 356	9.65	0.38
60 762	3.05	0.12	64 420	9.91	0.39
60 782	3.30	0.13	64 455	9.91	0.39
60 906	3.56	0.14	64 525	10.16	0.40
61 027	3.56	0.14	64 594	10.67	0.42
61 085	3.81	0.15	64 677	11.68	0.46
61 166	4.06	0.16	64 770	11.68	0.46
61 248	4.32	0.17	64 871	11.94	0.47
61 278	4.32	0.17	64 898	11.94	0.47
61 312	4.57	0.18	64 923	12.45	0.49
61 390	4.83	0.19	65 031	13.21	0.52
61 500	5.08	0.20	65 160	13.21	0.52
62 073	5.08	0.20	65 206	15.75	0.62
62 111	5.59	0.22	65 221	15.75	0.62
62 190	5.59	0.22	65 311	16.00	0.63
62 203	5.84	0.23	65 387	16.00	0.63
62 334	5.84	0.23	65 663	16.51	0.65
62 410	6.10	0.24	65 694	16.76	0.66
62 473	6.10	0.24	65 883	17.02	0.67
62 551	6.35	0.25	65 895	17.78	0.70
63 008	6.35	0.25	66 012	17.78	0.70
63 062	6.60	0.26	66 078	18.03	0.71
63 183	6.86	0.27	66 227	18.03	0.71
63 208	7.11	0.28	63 344	19.56	0.77
63 269	7.11	0.28	66 402	20.32	0.80
63 359	7.37	0.29	66 494	20.83	0.82
63 722	7.37	0.29	66 552	21.08	0.83
63 770	7.62	0.30	66 618	21.34	0.84
63 846	8.64	0.34	66 666	22.35	0.88
64 030	8.64	0.34	66 702	Complete failure	

(b) Specimen 39

Applied No. of Accelerated Flights (a)	Crack Length	
	mm	in.
40 000	2.54	0.10
41 000	3.56	0.14
43 000	6.35	0.25
43 500	8.13	0.32
43 800	12.70	0.50
44 000	20.83	0.82
44 040	Complete failure	

NOTE: (a) Specimen 39 had been subjected to 67 441 Real-Time Flights prior to the accelerated testing.

TABLE 8. - CRACK PROPAGATION RECORDS FOR TRIPLEX-ANNEALED Ti-8Al-1Mo-1V SHEET SPECIMENS

(a) Specimen AT-1

Applied No. of Real-Time Flights	Crack Lengths			
	One Side of Hole		Other Side of Hole	
	mm	in.	mm	in.
49 478	0	0	0.25	0.01
50 228			0.25	0.01
50 387			0.51	0.02
51 409			0.51	0.02
51 598			1.02	0.04
51 689			1.02	0.04
51 870			1.27	0.05
52 027			1.27	0.05
52 212			1.52	0.06
52 588			1.52	0.06
52 644			1.78	0.07
52 890			1.78	0.07
53 120			2.03	0.08
53 409			2.03	0.08
53 732			2.54	0.10
54 097			3.30	0.13
54 338			3.30	0.13
54 427			3.56	0.14
54 521			3.56	0.14
54 563			5.08	0.20
54 684			5.08	0.20
54 734			5.59	0.22
55 926			5.59	0.22
56 092			5.84	0.23
56 191			6.10	0.24
57 349			6.10	0.24
57 437			6.60	0.26
57 589	0	0		
57 729	1.52	0.06		
58 040	1.52	0.06		
58 125	2.03	0.08		
58 204	2.54	0.10		
58 268	2.54	0.10		
58 354	2.79	0.11	6.60	0.26
58 500	3.05	0.12	6.86	0.27
58 547	3.30	0.13	6.86	0.27
58 670	3.56	0.14	7.11	0.28
58 719	3.56	0.14	7.11	0.28
58 833	3.81	0.15	7.37	0.29
58 935	3.81	0.15	7.62	0.30
58 943	4.06	0.16	7.87	0.31
58 945	Complete failure			

(b) Specimen AT-2

Applied No. of Real-Time Flights	Crank Length (One Side of Hole)	
	mm	in.
65 399	3.05	0.12
65 420	3.05	0.12
65 486	3.05	0.12
65 533	3.30	0.13
65 646	3.30	0.13
65 713	3.56	0.14
	Test stopped	

(c) Specimen BT-1

Applied No. of Real-Time Flights	Crank Length (One Side of Hole)	
	mm	in.
62 962	3.56	0.14
63 195	3.56	0.14
63 303	3.81	0.15
63 432	3.81	0.15
63 478	4.32	0.17
63 935	4.32	0.17
63 966	4.57	0.18
64 499	4.57	0.18
64 616	5.08	0.20
64 824	5.08	0.20
64 890	5.33	0.21
65 233	5.33	0.21
65 352	5.84	0.23
65 399	7.11	0.28
65 486	7.11	0.28
65 533	7.62	0.30
65 646	7.62	0.30
65 713	8.89	0.35
	Test stopped	

TABLE 9. - CRACK PROPAGATION RECORDS FOR MILL-ANNEALED Ti-6Al-4V SHEET SPECIMENS

(a) Specimen CT-3

Applied No. of Real-Time Flights	Crack Lengths			
	One Side of Hole		Other Side of Hole	
	mm	in.	mm	in.
46 379	0	0	0.25	0.01
46 501			0.51	0.02
46 710			0.51	0.02
46 834			0.76	0.03
47 199			0.76	0.03
47 299			1.27	0.05
47 603			1.27	0.05
47 778			1.52	0.06
47 941			1.78	0.07
48 005			1.78	0.07
48 101			2.03	0.08
48 767			2.03	0.08
48 910			2.54	0.10
49 142			2.79	0.11
49 276			3.05	0.12
50 500			3.05	0.12
50 596			3.30	0.13
50 631			3.56	0.14
50 841			3.56	0.14
51 006			4.06	0.16
51 121			4.32	0.17
51 302			4.57	0.18
51 644			4.57	0.18
51 771			4.83	0.19
51 862			4.83	0.19
51 934			5.08	0.20
52 026			5.08	0.20
52 076			5.59	0.22
52 551			5.59	0.22
52 841			6.60	0.26
52 970			6.60	0.26
53 070			7.11	0.28
53 164			7.37	0.29
53 320			7.62	0.30
53 460			7.62	0.30
53 529	0	0	8.13	0.32
53 592	3.05	0.12	13.21	0.52
53 617	Complete failure			

TABLE 9. - Concluded

(b) Specimen CT-16

Applied No. of Accelerated Flights (a)	Crack Length (One Side of Hole)	
	mm	in.
13 000	0.76	0.03
13 200	1.27	0.05
13 700	1.78	0.07
14 000	2.54	0.10
14 300	2.54	0.10
14 600	2.54	0.10
14 800	3.05	0.12
14 900	3.30	0.13
15 000	3.56	0.14
15 300	3.56	0.14
15 600	3.81	0.15
15 900	4.06	0.16
16 300	4.57	0.18
16 600	6.10	0.24
17 000	6.60	0.26
17 400	7.62	0.30
17 700	8.64	0.34
17 996	Complete failure	

(c) Specimen DT-9

Applied No. of Real-Time Flights	Crack Length (One Side of Hole)	
	mm	in.
54 151	2.03	0.08
54 338	2.03	0.08
54 427	2.54	0.10
56 023	2.54	0.10
56 092	2.79	0.11
56 191	2.79	0.11
56 226	3.05	0.12
60 823	3.05	0.12
60 920	3.30	0.13
61 280	3.30	0.13
61 334	3.56	0.14
62 302	3.56	0.14
62 384	3.81	0.15
62 866	3.81	0.15
62 949	4.06	0.16
63 195	4.06	0.16
63 303	4.57	0.18
63 432	4.57	0.18
63 478	4.83	0.19
65 713	4.83	0.19
	Test stopped	

(d) Specimen DT-16

Applied No. of Accelerated Flights (a)	Crack Lengths			
	One Side of Hole		Other Side of Hole	
	mm	in.	mm	in.
32 400	5.59	0.22	5.33	0.21
32 500	5.59	0.22	5.84	0.23
32 600	5.59	0.22	6.35	0.25
32 700	5.59	0.22	6.86	0.27
32 800	5.84	0.23	7.62	0.30
33 000	5.84	0.23	8.89	0.35
33 100	Complete failure			

NOTE: (a) Specimens CT-16 and DT-16 were subjected to the following numbers of real-time flights prior to accelerated testing:

Specimen CT-16, 41 726 Real-Time Flights,
Specimen DT-16, 65 713 Real-Time Flights.

TABLE 10. - CRACK PROPAGATION RECORDS FOR SOLUTION-TREATED AND AGED Ti-6Al-4V EXTRUSION SPECIMENS

(a) Specimen J-1

Applied No. of Real-Time Flights	Crack Lengths			
	One Side of Hole		Other Side of Hole	
	mm	in.	mm	in.
57 172	2.03	0.08	0	0
57 485	2.03	0.08	0	0
57 552	2.03	0.08	1.52	0.06
57 589	2.03	0.08	1.52	0.06
57 729	3.30	0.13	2.03	0.08
57 813	3.30	0.13	2.03	0.08
57 909	4.06	0.16	3.05	0.12
57 948	4.06	0.16	3.05	0.12
58 040	4.57	0.18	3.05	0.12
58 125	5.08	0.20	3.30	0.13
58 195	Complete failure			

(b) Specimen J-2

Applied No. of Real-Time Flights	Crack Length (One Side of Hole)	
	mm	in.
40 779	1.27	0.05
40 914	2.54	0.10
41 200	2.79	0.11
41 318	2.79	0.11
41 422	3.05	0.12
41 637	3.30	0.13
41 844	3.81	0.15
41 892	3.81	0.15
41 979	4.06	0.16
42 297	4.57	0.18
42 431	5.08	0.20
42 589	5.33	0.21
42 750	5.84	0.23
42 830	Complete failure	

(c) Specimen K-1

Applied No. of Real-Time Flights	Crack Lengths			
	One Side of Hole		Other Side of Hole	
	mm	in.	mm	in.
53 434	0	0	1.52	0.06
53 545			1.52	0.06
53 621			1.78	0.07
53 736			2.03	0.08
53 913			2.29	0.09
54 093			2.29	0.09
54 293			2.54	0.10
54 502			3.56	0.14
54 797			4.06	0.16
56 030			4.06	0.16
56 120			4.57	0.18
56 187			5.08	0.20
56 260			5.08	0.20
56 327			5.59	0.22
56 455			6.10	0.24
56 561	0	0	6.10	0.24
56 632	1.02	0.04	7.11	0.28
56 720	Complete failure			

TABLE 10. - Concluded

(d) Specimen K-2

Applied No. of Real-Time Flights	Crack Length (One Side of Hole)	
	mm	in.
42 866	3.05	0.12
43 002	3.05	0.12
43 137	3.30	0.13
43 352	3.30	0.13
43 525	3.56	0.14
43 669	3.81	0.15
43 786	4.57	0.18
43 945	5.33	0.21
44 229	5.33	0.21
44 380	5.59	0.22
44 437	5.59	0.22
44 614	6.86	0.27
44 686	7.11	0.28
45 074	7.11	0.28
45 235	7.62	0.30
45 295	7.62	0.30
45 382	8.89	0.35
45 476	9.14	0.36
45 607	9.40	0.37
45 699	9.91	0.39
45 763	Complete failure	

(e) Specimen K-3

Applied No. of Real-Time Flights	Crack Length (One Side of Hole)	
	mm	in.
46 354	0.76	0.03
46 416	1.52	0.06
46 489	1.52	0.06
46 570	1.78	0.07
46 791	1.78	0.07
46 947	2.03	0.08
47 069	2.03	0.08
47 163	2.29	0.09
47 278	2.29	0.09
47 402	2.54	0.10
47 767	2.54	0.10
47 867	3.05	0.12
48 058	3.30	0.13
48 171	3.56	0.14
48 346	4.06	0.16
48 573	4.06	0.16
48 669	4.57	0.18
48 834	5.08	0.20
49 478	5.08	0.20
49 710	5.59	0.22
50 228	5.59	0.22
50 294	6.10	0.24
50 387	7.11	0.28
50 570	7.62	0.30
50 616	7.62	0.30
50 707	8.13	0.32
50 906	8.64	0.34
50 974	8.89	0.35
51 068	9.14	0.36
51 164	9.65	0.38
51 210	Complete failure	

TABLE 11. - LOG AVERAGES OF TEST RESULTS

Type of Specimen	Test Temperature	Log Average of Applied Flights	Ratio: Accelerated / Real-Time	Ratio: Accelerated / Real-Time+Acc.
Ti-8Al-1Mo-1V Mill-Annealed Sheet (f)	Constant Room Temp.	47 342(a)	0.86	0.75
	Constant 533K (500°F)	26 664(a)	0.49	0.42
	Cyclic 305-533K (90-500°F)	59 756(a)	1.09	0.94
	Real-Time	54 909(c)	—	—
	Real-Time+Acc.	63 308(d)	—	—
Ti-8Al-1Mo-1V Duplex-Annealed Sheet (Center-Notched) (b)	Constant Room Temp.	54 272(a)	0.82	0.54
	Constant 533K (500°F)	21 701(a)	0.33	0.21
	Constant 561K (500°F)	17 151(a)	0.26	0.17
	Cyclic 305-533K (90-500°F)	61 579(b)	0.93	0.61
	Cyclic 305-561K (90-550°F)	54 341(a)	0.82	0.54
	Real-Time	66 196(c)	—	—
	Real-Time+Acc.	101 197(d)	—	—
Ti-8Al-1Mo-1V Duplex-Annealed Sheet (Single Spotweld) (f)	Constant Room Temp.	34 204(a)	0.52	0.41
	Constant 533K (500°F)	18 718(a)	0.29	0.23
	Constant 561K (550°F)	14 141(a)	0.22	0.17
	Cyclic 305-533K (90-500°F)	46 292(a)	0.71	0.56
	Cyclic 305-561K (90-550°F)	35 370(a)	0.54	0.43
	Real-Time	65 658(c)	—	—
	Real-Time+Acc.	82 661(d)	—	—
Ti-8Al-1Mo-1V Triplex-Annealed Sheet (f)	Constant Room Temp.	78 857(b)	1.34	—
	Constant 533K (500°F)	31 510(a)	0.54	—
	Cyclic 305-533K (90-500°F)	79 950(b)	1.36	—
	Real-Time	58 842(e)	—	—
Ti-8Al-1Mo-1V Mill-Annealed Extrusion (g)	Constant Room Temp.	55 374(b)	2.24	—
	Constant 533K (500°F)	13 839(a)	0.56	—
	Cyclic 305-533K (90-500°F)	70 270(a)	2.84	—
	Real-Time	24 768(e)	—	—

TABLE 11. - Concluded

Type of Specimen	Test Temperature	Log Average of Applied Flights	Ratio: Accelerated / Real-Time	Ratio: Accelerated / Real-Time+Acc.
Ti-6Al-4V Mill-Annealed Sheet (f)	Constant Room Temp.	28 307(a)	0.61	0.51
	Constant 533K (500°F)	16 656(a)	0.36	0.30
	Cyclic 305-533K (90-500°F)	19 380(a)	0.42	0.35
	Real-Time	46 494(c)	—	—
	Real-Time+Acc.	55 982(d)	—	—
Ti-6Al-4V Solution-Treated and Aged Extrusion (g)	Constant Room Temp.	49 338(b)	1.07	—
	Constant 533K (500°F)	19 555(a)	0.42	—
	Cyclic 305-533K (90-500°F)	31 012(a)	0.67	—
	Real-Time	46 156(e)	—	—

NOTES: (a) Based on test results obtained from Reference 4.

(b) Based on test results obtained from Reference 4, including result(s) from unfailed specimen(s).

(c) Based on real-time flights to crack detection where available, or real-time flights to failure, or flights at the end of real-time testing for specimens which did not fail during real-time testing.

(d) Based on total flights to crack detection where available. Accelerated flights applied to unfailed real-time specimens added to the applied real-time flights.

(e) Based on flights to crack detection where available.

(f) Transverse grain direction (Figure 2).

(g) Longitudinal grain direction (Figure 2).

TABLE 12. - SUMMARY OF ACCELERATED TEST RESULTS AT ROOM TEMPERATURE

Type of Titanium Specimen	From Reference 4			Unfailed Real-Time Specimens		
	Specimen Heat Number	Flights to Crack		Specimen Number	Flights to Crack Detection	Flights to Complete Failure
		Individual Specimen	Log Average			
Ti-8Al-1Mo-1V Mill-Annealed Sheet	D 8141	35 300	47 342	FT-15	35 000	36 191
	D 8141	41 800				
	D 8733	49 700				
	D 8733	68 500				
Ti-8Al-1Mo-1V Duplex-Annealed Sheet, Center-Notched	D 4539	26 500	54 272	192	48 000	50 254
	D 4539	29 500		194	24 500	26 499
	D 4539	41 000		199	78 500	82 813
	D 4539	48 000		215	9 400	12 400
	D 4539	54 340		216	9 000	9 653
	D 4539	56 000		226	59 000	61 194
	D 4539	57 000				
	D 4539	69 000				
	D 4539	75 900				
	D 4539	82 000				
	D 4539	105 000				
Ti-8Al-1Mo-1V Duplex-Annealed Sheet With Spotweld	D 4539	29 000	34 204	33	40 000	5 000
	D 4539	30 000		38		35 300
	D 4539	38 000		39		44 040
	D 4539	41 400		41		15 625
				42		22 200
Ti-6Al-4V Mill-Annealed Sheet	D 8103	32 000	28 307	CT-16	13 000	17 996
	D 8103	39 000		DT-4		35 900
	D 8673	21 000		DT-16	32 400	33 100
	D 8673	24 500				

TABLE 13. - FAILURE STRENGTHS OF CRACKED REAL-TIME SPECIMENS

Specimen	Specimen Width		Crack Length (a)		Specimen Thickness		Failure Load		Net Area Strength	
	mm	in.	mm	in.	mm	in.	N	lbf	MPa	ksi
AT-2 (Ti-8Al-1Mo-1V T.A. Sheet)	39.50	1.555	3.56	0.14	1.23	0.0483	29 892	6720	823.2	119.4
BT-1 (Ti-8Al-1Mo-1V T.A. Sheet)	39.22	1.544	8.13	0.32	1.23	0.0483	25 889	5820	852.9	123.7
CT-14 (Ti-6Al-4V M.A. Sheet)	34.67	1.365	1.52	0.06	1.40	0.0550	33 139	7450	885.3	128.4
DT-9 (Ti-6Al-4V M.A. Sheet)	38.10	1.500	5.08	0.20	1.28	0.0502	27 312	6140	803.2	116.5
G-1 (Ti-8Al-1Mo-1V M.A. Ext.)	36.50	1.437	4.06	0.16	1.30	0.0510	29 136	6550	862.5	125.1
G-2 (Ti-8Al-1Mo-1V M.A. Ext.)	35.79	1.409	1.27	0.05	1.32	0.0520	25 800	5800	693.6	100.6
G-3 (Ti-8Al-1Mo-1V M.A. Ext.)	35.05	1.380	3.05	0.12	1.39	0.0546	34 162	7680	960.4	139.3
J-3 (Ti-6Al-4V STA Ext.)	36.50	1.437	2.54	0.10	1.33	0.0524	31 271	7030	850.8	123.4

NOTES: (a) The fatigue cracks had curved fronts, and the cracks usually appeared to be longer on one side of the specimen than on the other side. The crack propagation crack lengths were based on what was seen at the top surfaces of the specimens. In this table, the average crack lengths, as measured from the edge of the hole after failure, have been given. Only specimen G-1 had cracks on both sides of the hole, and the two average crack lengths have been added.

(b) The hole diameter was 6.35 mm (0.250 inch) for all specimens.

TABLE 14. - STANDARD DEVIATIONS ON LOG LIVES

Type of Titanium Specimen	Standard Deviations on Log Lives						
	Constant Room Temperature	Constant at 533 K (500 °F)	Constant at 561 K (550 °F)	Cyclic 305 - 533 K (90 - 500 °F)	Cyclic 305 - 561 K (90 - 550 °F)	Real-Time	Ranges of Standard Deviations
Ti-8Al-1Mo-1V Sheet (Mill-Annealed)	0.12	0.10	-	0.05	-	0.08 (b) 0.18 (c)	0.05 - 0.12 (b) 0.05 - 0.18 (c)
Ti-8Al-1Mo-1V Sheet (Duplex-Annealed; Center Notch)	0.18	0.11	0.04	0.13 (a)	0.10	0.01 (b) 0.12 (c)	0.01 - 0.18 (b) 0.04 - 0.18 (c)
Ti-8Al-1Mo-1V Sheet (Duplex-Annealed; Single Spotweld)	0.08	0.03	0.02	0.13	0.11	0.02 (b) 0.10 (c)	0.02 - 0.13
Ti-8Al-1Mo-1V Sheet (Triplex-Annealed)	0.01 (a)	0.30	-	0.00	-	0.07	0.00 - 0.30
Ti-8Al-1Mo-1V Extrusion (Mill-Annealed)	0.17 (a)	0.08	-	0.03	-	0.09	0.03 - 0.17
Ti-6Al-4V Sheet (Mill-Annealed)	0.12	0.17	-	0.05	-	0.17 (b) 0.24 (c)	0.05 - 0.17 (b) 0.05 - 0.24 (c)
Ti-6Al-4V Extrusion (Solution-Treated and Aged)	0.27 (a)	0.10	-	0.06	-	0.07	0.06 - 0.27
Ranges of Standard Deviations	0.01 - 0.27	0.03 - 0.30	(0.02 - 0.04)	0.00 - 0.13	(0.10 - 0.11)	0.01 - 0.17 (b) 0.07 - 0.24 (c)	0.00 - 0.30

NOTES: (a) Some specimens did not fail.

(b) Based on real-time test flights only.

(c) Accelerated test flights applied to the unfailed real-time specimens have been included.

TABLE 15. - FAILED CENTER-NOTCHED SPECIMENS SUBJECTED TO METALLURGICAL ANALYSIS

Titanium Material	Heat Number	Specimen Number	Test Temperature	Applied Flights	Remarks
Ti-8Al-1Mo-1V Mill-Annealed Extrusion	3093	G-1	Real-Time	27 612	
		G-3	Real-Time	23 470	
		GL-10	Room Temp.	42 800	Nonstandard specimen (Ref. 4)
	3227	H-1	Real-Time	22 956	
		H-2	Real-Time	22 725	
		H-3	Real-Time	19 618	
		H-8	Room Temp.	46 000	
		H-9	Const. 533 K (500 °F)	15 700	
		H-10	Room Temp.	35 000	
		HL-6	Const. 533 K (500 °F)	11 800	
		HL-8	Cyclic 305 - 533 K (90 - 500 °F)	67 000	
		HL-9	Const. 533 K (500 °F)	14 000	Nonstandard specimens (Ref. 4)
		HL-10	Cyclic 305 - 533 K (90 - 500 °F)	21 000	

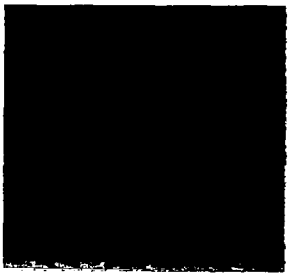

(a) M.A. 8-1-1 sheet, heat D8141

(b) M.A. 8-1-1 sheet, heat D8733

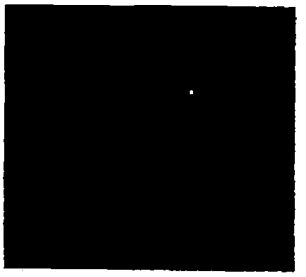

(c) D.A. 8-1-1 sheet, heat D4539

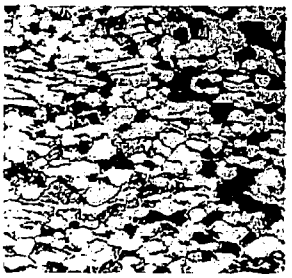

(d) T.A. 8-1-1 sheet, heat D8647

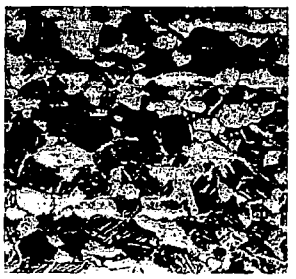

(e) T.A. 8-1-1 sheet, heat D6512

(f) M.A. 8-1-1 extrusion, heat 3093

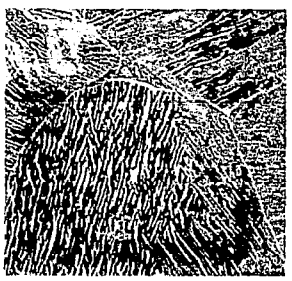

(g) M.A. 8-1-1 extrusion heat 3227

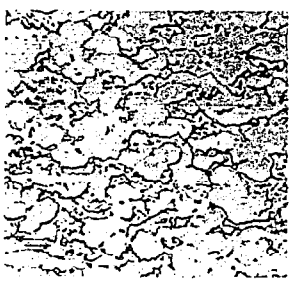

(h) M.A. 6-4 sheet, heat D8673

(i) M.A. 6-4 sheet, heat D8103

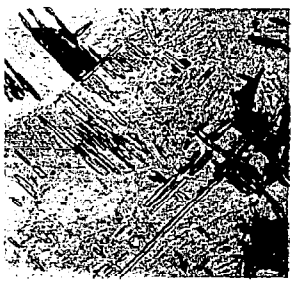

(j) STA 6-4 extrusion heat 3701

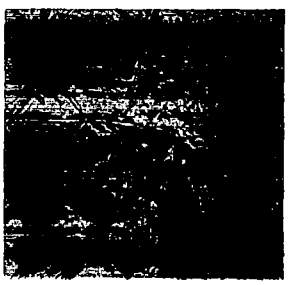

(k) STA 6-4 extrusion heat 3712

Figure 1. - Photomicrographs of sections through untested samples of Ti-8Al-1Mo-1V and Ti-6Al-4V. Mag. 450X for sheet and 200X for extrusion.

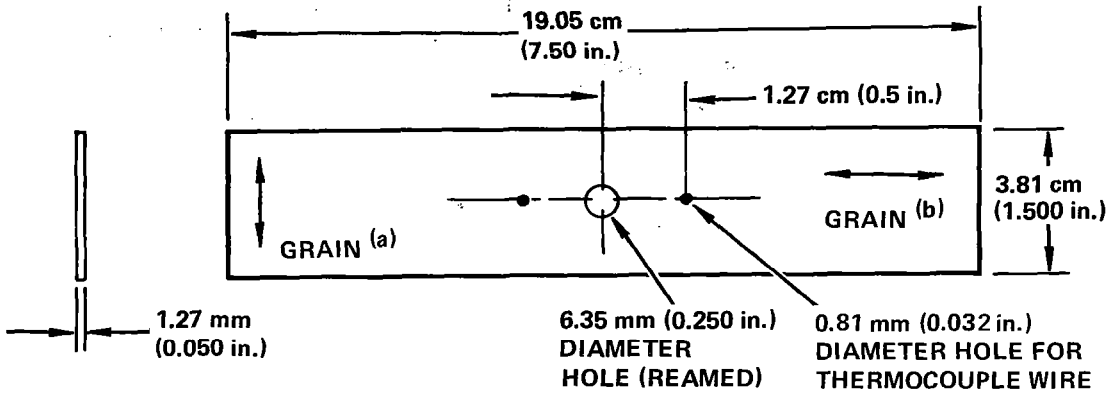

NOTES:

(a) SHEET SPECIMENS.

(b) EXTRUSION SPECIMENS, EXTRUDED DIRECTION.

(a) CENTER-NOTCHED FATIGUE SPECIMEN.

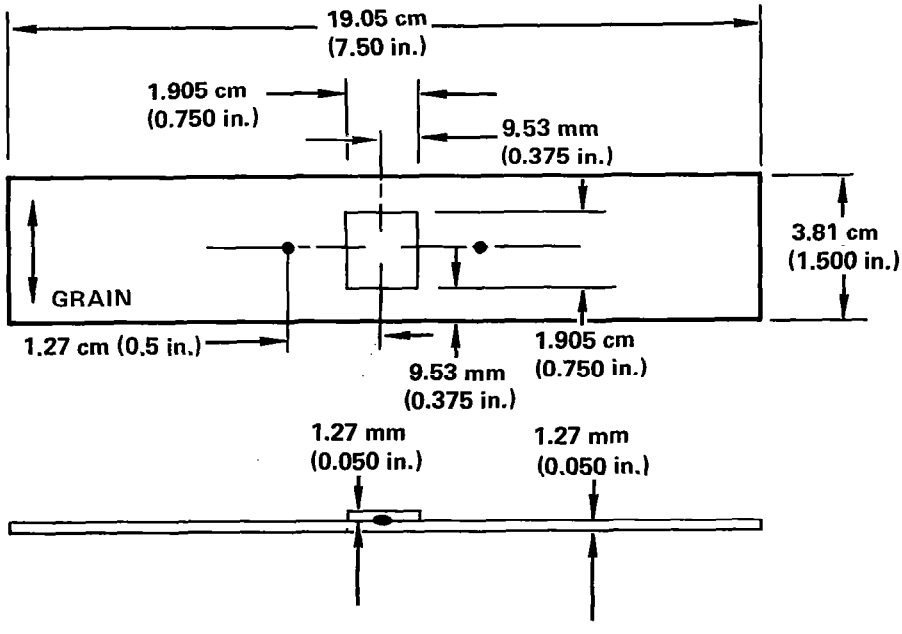

(b) FATIGUE SPECIMEN WITH SINGLE SPOTWELD DOUBLER.

Figure 2. - Test specimen geometries.

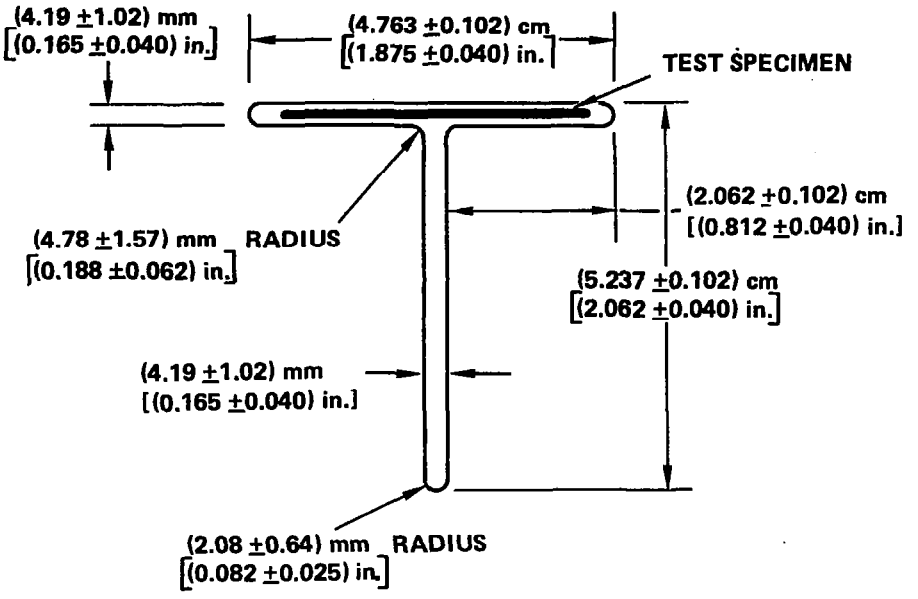

NOTES:

(a) 0.38 mm (0.015 in.) MAXIMUM DEPTH OF SURFACE DEFECT.
(b) 0.63 mm/30 cm (0.025 in./ft) STRAIGHTNESS TOLERANCE.
(c) 0.10 mm/cm (0.010 in./in.) DEVIATION FROM FLATNESS.
(d) 1 DEGREE/30 cm (1 DEGREE/ft) TWIST TOLERANCE, NOT TO EXCEED 5 DEGREES FOR ANY TOTAL LENGTH.

Figure 3. - Shape of Ti-8Al-1Mo-1V and Ti-6Al-4V titanium extrusions.

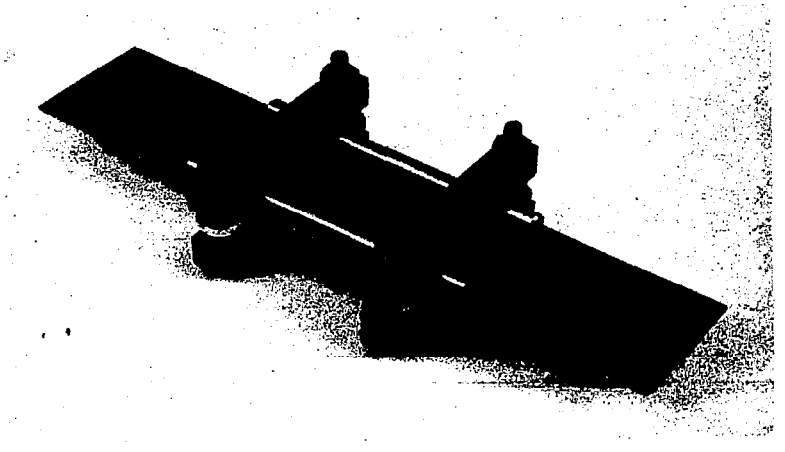

Figure 4. - Test specimen with edge support installed.

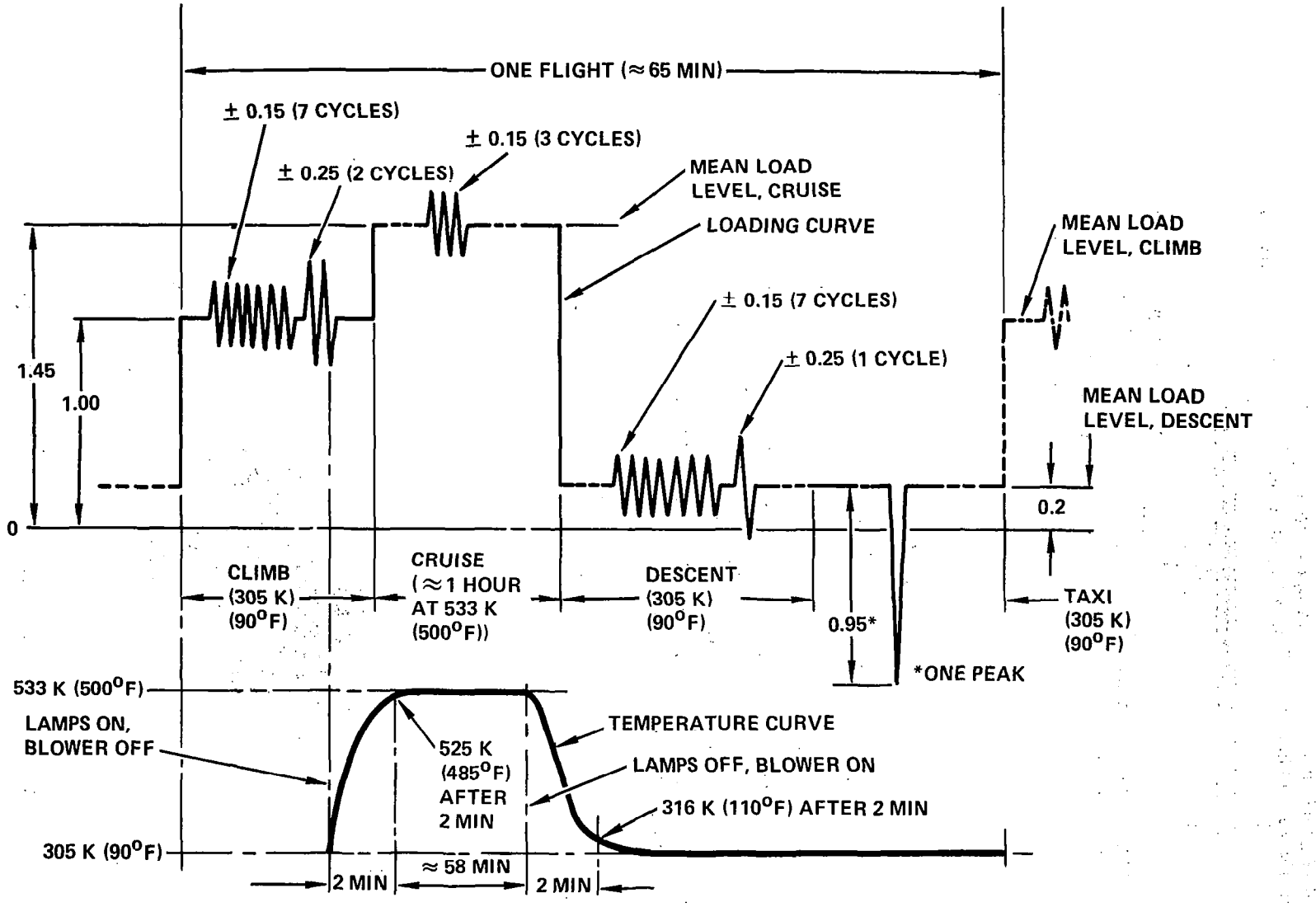

NOTE: ORDINATE INDICATES RATIO OF STRESS TO $f_{1g_{REF}}$

WHERE $f_{1g_{REF}}$ = 172 MPa (25 KSI) (GROSS AREA).

THE GROWTH IN MAGNITUDES OF CYCLIC LOADS WITH TIME IS GIVEN IN TABLE 3.

Figure 5. - Loading and temperature sequences and magnitudes for the real-time unit flight.

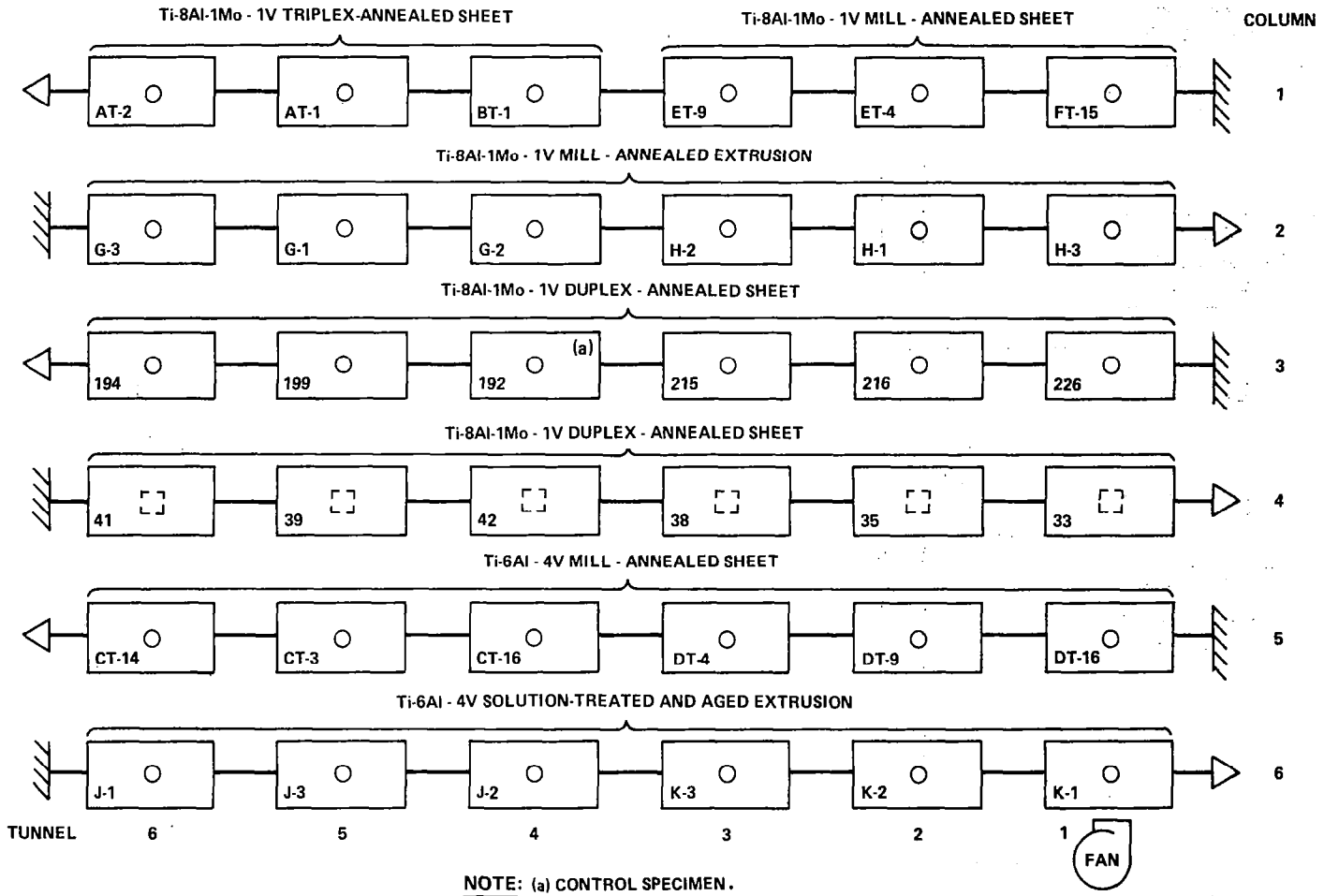

Figure 6. - Specimen positions in the real-time testing machine.

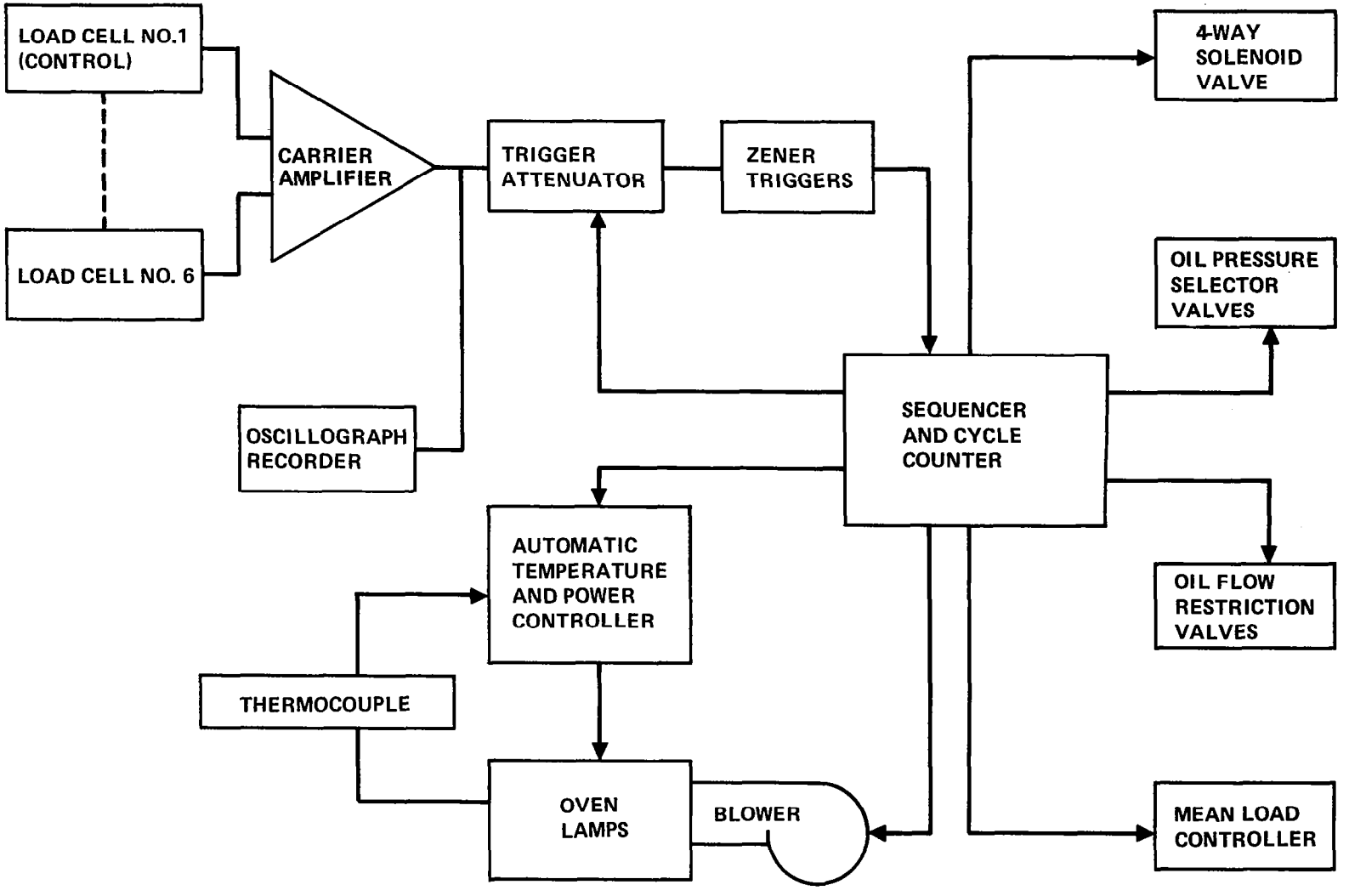

Figure 7. - Block diagram of control equipment for the real-time spectrum loading tests.

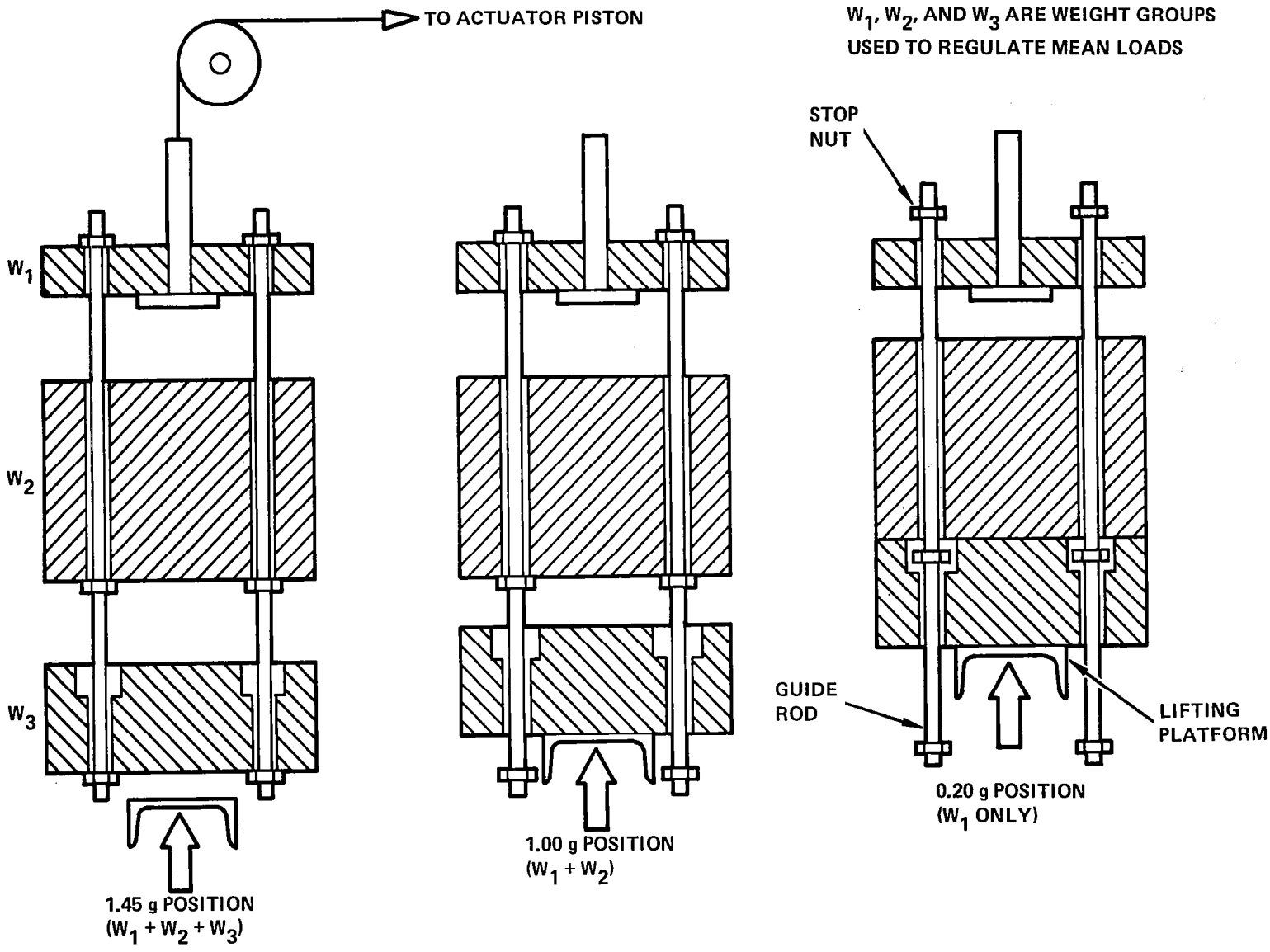

Figure 8. - Static weight loading system for maintaining the mean loads on the real-time spectrum loading machine.

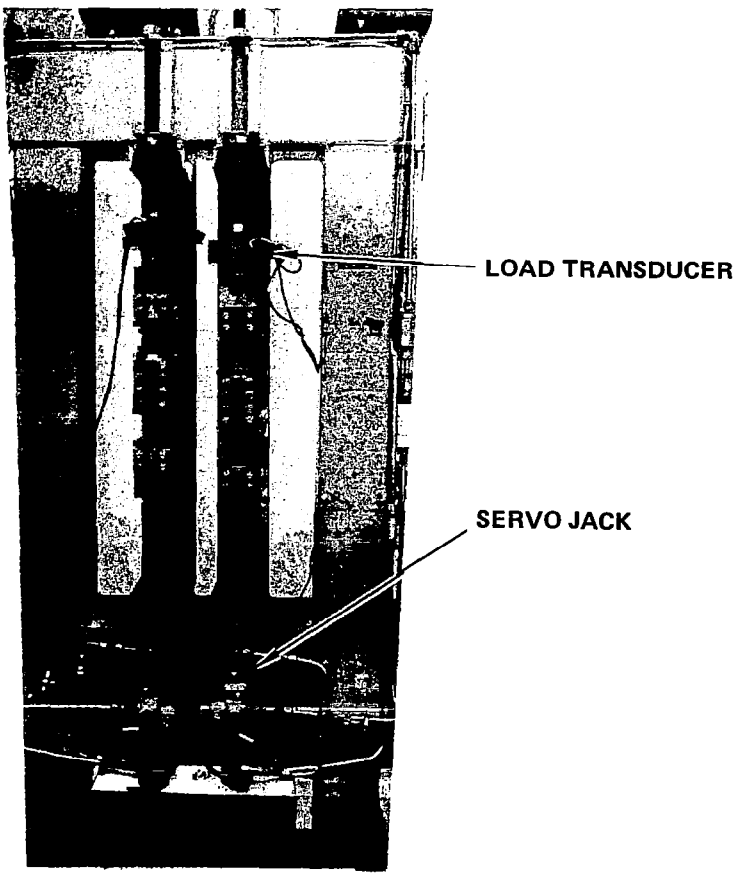

Figure 9. - Accelerated fatigue testing machine.

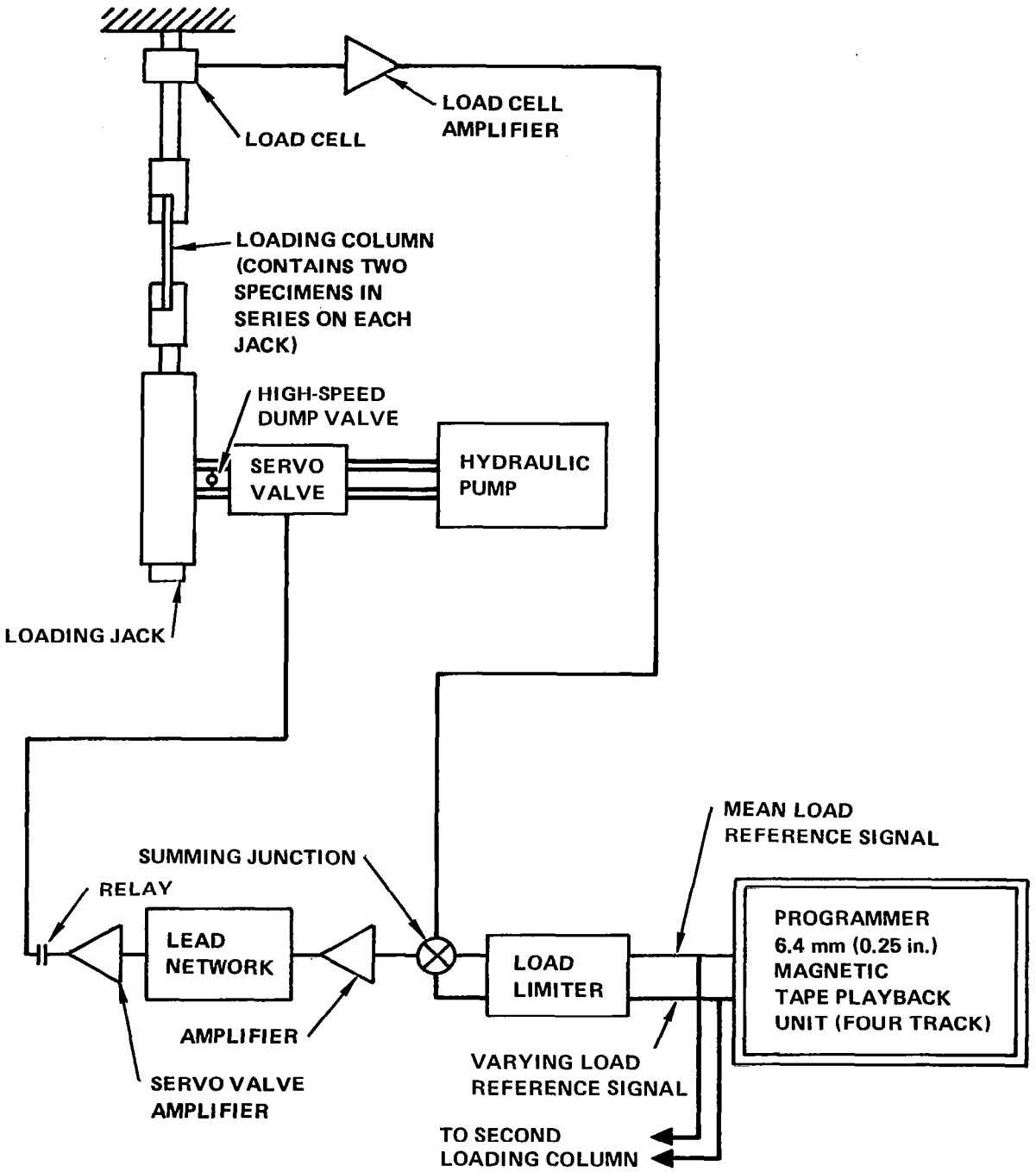

Figure 10. - Block diagram of test setup for accelerated flight-by-flight loading tests.

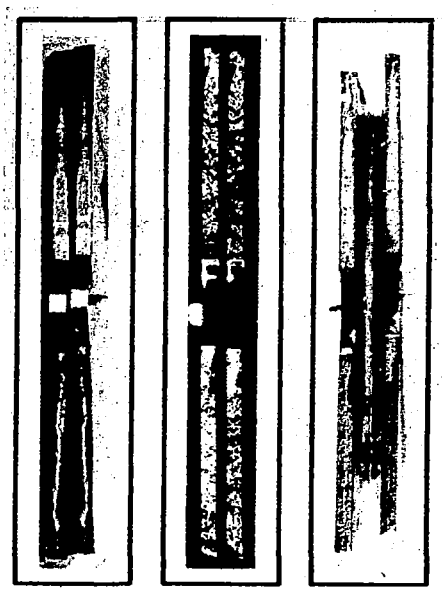

(a) ET-4 (b) ET-9 (c) FT-15

(a) and (b) failed during real-time testing.
(c) failed during accelerated testing.

Figure 11. - Photomacrographs showing mating fracture surfaces for mill-annealed Ti-8Al-1Mo-1V sheet specimens.

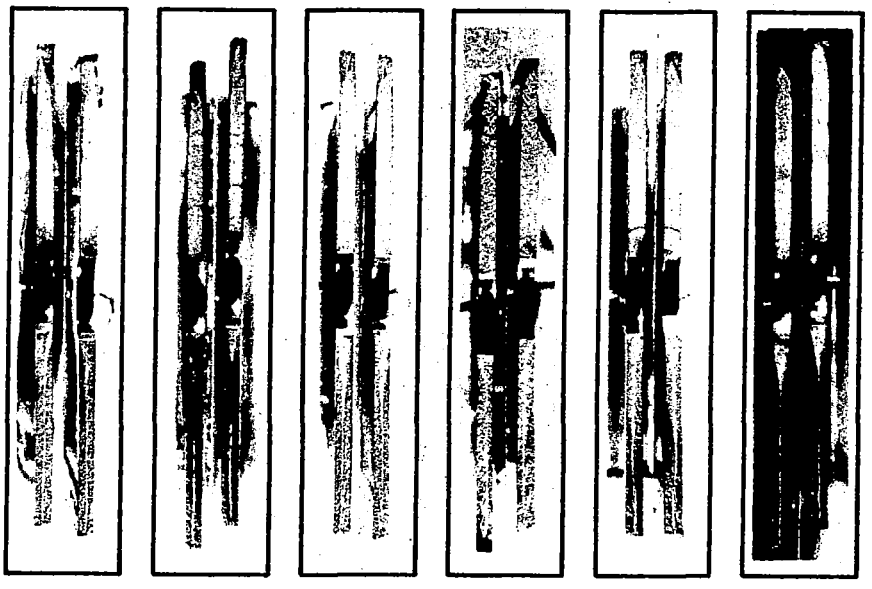

(a) 192 (b) 194 (c) 199 (d) 215 (e) 216 (f) 226

All specimens failed during accelerated testing.

Figure 12. - Photomacrographs showing mating fracture surfaces for duplex-annealed Ti-8Al-1Mo-1V sheet specimens with center notch.

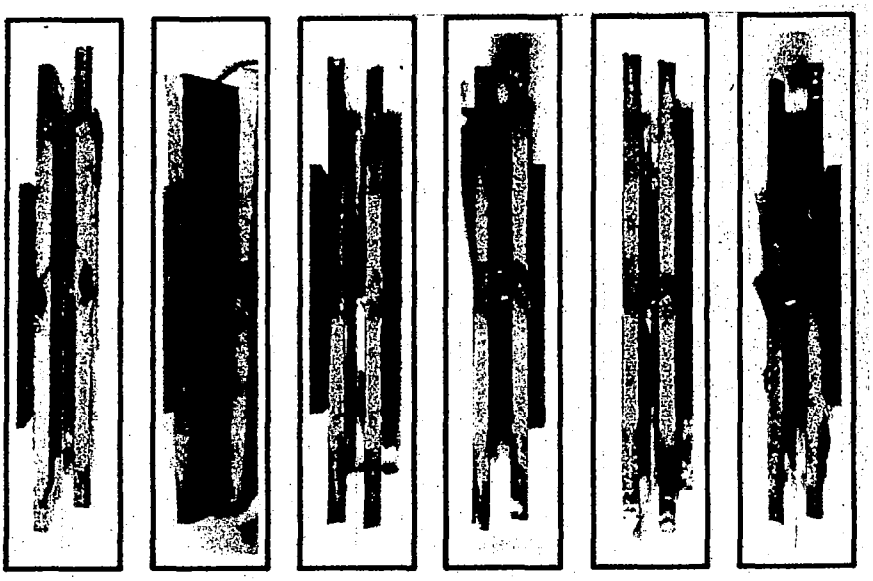

(a) 33 (b) 35 (c) 38 (d) 39 (e) 41 (f) 42

(b) failed during real-time testing.

(a), (c), (d), (e), and (f) failed during accelerated testing.

Figure 13. - Photomacrographs showing mating fracture surfaces for duplex-annealed Ti-8Al-1Mo-1V sheet specimens with single spotweld.

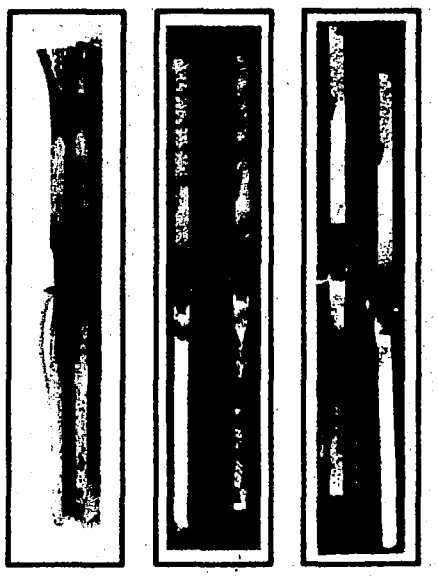

(a) AT-1 (b) AT-2 (c) BT-1

All specimens failed during real-time testing.

Figure 14. - Photomacrographs showing mating fracture surfaces for triplex-annealed Ti-8Al-1Mo-1V sheet specimens.

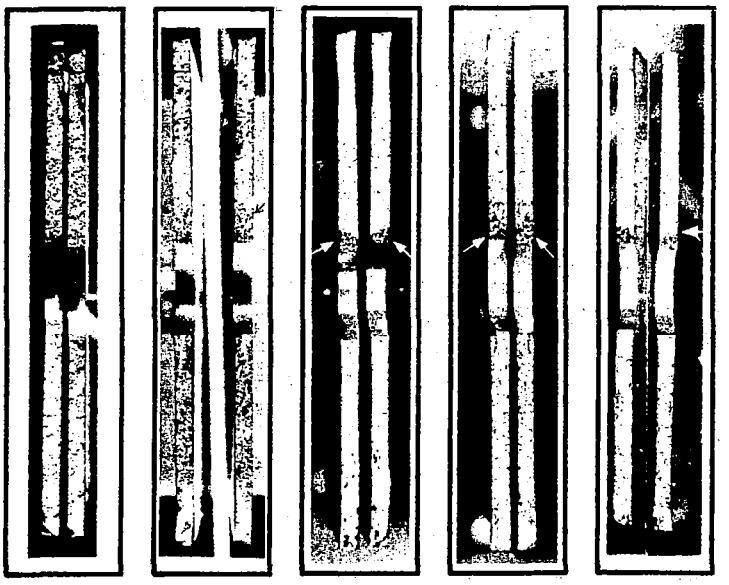

(a) G-2 (b) G-3 (c) H-1 (d) H-2 (e) H-3

All specimens failed during real-time testing.

Figure 15. - Photomacrographs showing mating fracture surfaces for mill-annealed Ti-8Al-1Mo-1V extrusion specimens.

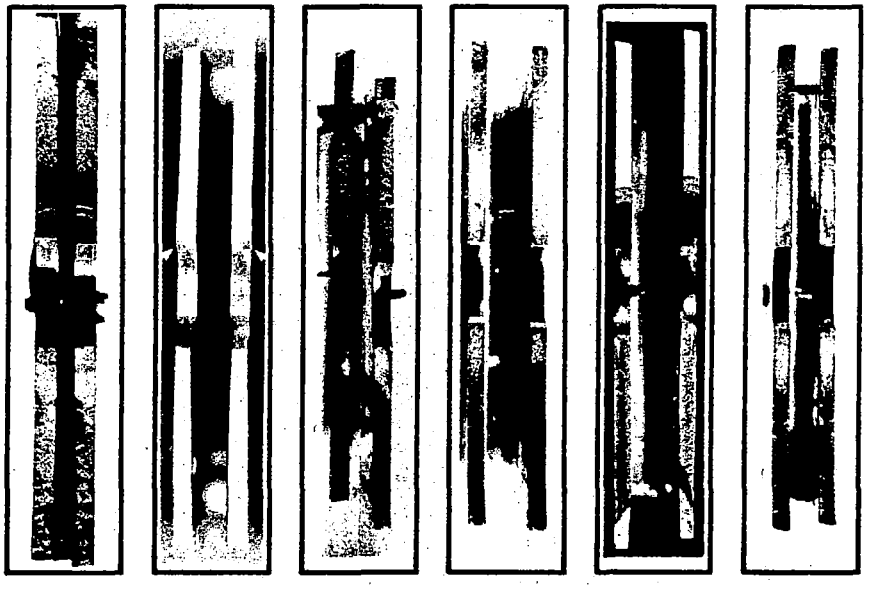

(a) CT-3 (b) CT-14 (c) CT-16 (d) DT-4 (e) DT-9 (f) DT-16

(a), (b), and (e) failed during real-time testing.
(c), (d), and (f) failed during accelerated testing.

Figure 16. - Photomacrographs showing mating fracture surfaces for mill-annealed Ti-6Al-4V sheet specimens.

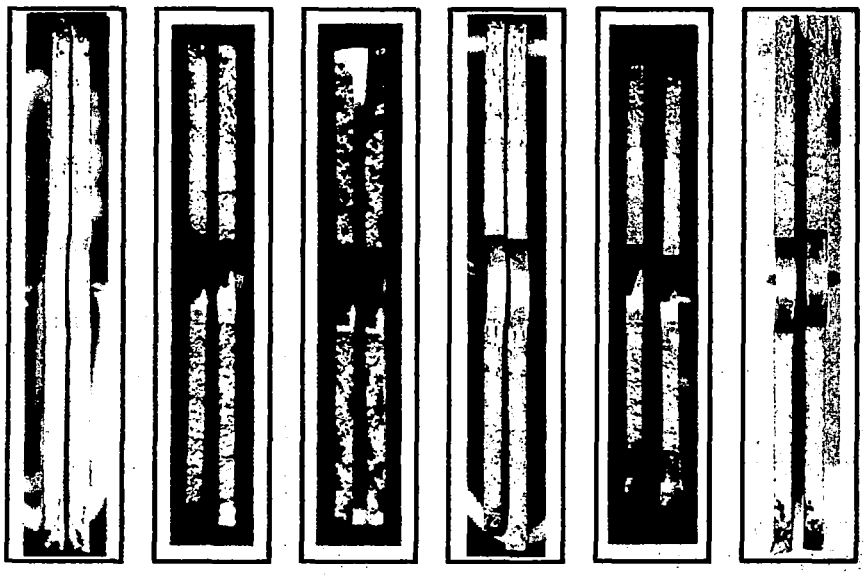

(a) J-1 (b) J-2 (c) J-3 (d) K-1 (e) K-2 (f) K-3

All specimens failed during real-time testing.

Figure 17. - Photomacrographs showing mating fracture surfaces for solution-treated and aged Ti-6Al-4V extrusion specimens.

FOR SYMBOLS, SEE NOTES ON FIGURE 24.

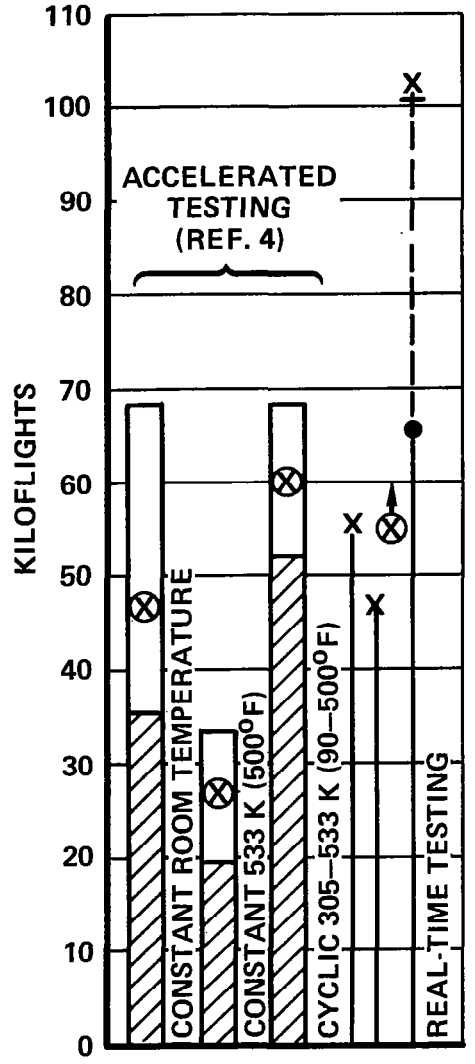

Figure 18. - Comparative test results for mill-annealed Ti-8Al-1Mo-1V sheet specimens.

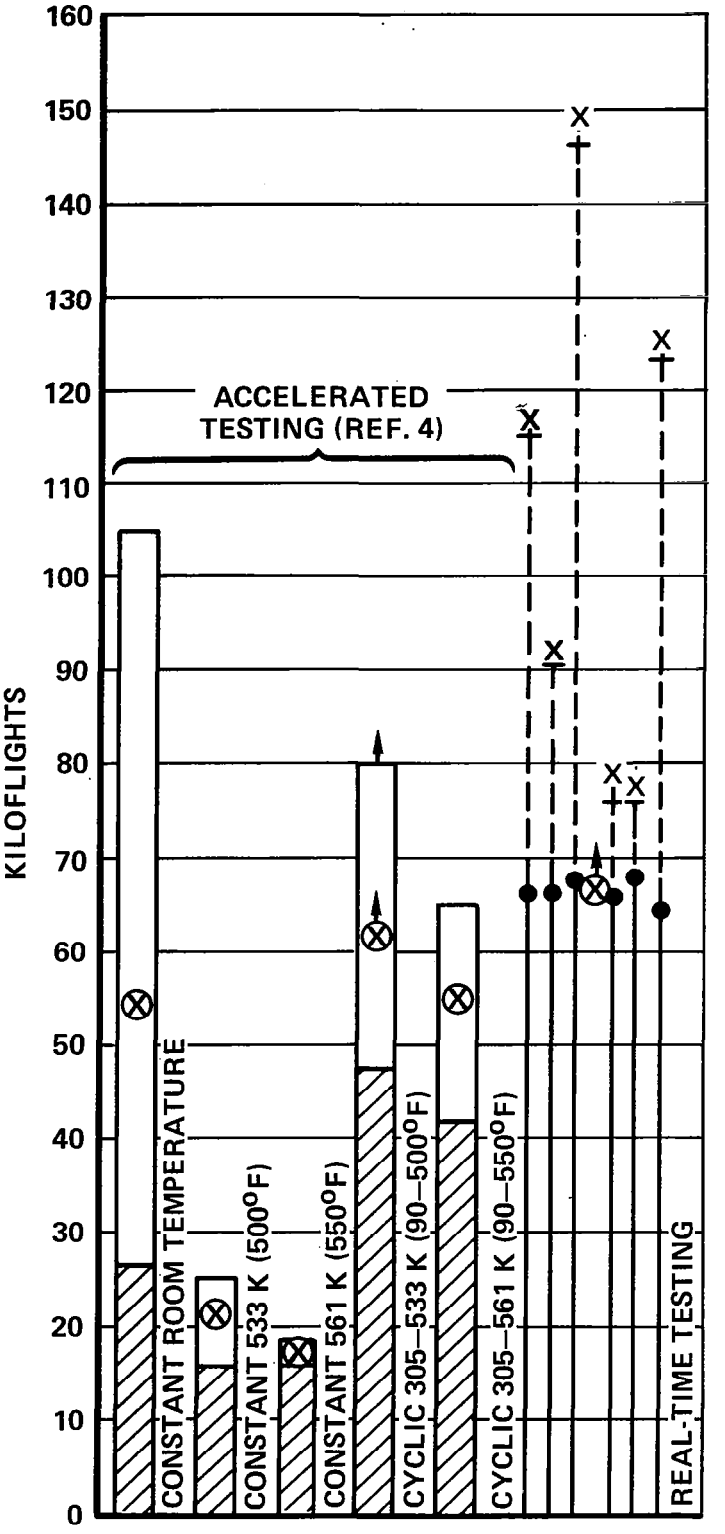

Figure 19. - Comparative test results for duplex-annealed Ti-8Al-1Mo-1V sheet specimens with center notch.

FOR SYMBOLS, SEE NOTES ON FIGURE 24.

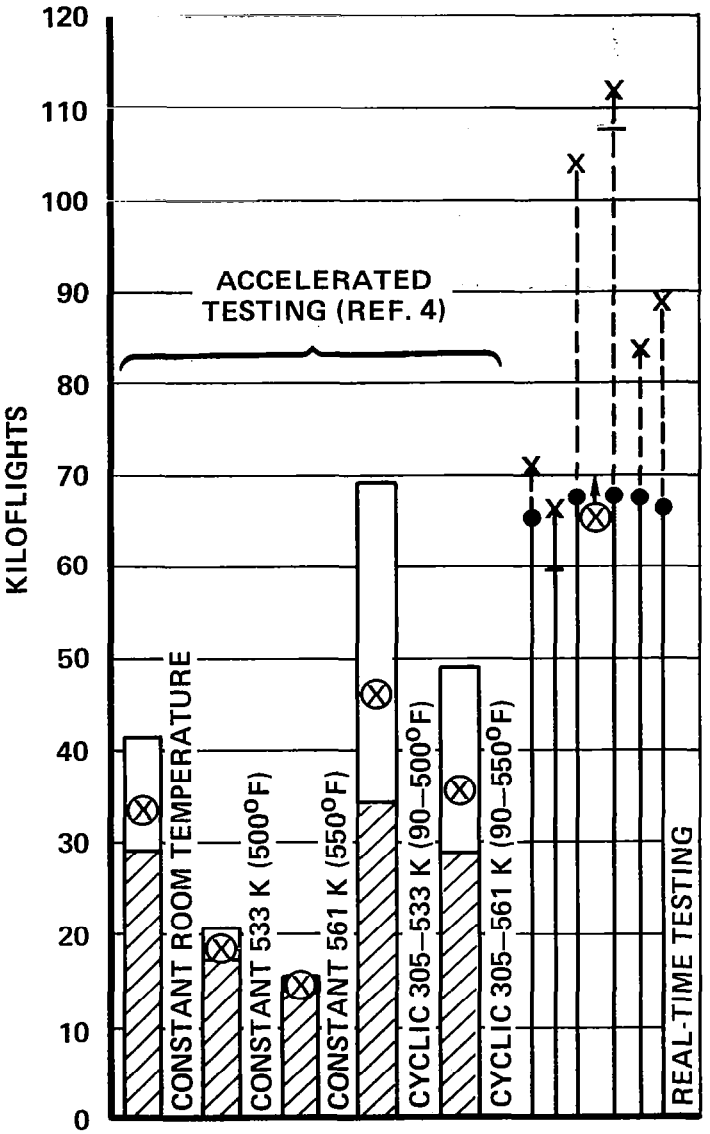

Figure 20. - Comparative test results for duplex-annealed Ti-8Al-1Mo-1V sheet specimens with single spotweld.

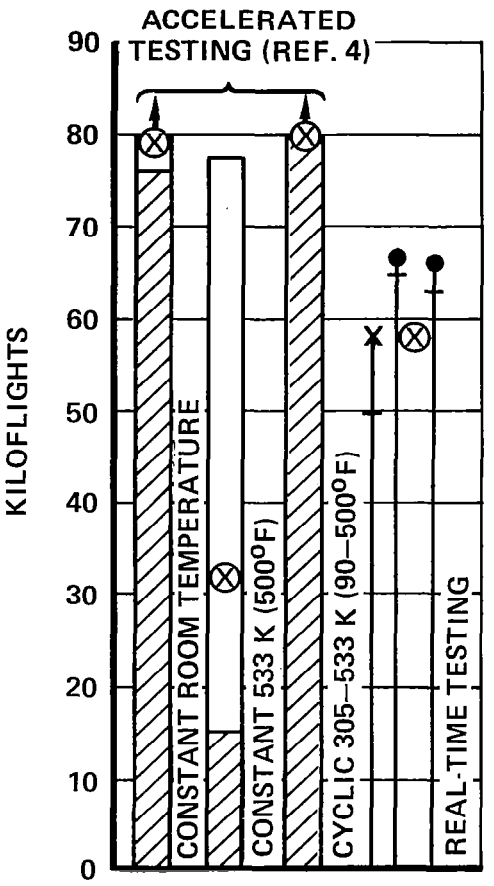

Figure 21. - Comparative test results for triplex-annealed Ti-8Al-1Mo-1V sheet specimens.

FOR SYMBOLS, SEE
NOTES ON FIGURE 24.

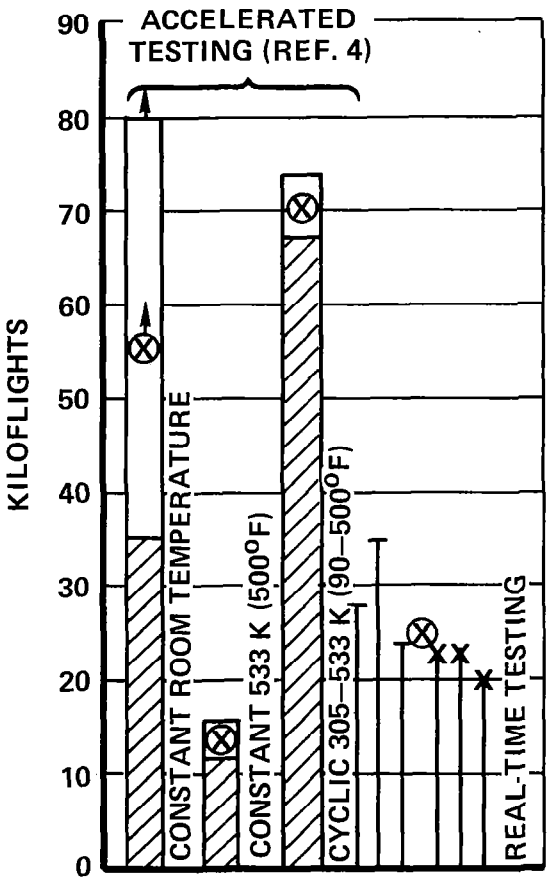

Figure 22. - Comparative test results for mill-annealed Ti-8Al-1Mo-1V extrusion specimens.

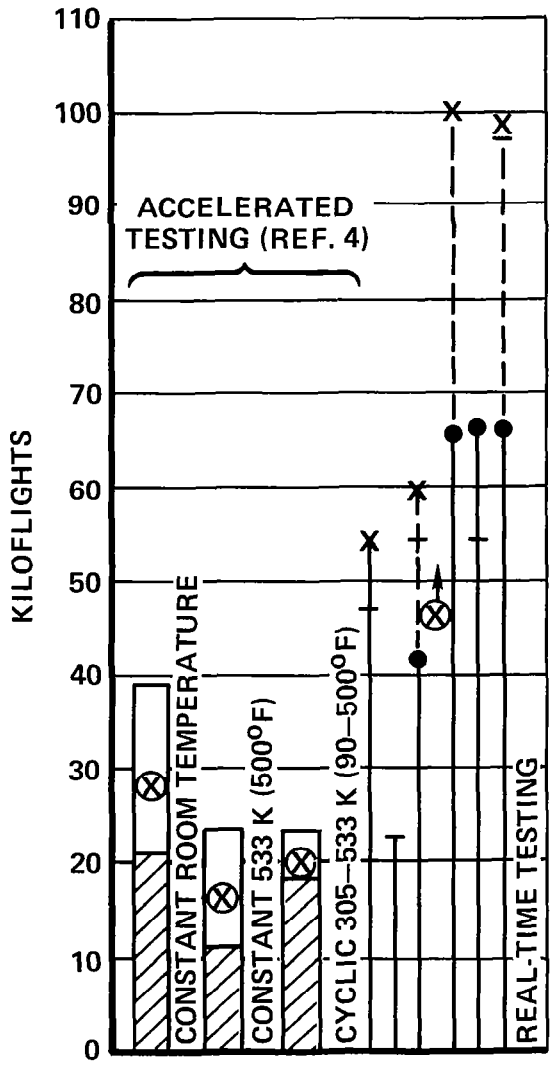

Figure 23. - Comparative test result for mill-annealed Ti-6Al-4V sheet specimens.

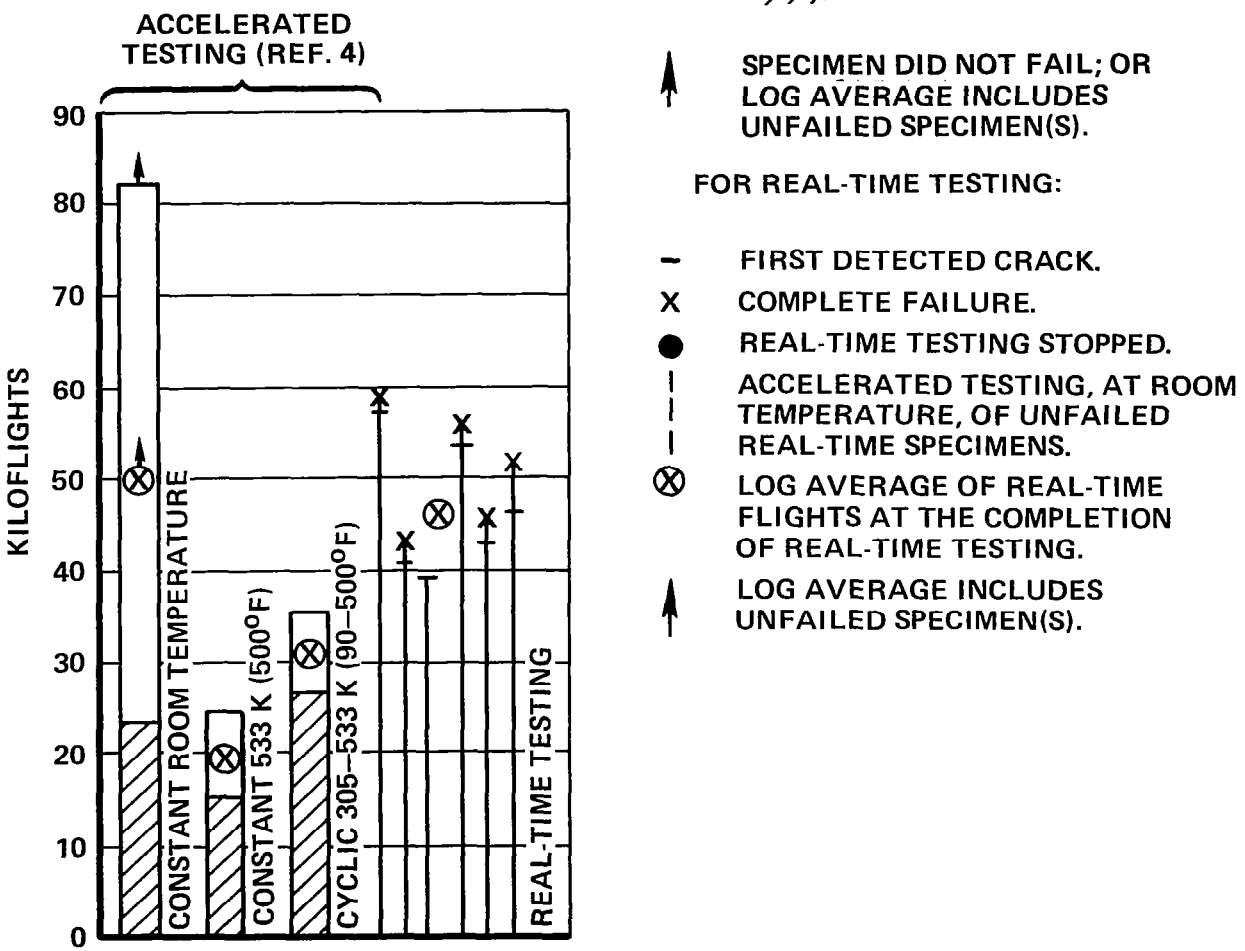

Figure 24. - Comparative test results for solution-treated and aged Ti-6Al-4V extrusion specimens.

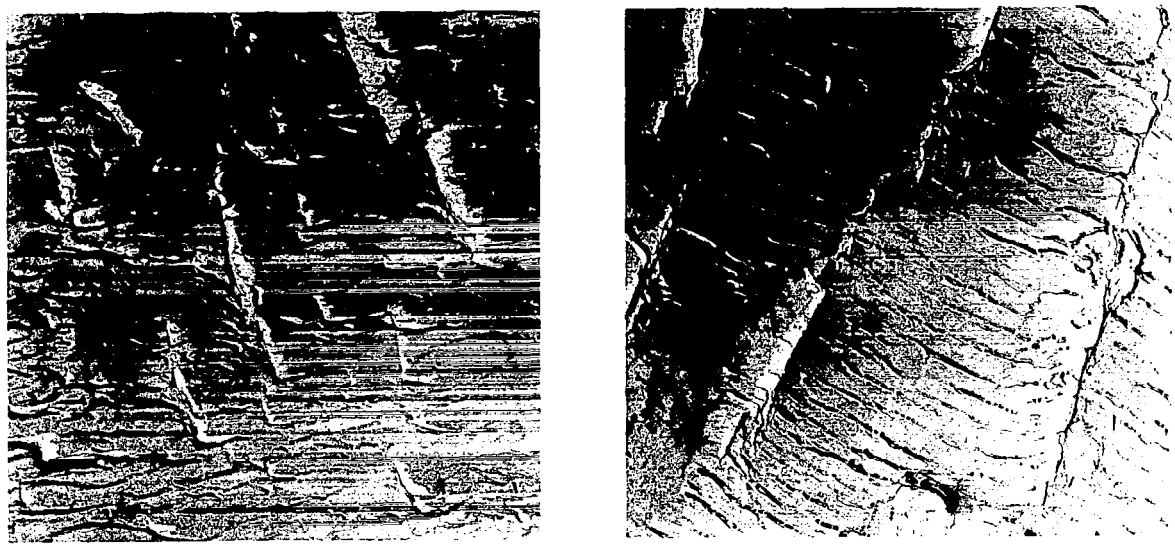

a b

(a) and (b) Fatigue striations interrupted by cleavage steps which were predominant in the fatigue regions.

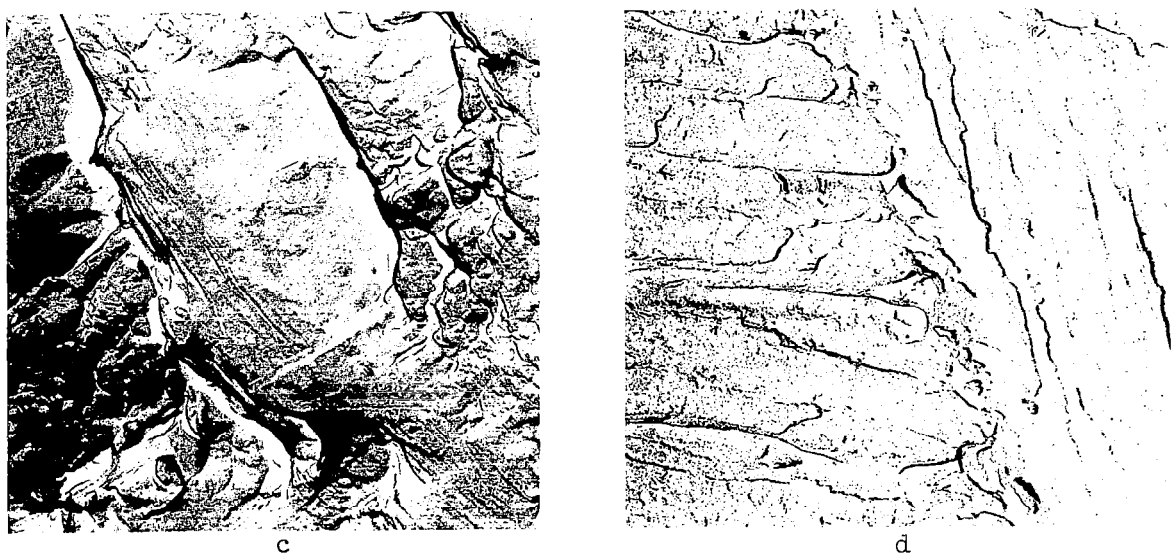

c d

(c) Dimples and second phase particles; and
(d) Cleavage-type fracture features; in the area adjacent to the larger fatigue region.

Figure 25. - Electron fractographs from mill-annealed Ti-8Al-1Mo-1V extrusion specimen G-1. Mag. 6500X

e

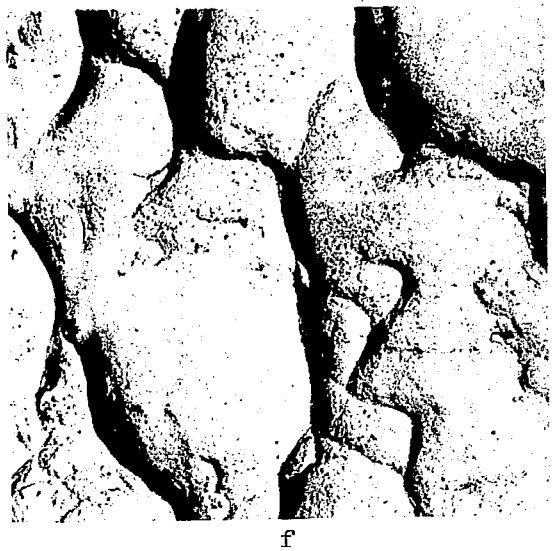

f

Well formed dimples: (e) In an area half-way along the shear regions; and
(f) At the end of the shear regions.

Figure 25. - Concluded.

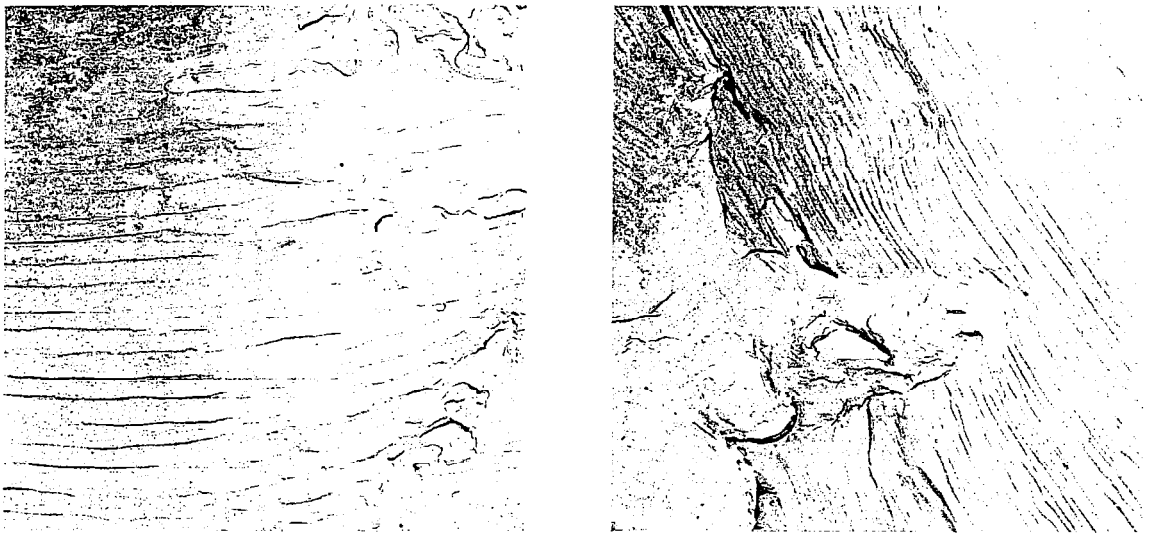

a b

(a) and (b) Well defined fatigue striations with very little cleavage in the fatigue regions.

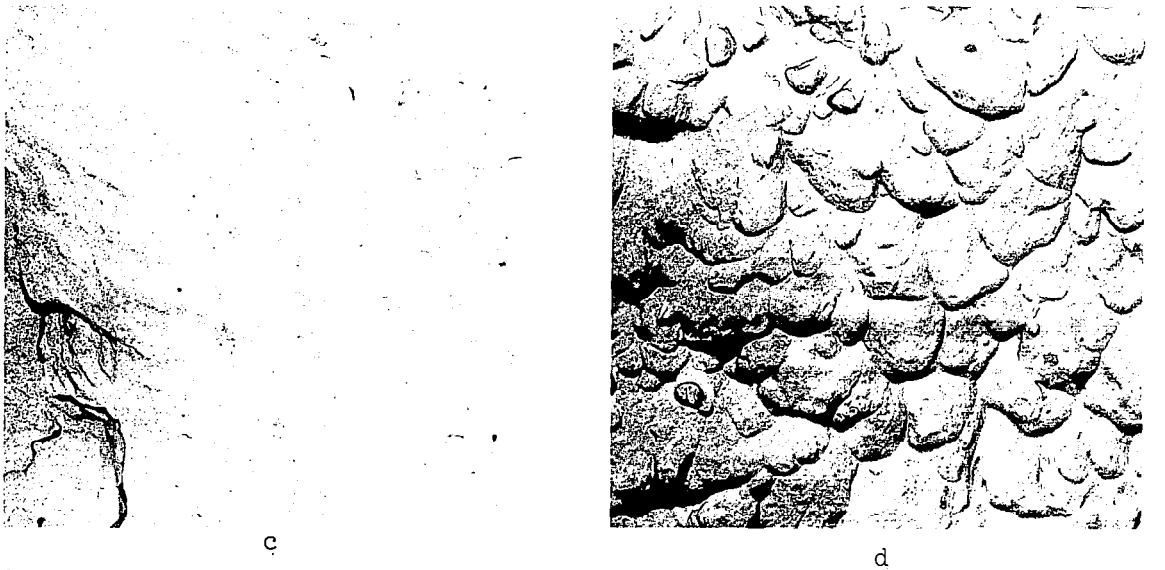

c d

(c) An isolated area of fatigue striations; and (d) An area of well formed dimples of both equiaxed and elongated types; in the fatigue-to-overload transition regions.

Figure 26. - Electron fractographs from mill-annealed Ti-8Al-1Mo-1V extrusion specimen GL-10. Mag. 6500X.

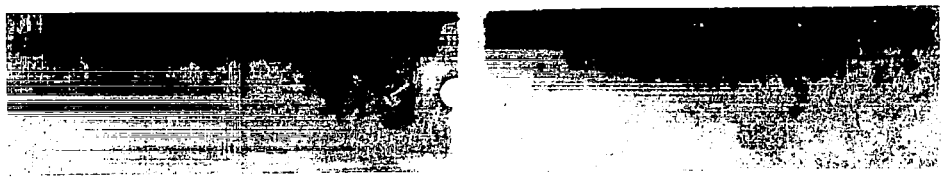

Figure 27. - Overall view of failed mill-annealed Ti-8Al-1Mo-1V extrusion specimen H-3. Mag. 1/2X

(a) The center hole with rough scored surface and raised annular ring. Mag. 8X

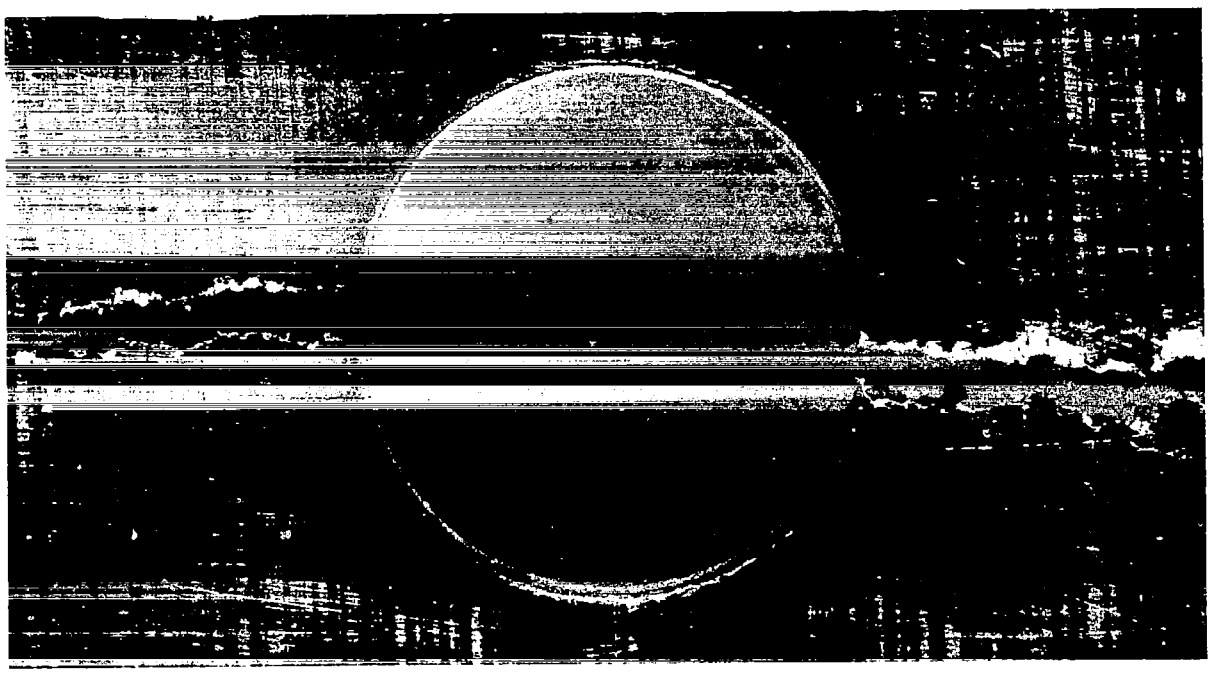

(b) The center hole with raised annular ring and deformed radius. Mag. 10X

Figure 28. - Photomacrographs of the hole region of mill-annealed Ti-8Al-1Mo-1V extrusion specimen H-3.

(a) Grip area (specimen H-3). Mag. 200X

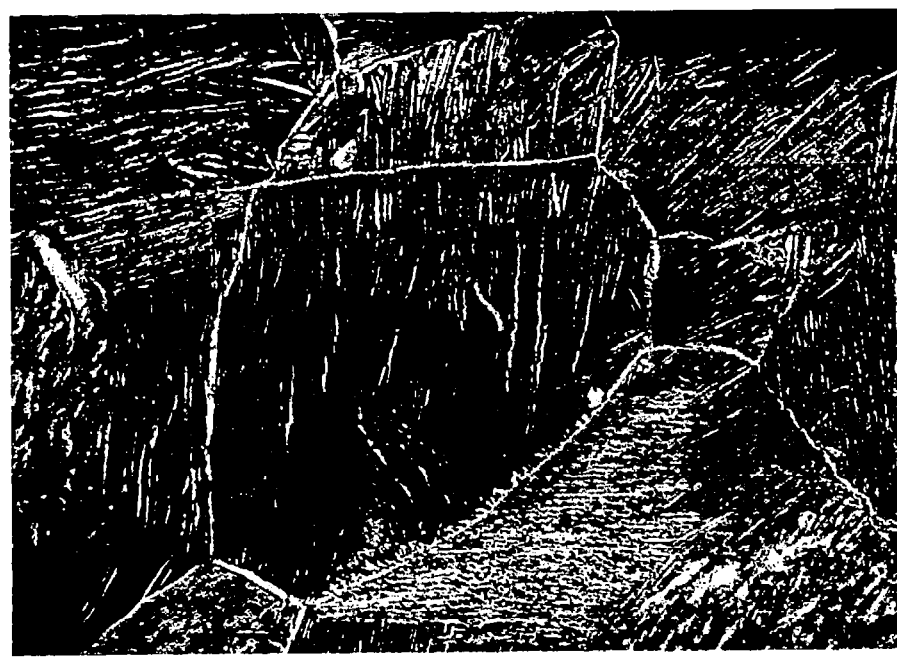

(b) Fatigue area near the center hole. Mag. 450X

Figure 29. - Typical microstructures for the mill-annealed Ti-8Al-1Mo-1V extrusion specimens.

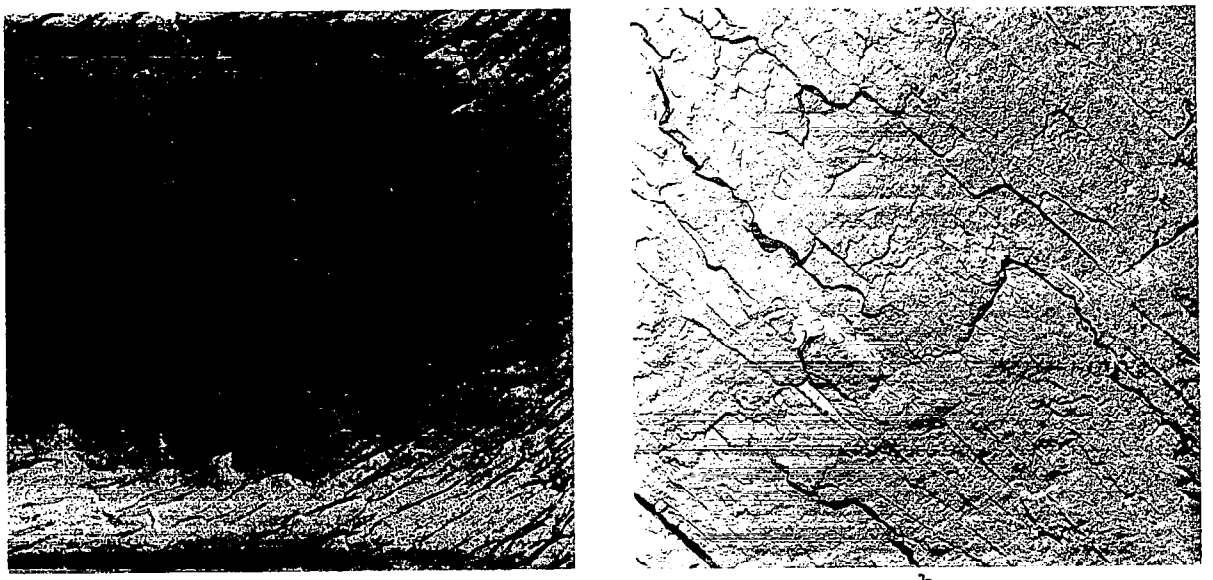

a b

(a) Fatigue striations with occasional striation cracking found in the oxidized fatigue area; and (b) Cleavage rupture mode found in the rapid overload failure area.

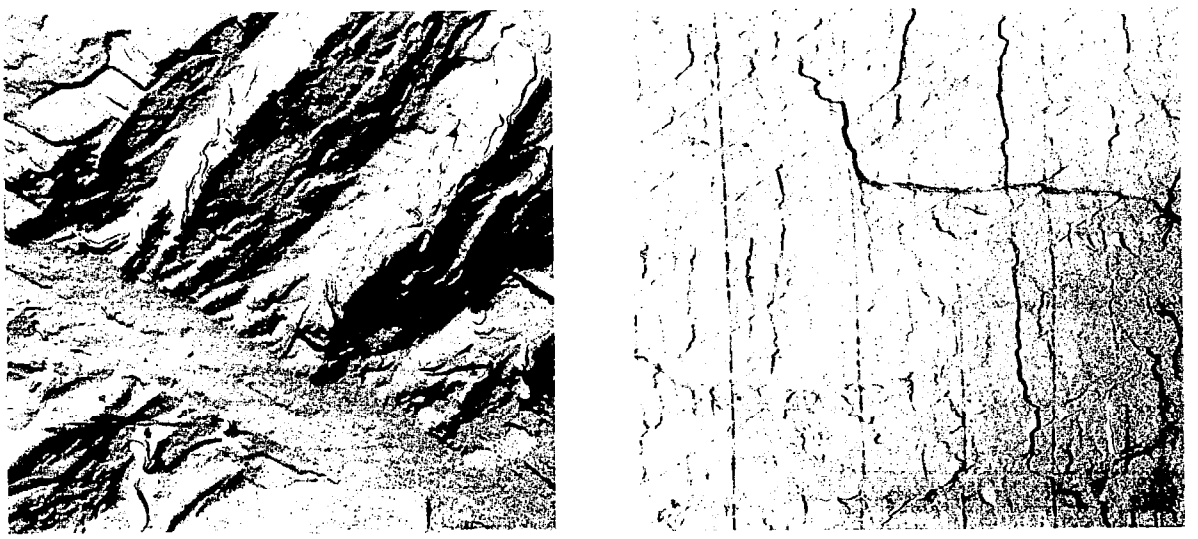

c d

(c) and (d) Cleavage-type fracture features found intermixed with fatigue striations in the fatigue region.

Figure 30. - Electron fractographs from mill-annealed Ti-8Al-1Mo-1V extrusion specimen H-3. Mag. 6500X

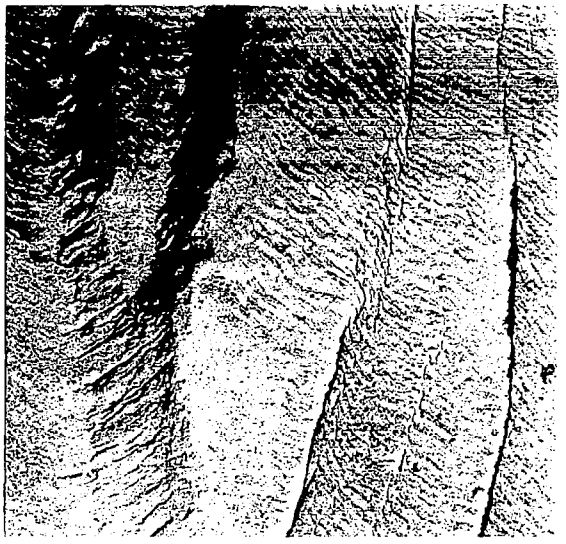

e

f

(e) Fatigue striations interrupted by cleavage steps; and
(f) Uninterrupted fatigue striations; in the fatigue region.

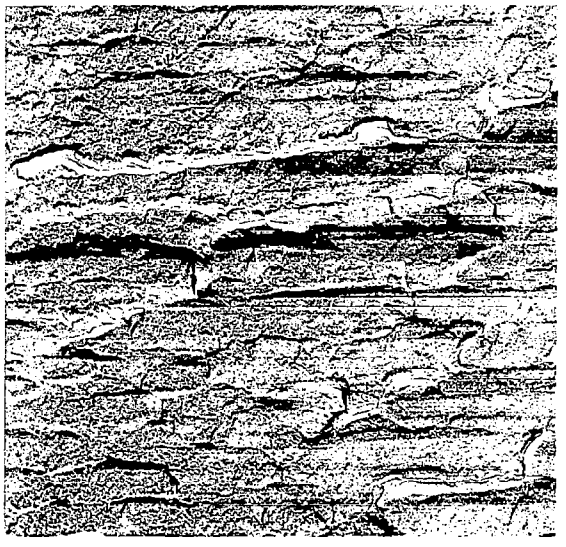

g

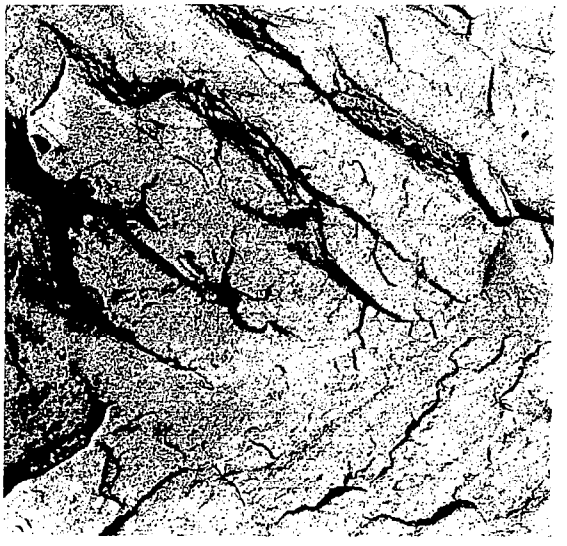

h

Predominant cleavage-type fracture features in an area: (g) Adjacent to the fatigue region; and (h) Half-way towards the specimen outer edge.

Figure 30. - Continued.

i

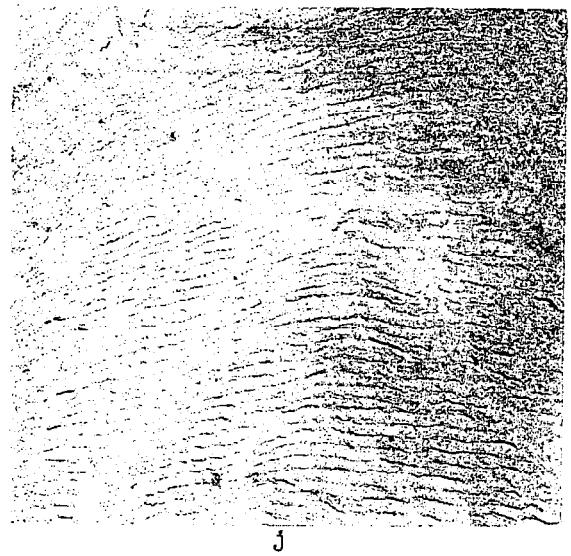

j

(i) Dimple rupture mode found in areas adjacent to the fatigue region and mid-way towards the specimen outer edge; and (j) Fatigue striations found in area adjacent to the visual fatigue region.

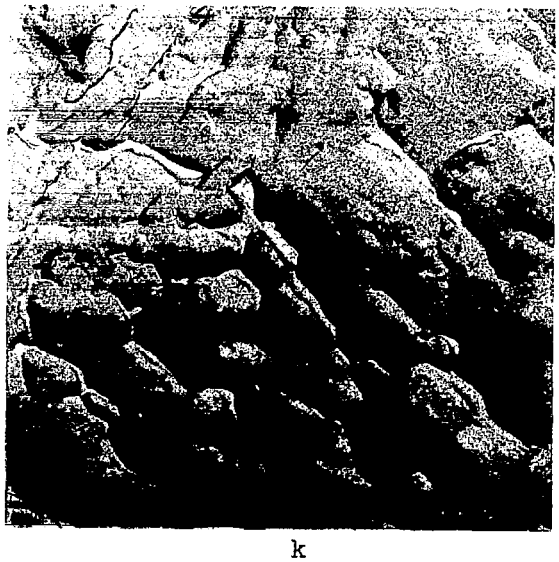

k

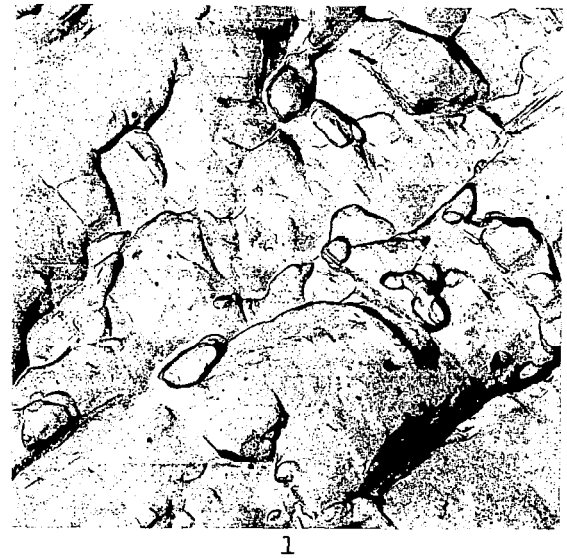

l

(k) and (l) Dimples in the fracture surface opposite the fatigue crack side of the hole.

Figure 30. - Concluded.

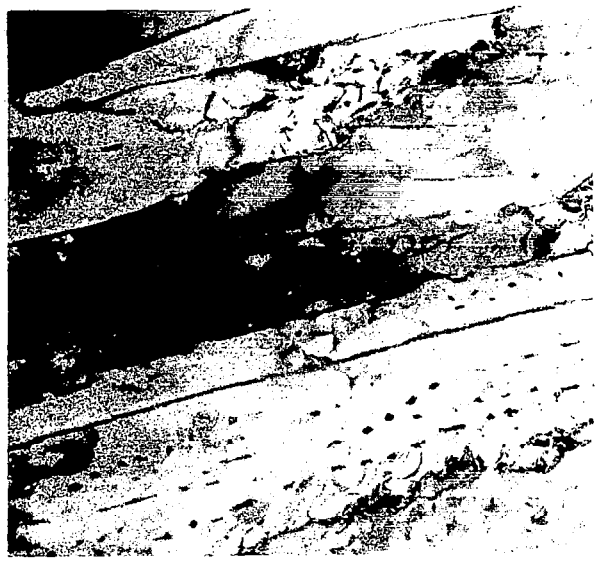

a Mag. 15000X

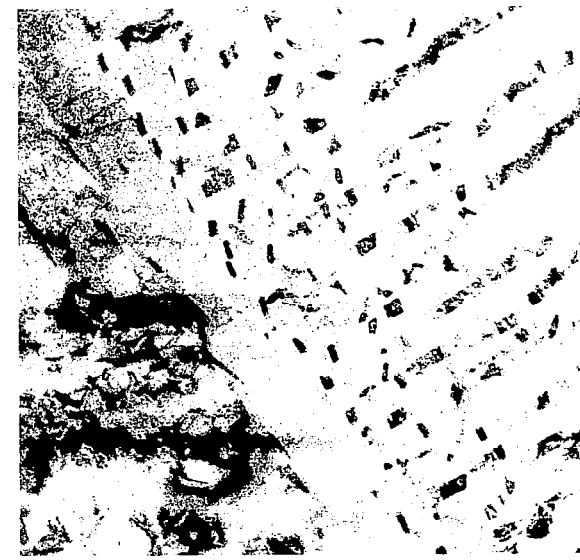

b Mag. 15000X

(a) Parallel lamellae separated by relatively low angle boundaries with clear grain interiors; and (b) Prominent grain boundary (upper left to lower right) with numerous partial dislocations and associated stacking faults evident in the right grain.

c Mag. 15000X

d Mag. 34500X

(c) Parts of two grains with stacking faults and several dislocation pile-ups; and (d) High magnification electron micrograph of area with apparent second phase particles interconnected by dislocations.

Figure 31. - Transmission electron micrographs from mill-annealed Ti-8Al-1Mo-1V extrusion specimen H-3.

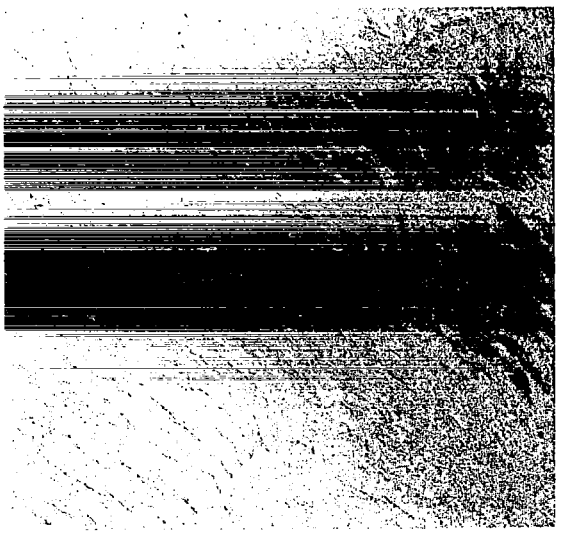

a

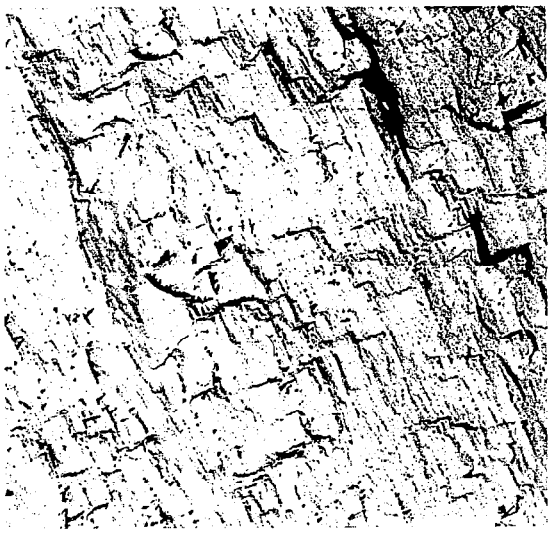

b

(a) Uninterrupted fatigue striations; and (b) Fatigue striations interrupted by cleavage steps; in the fatigue region.

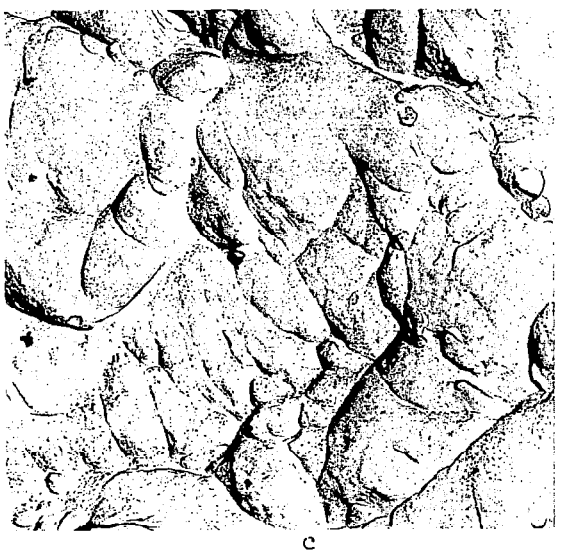

c

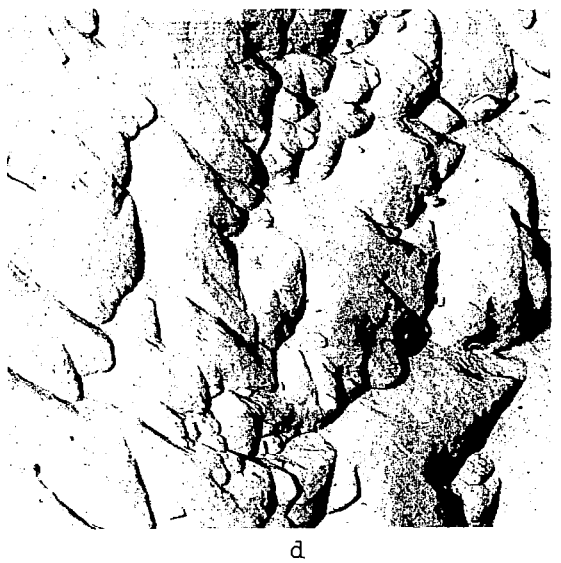

d

(c) and (d) Well formed dimples of both equiaxed and elongated types in the overload region.

Figure 32. - Electron fractographs from mill-annealed Ti-8Al-1Mo-1V extrusion specimen HL-9. Mag. 6500X

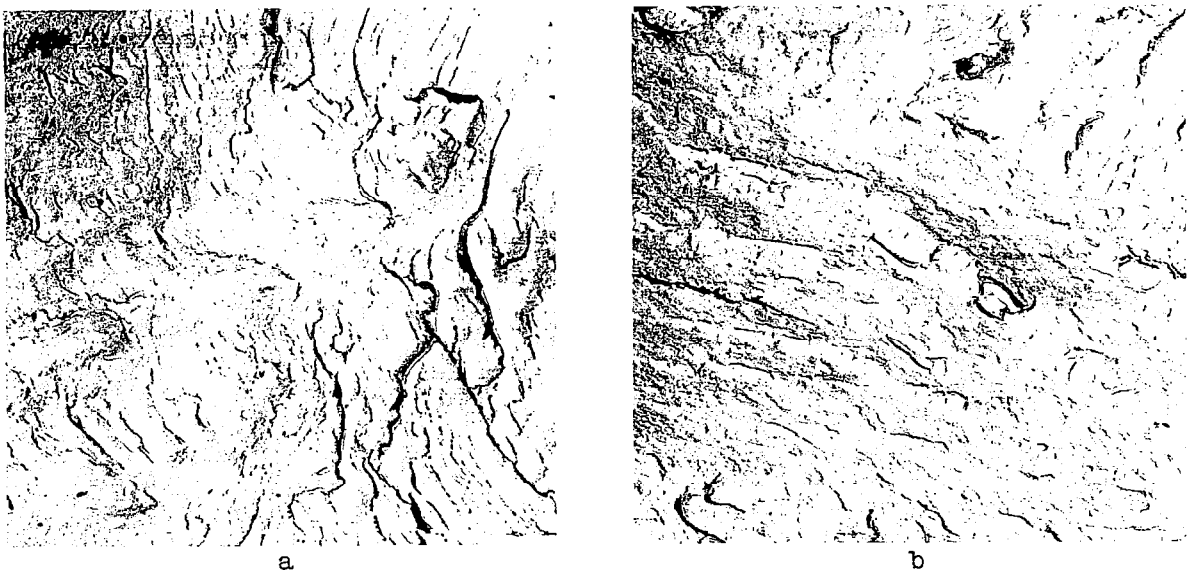

(a) Fatigue striations interrupted by cleavage steps; and
(b) Cleavage-type fracture; in the fatigue region.

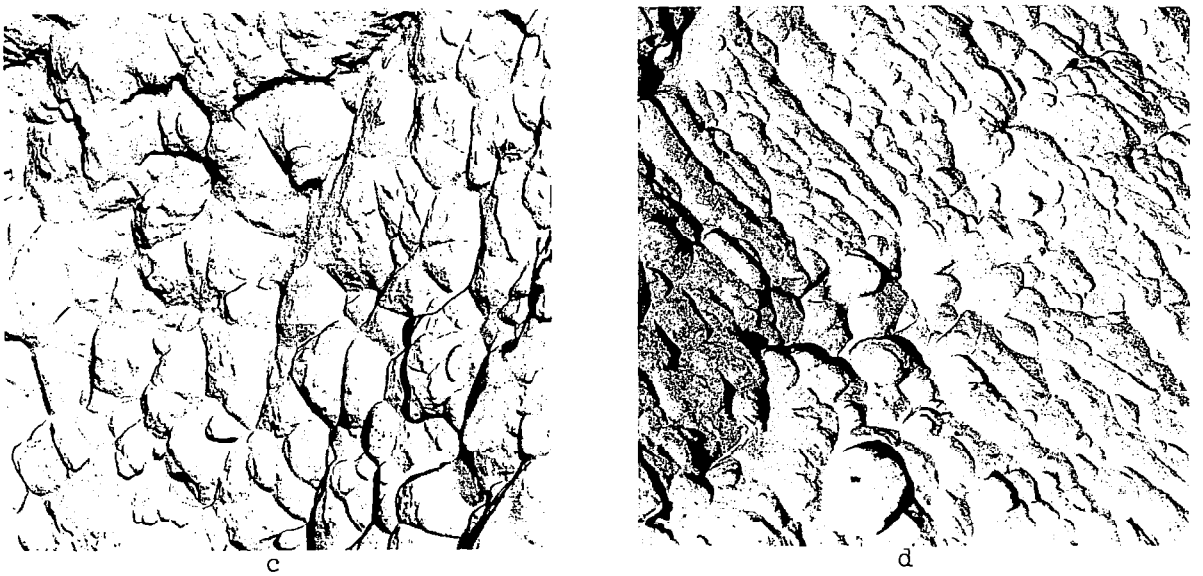

(c) and (d) Well formed dimples of both equiaxed and elongated types in the overload region.

Figure 33. - Electron fractographs from mill-annealed Ti-8Al-1Mo-1V extrusion specimen HL-10. Mag. 6500X